National Library of Canada
Acquisitions and Bibliographic Services Branch
395 Wellington Street
Ottawa, Ontario
K1A 0N4

Bibliothèque nationale du Canada
Direction des acquisitions et des services bibliographiques
395, rue Wellington
Ottawa (Ontario)
K1A 0N4

Your file Votre référence

Our file Notre référence

NOTICE

The quality of this microform is heavily dependent upon the quality of the original thesis submitted for microfilming. Every effort has been made to ensure the highest quality of reproduction possible.

If pages are missing, contact the university which granted the degree.

Some pages may have indistinct print especially if the original pages were typed with a poor typewriter ribbon or if the university sent us an inferior photocopy.

Reproduction in full or in part of this microform is governed by the Canadian Copyright Act, R.S.C. 1970, c. C-30, and subsequent amendments.

AVIS

La qualité de cette microforme dépend grandement de la qualité de la thèse soumise au microfilmage. Nous avons tout fait pour assurer une qualité supérieure de reproduction.

S'il manque des pages, veuillez communiquer avec l'université qui a conféré le grade.

La qualité d'impression de certaines pages peut laisser à désirer, surtout si les pages originales ont été dactylographiées à l'aide d'un ruban usé ou si l'université nous a fait parvenir une photocopie de qualité inférieure.

La reproduction, même partielle, de cette microforme est soumise à la Loi canadienne sur le droit d'auteur, SRC 1970, c. C-30, et ses amendements subséquents.

Canada

Design Synthesis and Testing of a Capacitive Type Pressure Transducer Using Micro-machining Techniques

Soumitra Chowdhury

A Thesis

in

The Department

of

Mechanical Engineering

Presented in partial fulfillment of the Requirements

for the Degree of Master of Applied Science at

Concordia University

Montreal, Quebec, Canada

November 1993

© Soumitra Chowdhury, 1993

National Library of Canada

Acquisitions and Bibliographic Services Branch

395 Wellington Street
Ottawa, Ontario
K1A 0N4

Bibliothèque nationale du Canada

Direction des acquisitions et des services bibliographiques

395, rue Wellington
Ottawa (Ontario)
K1A 0N4

Your file Votre référence

Our file Notre référence

The author has granted an irrevocable non-exclusive licence allowing the National Library of Canada to reproduce, loan, distribute or sell copies of his/her thesis by any means and in any form or format, making this thesis available to interested persons.

L'auteur a accordé une licence irrévocable et non exclusive permettant à la Bibliothèque nationale du Canada de reproduire, prêter, distribuer ou vendre des copies de sa thèse de quelque manière et sous quelque forme que ce soit pour mettre des exemplaires de cette thèse à la disposition des personnes intéressées.

The author retains ownership of the copyright in his/her thesis. Neither the thesis nor substantial extracts from it may be printed or otherwise reproduced without his/her permission.

L'auteur conserve la propriété du droit d'auteur qui protège sa thèse. Ni la thèse ni des extraits substantiels de celle-ci ne doivent être imprimés ou autrement reproduits sans son autorisation.

ISBN 0-315-90827-0

Canada

Abstract

Design Synthesis and Testing of a Capacitive Type Pressure Transducer using Micro-machining Techniques

Soumitra Chowdhury

IC fabrication technology is being used to fabricate micro-dimensional mechanical devices out of Silicon. Micro-mechanical devices and components such as micro-gears, micro-calipers and micro-valves are being developed by scientists around the world. This technology has ample applications, in fields ranging from aerospace to bio-medical, robotics to information processing. It is especially the field of sensors which holds the maximum application potential as the scope of such devices to revolutionise the industrial scene is enormous.

This thesis describes the design, fabrication using micro-machining techniques and testing of a capacitive type micro pressure sensor. The sensor consists of a silicon membrane bonded to a glass backing plate that has a small cavity. When under pressure, the membrane deflects causing a change in the gap between itself and the cavity bottom. This results in a change in the capacitance of the gap, the change in capacitance being a measure of the pressure that caused the deflection. A simulation of the response of the device is provided.

Several fabrication techniques were tried out before arriving at a satisfactory method. A novel method for the etching of silicon with an anisotropic etchant, potassium hydroxide, was used for making the membrane; anodic bonding was used for the assembly of the sensor.

The pressure sensor was tested to study its performance characteristics. These test results are compared with the simulation results. Based on the experience gained from the fabrication process and the testing, some suggestions for future research are provided.

Acknowledgements

The author expresses his sincere gratitude to the thesis supervisors - Professor R.M.H Cheng and Professor R.B. Bhat for their invaluable guidance and consistent encouragement throughout the course of this research. The author is indebted to Professor J.F. Currie, who has played a very significant role in this endeavour - his invaluable suggestions and ideas have played a significant role in the realization of this device and completion of the project. Thanks are also due to him for making the facilities of the MODFAB group at Ecole Polytechnique available for the work. Mention must also be made of the contributions made by his colleagues Drs. Chetlur Sundaraman and Yacouba Diawara. Special thanks are due to Professor Les Landsberger for his help and guidance at crucial stages, especially in the revision of the thesis. He and Professor Ion Stiharu have both contributed greatly towards bringing this work to a satisfactory end. Suggestions and ideas have also been received from Professors Arthur Yelon and M. Kahrizi, the author wants to convey his sincere thanks to them.

Deep appreciation is conveyed to the staff and friends at the Genie Physique laboratories at Ecole Polytechnique and the Centre for Industrial Control of Concordia University for their help. Special mention is to be made of friends like Gautam Mundkur, Chandrasekhar Rao and Gegi George who have helped at some crucial stages.

Finally, I am grateful to my wife for her constant encouragement through these years of toil.

TABLE OF CONTENTS

	List of Figures	ix
	List of Tables	xi
	Nomenclature	xii
Chapter 1	**Introduction and Literature Survey**	1
1.1	Introduction	1
1.2	Survey of the Field of Micro-machined Sensing Devices	4
	1.2.1 Types of Sensing Devices	4
	1.2.2 Literature Survey of the Field of Sensing Devices	9
1.3	Objectives and Scope of the Thesis	17
Chapter 2	**Capacitive Type Pressure Sensors**	19
2.1	Material of Construction	19
2.2	Capacitive Type Silicon Pressure Sensing Devices	22
2.3	Description of the Pressure Sensor	26
	2.3.1 Etching of Crystalline Silicon	27
	2.3.1.2 Different Etchants for Silicon	27
	2.3.2 Deposition of Metals	36
	2.3.3 Bonding Techniques	39

Chapter 3	**Analytical Design and Simulation of the Sensing Device**	46
3.1	Derivation of the Relation Between Pressure and Capacitance	46
	3.1.1 Behaviour of a Circular Plate Clamped at the Edge Under Uniform Loading	49
	3.1.2 Stress Calculations	55
	3.1.3 Capacitance Calculations	57
3.2	Simulation of Response of Device	60
Chapter 4	**Fabrication of The Capacitive Type Pressure Sensor**	66
4.1	Description of the Pressure Sensor	66
4.2	Description of the Process of Fabrication	75
	4.2.1 The Etching of Silicon	75
	4.2.2 Characterisation of the Etchant	76
	4.2.3 Fabrication of the Membrane	84
4.3	Bonding of the two partss of the Device	91
4.4	Deposition of Aluminium	93
Chapter 5	**Testing of the Device**	94
5.1	Test set-up	96
5.2	Test Procedure	98

5.2.1 Characterisation of Pressure Sensor 98

5.2.2 The Effect of DC Bias on the Capacitance Variation with Change in Pressure 102

5.3 The Effect of Pressure Change on the Capacitance of the Device 103

5.4 The Effect of Glass Thickness and the Membrane Thickness on the Device Capacitance 107

5.4.1 The Effect of Parasitic Capacitance 110

5.4.2 Comparison of the Simulated Results with Experimental Results 115

5.5 Summary of Results 119

Chapter 6 Conclusions and Recommendations for Future Work 120

6.1 Conclusions 120

6.2 Recommendations for Future Work 123

References 125

Appendix Program used for Simulation 130

List of Figures

Figure 2.1	The Operation of a Capacitive Type Pressure Sensing Device Under Uniform Load	21
Figure 2.2	Miller Indices of Some Important Planes of Silicon	28
Figure 2.3	Anisotropic Etching of Silicon	28
Figure 2.4	Field Assisted Glass Silicon sealing	38
Figure 3.1	Detailed Structure of Device	47
Figure 3.2	Behaviour of a Parallel Plate Capacitive type Sensor under Uniform Load	48
Figure 3.3	Equivalent Circuit	58
Figure 3.4	Deflection of Membrane under Uniform Load	61
Figure 3.5	Stress distribution in Membrane under Load	62
Figure 3.6	Capacitance variation under load	63
Figure 4.1	Three devices made	67
Figure 4.2	Fabrication Sequence for Device1	71
Figure 4.3	Fabrication Sequence for Device2	73
Figure 4.4	Fabrication Sequence for Device3	74
Figure 4.5	Teflon cell used for Etching	82
Figure 4.6	Details of Teflon Cell	83
Figure 4.7	DEKTAK printout depth of etch	86
Figure 4.8	DEKTAK printout showing surface finish	86

Figure 4.9 DEKTAK printout for membrane for Device3 87

Figure 4.10 Detailed Structure of Device3 89

Figure 5.1 Detailed Structure of Device 95

Figure 5.2 Details of the Pressure Chamber 96

Figure 5.3 The Test Set-up 97

Figure 5.4 Capacitance variation with frequency 100

Figure 5.5 Capacitance variation with frequency 101

Figure 5.6 Capacitance variation with Pressure 104

Figure 5.7 Capacitance variation with Pressure (full cycle) 105

Figure 5.8 Capacitance variation with Pressure 106

Figure 5.9 Capacitance variation with Pressure (after thinning) 108

Figure 5.10 Capacitance variation with pressure (full cycle) 109

Figure 5.11 Equivalent Circuit with Parasitic Capacitance 111

Figure 5.12 Capacitance variation with Pressure (after thinning) 112

Figure 5.13 Capacitance variation with Pressure (after thinning) 113

Figure 5.14 Capacitance variation with Pressure (after thinning) 114

Figure 5.15 Comparison of Simulated Results with Experimental 115

List of Tables

Table 2.1	Mechanical Properties of Silicon	20
Table 4.1	Details of Wafer used for Membrane Fabrication	75
Table 4.2	Etch Rates for Silicon with KOH	78
Table 4.3	Experimentally Obtained Etch Rates	81
Table 5.1	Rates of change of Capacitance with Pressure	110

Nomenclature

w	Deflection of membrane (micrometers, μm)
P	External Pressure on membrane (MPa, Psia)
D	Flexural rigidity of the membrane (N-m)
E	Young's Modulus (N/m^2)
h	Thickness of membrane (μm)
ν	Poisson's Ratio
r	Radial distance of any point on the membrane from its centre (μm)
a	Radius of membrane (μm)
b	Distance of point of contact of membrane with cavity bottom, when under pressure, from the centre (μm)
δ	Gap between the membrane and cavity bottom (μm)
M_r	Bending moment, radial component (N-m)
M_t	Bending moment, tangential component (N-m)
z	Section modulus (m^4)
σ_r	Stress on the membrane, radial component (N/m^2)
σ_t	Stress on the membrane, tangential component (N/m^2)
ε_0	Vacuum Permittivity (F/cm)
ε_r	Relative Permittivity
C_{air}	Capacitance of air-gap (F, pF)
C_{ins}	Capacitance of insulation (F, pF)
C_{gl}	Capacitance of glass (F, pF)

C_{eq}	Equivalent Capacitance (F, pF)
C_{total}	Total Capacitance (F, pF)
t	Thickness of insulation layer (μm)
R	Radius of area in contact (μm)
Å	Unit of thickness measurement
μm	Unit of thickness measurement
mm	Unit of width measurement
cm	Unit of width measurement

Chapter 1

Introduction and Literature Survey

1.1 Introduction

The field of micro-electronics using IC fabrication technology had miniaturized electronic components to a point where it is possible to pack thousands of components into a single chip. Recently, the use of this technology has made it possible to fabricate mechanical devices along with the electronic circuitry to sense, activate and control. Silicon micro-machining has made it possible for this new breed of sensing devices, the application potential for which are immense. A revolution in the field of physical sensing devices has been brought about, and this field encompasses not just sensing devices but also structures that were previously inconceivable, or unimaginable; these are now being designed and fabricated out of silicon, using techniques that were pioneered in the original silicon revolution. Other devices like actuators, pumps, valves, motors etc. are being made, however, it is the field of sensors which is growing the fastest, possibly because the devices that have already been fashioned have found ready acceptance in the market, replacing existing sensors not only due to their cost advantages but also due to other features like reliability, size, self-testing abilities, and most of all the ability to combine more than one sensing feature in one device.

Silicon sensors have been in the market for quite some time; there have been devices that were based on silicon since the early 1960's. However these were

large in size, especially when compared to the devices that are made with IC fabrication technology today. They had their limitations, mostly due to the fact that the silicon structures that were used were usually built up, ie. epoxy bonding had to be extensively used. Improvements in manufacturing techniques along with advances in the IC industry have brought about a drastic reduction in the size of the structures that one can possibly build without having to resort to bonding. Moreover, epoxy can be altogether done away with since the discovery of anodic bonding techniques. It has come to a point where almost all new sensor applications are silicon-based, because it is the best suited to meet the cost/performance requirements of most new applications. New sensor-based applications are becoming feasible, thus leading to the development of newer and innovative designs, which in turn bring about newer applications.

Initially, silicon based sensors made with IC-technology were expensive, mostly due to the high cost of equipment and R&D that was required. However, due to the advances in the technology itself and also due to the very large increase in demand, the cost has been coming down as it has done for ail electronic components. For example, [1], the price of the MAPS (manifold absolute pressure) sensors, used to measure the pressure in the IC engine for automobiles, has come down from $40 per unit in 1976, when the demand was about 10,000 units, to $15 in 1989 when the demand had jumped to 20 million units. Similarly for the disposable blood pressure transducer, which cost about $40 in 1982, when only

40,000 units were made, the demand had risen to 8 million units in 1989, and the cost came down to $10 per unit.

The development in the silicon-sensor market is thus linked directly with the development in the IC-technology. First, there was the discovery period, which was followed by the commercialisation and the market development, with cost reduction and the expansion of the application. Micro-machining techniques have helped in reducing sizes, by allowing better packaging techniques, thus enabling designers to meet the price/performance ratio. The advent of VLSI also enabled sensor designers to incorporate those techniques to their designs, thus creating devices that not only improved upon the price/performance ratio but also opening up newer applications that could not be thought of previously. Silicon micro-machining is a complex process, especially since it brings about the study of both the mechanical and electrical properties of silicon and it has taken place only in a limited number of places. Silicon is stronger than steel, it does not show mechanical hysteresis, it is very sensitive to stresses and it has the ability to become almost the perfect mechanical material. However, it needs to be seen whether the commonly accepted values of certain physical properties that are valid for the 'macro' sizes, would still continue to hold good in the micro-dimensional range.

After temperature sensors, the largest number of sensors that are being developed are the acceleration sensors, growing at the rate of 27% per year, with sensors for

pressure growing at 20% per year[1]. The automotive market is a big growth area, with a step increase expected in the sector from 1992 onwards with uses like the deployment of air bags, and smart suspensions. It is the pressure sensor market that has the fastest increase in the consumer segment, 75% per year.

1.2 Survey of the field of Micro-machined Sensing Devices

1.2.1 Types of Sensing Devices

There are six basic types into which micro-machined silicon sensing devices may be classified, the method of classification being based on the type of signal the sensor is designed to pick up.

The classification of such sensors is done based on the different measurement environments as follows [1], [2]:

Radiant Signal Domain, where the electromagnetic radio waves, microwaves, infrared waves, visible light waves and waves like ultraviolet, X-rays, gamma rays etc. are used.

Here the variables measured are the light intensity, wavelength, polarization, reflectance, transmittance, etc.

Mechanical Signal Domain, where gravitation and mechanical energy forms are used. Thus the gravitational attraction between the mass and the earth is used for the first form, whereas parameters such as displacement, force, pressure, torque, vacuum, flow, volume, thickness, mass, level, velocity, acceleration, tilt, roughness, etc. are used.

Thermal Signal Domain, relates the kinetic energy of atoms and molecules. Measured variables include temperature, heat, specific heat, entropy, heat flow, etc.

Electrical Signal Domain uses electrostatic fields, current and voltages. Variables that are measured here include the voltage, current, charge, capacitance, inductance, dielectric constant, electric polarization, frequency, pulse duration, etc.

Magnetic Signal Domain, where magnetic fields, current and voltages are dealt with. Field intensity, flux density, moment, magnetisation, permeability, etc. are the variables used.

Chemical Signal Domain makes use of the molecular and atomic energy. Thus the bond energy that holds atoms together in molecules, and the energy that holds the nucleus and the electrons together are used. The variables measured here are the composition and the concentration, reaction rate, toxicity, oxidation-reduction potential, pH, etc.

A more detailed discussion of the various classes of silicon sensors can be made by studying the different 'effects' that could be grouped in each signal domain. For instance, in the **Mechanical signal domain**, it could be the **Deflection** effect, where the external force causes the bending of the silicon structure (in most cases a membrane, ie. a thin plate) which in turn will cause stresses in the plate (or beam), the bending also causes the distance with an adjacent plate to change, which would affect the capacitance. There could be a **Piezoelectric** effect, where the mechanical force could cause surface changes to appear in a crystal which

lacks a centre of symmetry. This piezoelectric effect could be utilised to use the sensor as an actuator too. Then there is the **Acoustoelectric** effect where an electric current can be generated in a crystal by a travelling longitudinal acoustic wave interacting with the conduction electronics. **Triboelectrification**, where rubbing surfaces of suitable materials together will produce positive or negative charges on the surfaces. **Piezoresitivity**, when a mechanical force, by acting on a semiconductor, causes a substantial change in its resistivity, is another phenomenon which may be utilised. Similarly, it could be the **Piezojunction** effect, which is the change in the characteristics of a *pn* junction when the semiconductor in under mechanical stresses. The following phenomenon may also be considered as applicable within the realm of the Mechanical signal domain; **Lateral Photovoltaic effect** is when a junction of two dissimilar materials are locally illuminated by radiant energy giving rise to a lateral voltage along the junction. The **Lateral Photoelectric effect** is the measure of the radiant energy incident on a junction by considering the current division across two contacts at one side of the reverse-biased semiconductor junction. The **Faraday-Henry** induction is the phenomenon when a closed electric circuit is moved in a magnetic field, a current is induced proportional to the embraced flux change per unit time.

The whole concept of sensor technology is being revised, with new possibilities arising. All the effects mentioned above can be discussed in greater detail, and the other signal domains have individual phenomenon which may also be discussed in greater detail. Every effect, within every domain, could be utilised to design a

sensor, and hence the variety and the range of the such devices is tremendous. The effects can also be used in combination, thus increasing the possibilities even further. However, the discussion in this thesis will concentrate on the capacitive type pressure sensing devices. With the wide choice of devices that are becoming available (some are already in the market), the market for silicon sensors seems to be exploding. A survey conducted in 1985 showed that the market then was around $2.5 billion (US). It is predicted that the growth rate in the market for silicon sensors is 20% per year, with the consumer segment growing the fastest.

To summarize, silicon-sensors are widely perceived to be the most widely used sensor type in the future, the growth is expected to be much faster than what it was till now. This is since the technology has reached a certain stage where the ability already exists to manufacture in very large numbers and very high quality standards. The cost is also expected to come down, more so since the volume of the demand is yet to reach its peak. Of all the sensors, the pressure sensors represent the largest established market, with the acceleration sensors representing the largest potential market. The automotive market represents a large potential demand, increasing with time as products become more sophisticated. The medical market also holds enormous possibilities of becoming another high volume consumer, especially with the advent of newer designs with newer uses. The industrial and process control segment, the traditional market for sensors, is yet another field where the growth is expected, perhaps less

spectacular, since silicon-sensors are already in use to a certain extent. Condition monitoring of machinery will involve use of micro-machined sensors, and hence it promises to be a growth area. Apart from the above, the consumer applications of silicon sensors in recreational, personal and home uses will hold the promise of very good growth with the development of newer designs with newer abilities of the sensors. Of these, the HVAC market has the potential for becoming the second largest market, next to the automotive market. The trend in the market is towards a higher level of integration, both electronic and mechanical. The appropriate signal conditioning circuitry, till now done outside the sensor chip, is being integrated into the chip. Compensation for the offset and temperature; signal normalisation are the different areas of work being carried out for electronic integration. However the cost benefits of this exercise is still to be worked out since the increase in levels of integration will mean increase in the masking steps required in the fabrication processing. Mechanical integration on the other hand holds more promise as this would mean direct benefit to the user, like decrease in size, integration of air-damping for accelerators, etc. All this leads us to the conclusion that the sensor is assuming a new role; it is becoming more of an electro-mechanical component instead of merely an instrument as before. By becoming a commodity component its price/performance ratio changes, thus encouraging more research into this field.

1.2.2 Literature Survey of the Field of Sensing Devices

A survey of the field of Micro Electro Mechanical Systems (MEMS) reveals that the fabrication techniques that had been developed for the semiconductor industry are the mainstay for the different devices that are being produced. The survey has shown some interesting usages of existing techniques and in some cases new methods. A brief description of the various types of micro-machined sensing devices is given here.

A micro-machined sensing device of the capacitive type has been described by Rosengren et al. [3]. There are two parallel plates that constitute the device, the upper plate when subjected to the load deflects through a gap and comes in contact with the lower plate. In the process, the capacitance varies and this actual change is measured to estimate the load. The authors have highlighted the concept of the membrane deflecting and coming in contact with the back plate of the capacitor. They show that as the area of contact increases with the deflection, the linearity of the response of the device also increases. To facilitate such contact, they have proposed four designs which show ways in which the edge of the top circular plate can be weakened. This can be done by corrugating the edge or even by using a combination of the corrugation and weakening. The two halves of the sensor are assembled using silicon fusion bonding where the parts are brought together at room temperature and then heated to a temperature of around 1100°C to achieve the bonding. This heating also serves to force out the trapped air inside the cavity. The membrane is then obtained by etching the top wafer

using Potassium Hydroxide after having diffused an etch stop.

A design from NOVASENSOR [1] has a capacitive type absolute pressure sensor where the gap between the two plates of the capacitor is defined by the thickness of a layer of oxide which is grown on one plate. High temperature metals can also be used to make the plate. The oxide layer is grown as an insulating layer between the two plates and this separates the two.

High pressure sensors have also been designed by NOVASENSOR [1] with thick diaphragms. The thickness of the diaphragms actually depend on the pressure range at which the device is to be used. NOVASENSOR uses silicon fusion bonding to bond two wafers so as to form a sealed reference cavity of approximately 10μm in depth. This cavity had been etched out of the wafer by using an anisotropic etchant like potassium hydroxide (KOH) or Ethylene Diamine Pyrocatechol (EDP) or even plasma etching. The top plate is the n type wafer which is then ground and polished to the desired thickness for the pressure range for which it is designed. The typical diameter of a diaphragm is 900μm with a thickness of 200μm and the pressure sensor can read pressures of upto 4000psi. The fact that such sensors are built out of 100% single crystal silicon provides the advantage of very low temperature coefficient of offset.

An ultraminiature solid-state pressure sensor for use in a cardiovascular catheter has been described by Chau et al. [4]. The authors have designed and fabricated a capacitive type pressure sensor that can be mounted on a 0.5mm OD catheter suitable for multi-point pressure measurements from within the coronary artery of

the heart. The pressure transducer consists of a silicon micro-diaphragm measuring 290x550x1.5 μm surrounded by a 12μm thick silicon supporting rim, both defined by a boron etch-stop technique. A hybrid interface circuit chip provides a high level output signal and allows the sensor to be compatible with use on a multisite catheter having only two leads.

A capacitive type tactile imaging array has been described by Chun et al. [5] where an 8x8 element array on 2mm centres have been fabricated. The capacitive transducer uses a diaphragm made by using a boron etch-stop and metal plates isolated from silicon substrate. The off-chip electronics are used which reduce the fabrication sequence to only five non-critical masks. Such arrays are used to provide industrial robots with information on the distribution and amount of contact force (pressure) between the work-piece and the robot gripper.

Various types of micro-machined silicon accelerometers using capacitance variation between elements have been designed. Lynx Reliance et al. [6] had described the design and development of a batch fabricated accelerometer using IC technology. The device was 2x3x0.6mm and weighed 0.02g and was capable of measuring accelerations from 0.001 to 50g over a 100Hz bandwidth. The device is a silicon wafer sandwiched between two glass pieces. The wafer has a very thin silicon cantilevered beam surrounded by a 200μm thick rim. The rim provides a rigid support for one end of the beam, a region for contact pads and mounting surfaces parallel to the plane of the beam. The beam widens into a rectangular paddle at its free end to which is fixed a mass of some dense substance like gold (or silicon). A resistive half-bridge composed of two p-type resistors, one centred

on the top surface of the beam and the other placed in an unstressed region of the rim, and three large p+ contact regions complete the silicon portion of the accelerometer. The beam resistor changes its value with the change in the stress induced in the beam whereas the second resistor is used for temperature compensation. A well etched into the glass covers allows for space for the beam to deflect. The glass covers are hermetically sealed to the thick silicon rim by anodic bonding. The major goal of this device is the miniaturisation of the accelerometer without sacrificing the characteristics in comparison with larger conventional devices. Companies like NOVASENSOR [1] have come out in the market with products similar in design, where a mass called proof mass, usually silicon, is suspended by silicon beams. Ion-implanted piezoresistors on the suspension beams sense the motion of the proof mass produced by the acceleration. The movement of the proof mass may also be detected by change in capacitance. Two wafers used to enclose the proof mass act as capacitor plates and apply a restoring electrostatic force to the mass to null its displacement. In another design the proof mass is suspended from its corners by eight beams (four each on top and bottom surfaces). A switched capacitor specific IC (ASIC) measures the variation in capacitance between the proof mass and the metal electrodes located in wells etched in the upper and lower glass capping wafers. Yet another design has the deflection of the proof mass change the axial load on the resonant micro-structure shifting its frequency of resonance. Thermal expansion drives the micro-structures vibrations which is sensed by a diffused

piezoresistor.

A design by GENERAL MOTORS CORPORATION Research Laboratory (Warren Michigan) has a bulk micro-machined proof mass suspended by four polysilicon micro-bridges whose vibrations are both driven and sensed capacitively. The difference in resonant frequency in a pair of opposing micro-bridges is proportional to the component of acceleration aligned with that pair.

The product that NOVASENSOR [1] is set to introduce is for 'smart' automotive suspensions. Micromachined accelerometers monitor the road condition and the vehicle's speed and load and accordingly adjust the suspension so as to maintain constant firmness and handling. Projected production cost is $10.00 per unit, (non-micro-machined silicon sensors that are available at present cost $600.00 apiece). The projected demand is over one million units per year. The current requirement of Manifold Absolute Pressure (MAP) sensors annually for the automotive industry is about 20 million units. It is expected to increase to 30 million. For the air-bag deployment systems the market is expected to grow from $136.5 million in 1990 to $315 million in 1996. NOVASENSOR is in the process of developing sensors for the air-bag deployment system and the anti-lock braking system. The company at present makes silicon micro-machined sensors of both the pressure and accelerometer types.

A pressure switch developed by IC SENSORS [7] uses thin flexible structures to contact a stiffer substrate under pressure. The silicon diaphragm has a multiplicity of metal paths, as pressure is applied more and more of these paths are forced

against a top cap bonded against the silicon structure, thus forming mechanical contact between the two substrates. Using a metallised top cap the mechanical closure is converted to an electrical closure. For the fabrication, an oxide is first grown on the wafer as an insulator. The metal for the moving contacts is then deposited and patterned lithographically. A glass cap is then patterned to define the gap; the fixed electrode is deposited on the glass. The field oxide on the silicon is then stripped and the two substrates are anodically bonded under a high electric field and at elevated temperatures, thus giving a fully hermetic, absolute pressure cavity. After the bonding, the silicon substrate is patterned and etched on the reverse side to thin the diaphragm area into the desired operating range. The advantages of this device is its small size and high reliability. The switch has a size of 1/10 of the more conventional pressure switches; further constant static pressure does not degrade its performance. The packaging allows it to be directly interfaced to air and pressure lines. Another application for this switch is in tire pressure monitoring. These switches can be fabricated in thousands on a single 4in. wafer, thus opening applications that were previously not possible. Short pressure pulses can be detected by these switches because of their high mechanical resonances (in excess of 500kHz), unlike the more conventional devices. The advantage of this ability lies in the capability to detect instant pressure or acceleration impulses.

A capacitive type silicon pressure sensor described by Matsumoto, et al. [8] consists of a Pyrex glass and a silicon chip. A silicon diaphragm and a CMOS

capacitance to frequency converter are integrated on the same chip. The silicon chip is hermetically sealed by the Pyrex glass using anodic bonding. Piezoresistive devices have high temperature coefficients and suffer from packaging stress, necessitating the use of individual compensation circuits. The advantage of capacitive pressure sensors is that they have higher sensitivity than the piezoresistive sensors apart from not having the problems mentioned above. They have lower temperature drift and lower power consumption than the piezoresistive sensors. The sensor capacitor is formed by a metal electrode on the Pyrex glass and a silicon diaphragm which has a mesa structure at its centre. The capacitance to frequency converter is integrated on the same chip. The sensor size is 2.2mmx1.7mm and 500μm thick. The gap between the silicon diaphragm and the metal electrode is 1.75μm, the diaphragm size being 1.2mmx1.2mm and 15μm thick. The mesa is 740μmx740μm and 45μm thick. The glass cover and the silicon wafer are sealed hermetically by anodic bonding at 390°C and 600V.

Pressure Sensor signals are produced by a wide variety of techniques, including piezoelectric, piezoresistive, bonded strain gauges and LVDTs (linear variable differential transformers). Diffused and implanted piezoresistors and thin-film technologies are however taking the lead. Typically, piezoresistive pressure sensors are constructed using planar IC technology. Impurities such as boron are implanted or diffused into the lattice to form PN junctions. These junctions behave as piezoresistors and sense silicon stresses. Discrete resistors may also be bonded to a diaphragm by using a silicon fusion bonding process. An insulator separates the resistors from the silicon, greatly extending their operating

temperature range. Pressure sensing resistors are connected in a Wheatstone bridge configuration. In constructing the sensor, the resistors can be bonded, implanted or diffused to the silicon diaphragm at precise locations where they experience the highest stresses under externally applied forces. The silicon substrate is etched on the reverse side to produce a small square or rectangular well. The thin membrane remaining after chemical etching or machining is called the diaphragm. The etching is done with KOH, EDP or other etchant, after masking the chip with a protective layer. This diaphragm may be from 5 to 250μm thick on an overall chip size of 2.5x2.5x0.4mm. A single wafer may contain from 500 to 15000 sensors making high production volumes and thus lowering costs. The opposite side of the wafer is processed to form the sensing resistors, the interconnections between them and the bonding pads for the connection between chips and external circuits. One drawback of the etching process is that the backside cavity walls of the etched well slope outwards from the thin diaphragm. Thus in conventional etched pressure sensors chips, overall chip area is substantially larger than would theoretically be required by the active sensing diaphragm area. This drawback is overcome by using silicon fusion bonding. Differential pressure across the diaphragm causes stress that increases the resistance in two resistors and decreases resistance in the other two. The output voltage of the Wheatstone bridge is proportional to the pressure. Resistors are connected in series with the bridge arms that can compensate for the effects of temperature and packaging stresses. Similarly, resistors connected in parallel with

the two arms of the bridge affect the bridge-arm temperature coefficient and provide a means to compensate for the temperature coefficient.

An ultra miniature pressure sensor is fabricated with a shallow depression on the substrate wafer, defining the sensing diaphragm. Next a silicon wafer is fusion bonded over the depression and etched back to form a thin sensing diaphragm. Finally, the piezoresistive bridge resistors and metal interconnects are aligned on the diaphragm and fabricated.

Having outlined the basic concepts and considerations that go into the design of the silicon micro-machined sensing devices, and also discussing a few such devices that have been fabricated by different scientists around the world, the objective and scope of this thesis is discussed.

1.3 Objectives and Scope of the Thesis

The discussion above has shown that there are a number of devices that have been designed and fabricated using micro-machining techniques. The capacitive type pressure sensors are simple in design and have numerous possible applications. Many are already in the market. A feature that should be highlighted is an aspect of the performance which is particularly relevant to our efforts, namely the linearity of the response of the device. Normally, the response of the capacitive type sensor has an apparent non-linearity, this being further influenced by the magnitude of the deflection of the flexing diaphragm. Larger deflections will result in an increase in the nonlinearity, as will deflections in different directions and the

variation of the deflection along the diaphragm.

The objective of this thesis is to design, fabricate and test a micro-machined device that uses the principle of capacitance variation with pressure. The objective will be achieved keeping the following considerations in mind:

1. The linearity of the pressure-capacitance relation is enhanced by allowing the silicon membrane to touch the bottom surface forming the capacitor, and to spread over it as it further deflects.

2. Simple procedure for fabrication, without the use of photo-lithography and the use of a diffused boron etch-stop.

3. Use of material combinations of silicon-glass which would allow the utilization of anodic bonding techniques.

The thesis continues in the next chapter with a discussion of the choice of silicon as the material of construction for micro-machined sensing devices. A description of the principle of capacitive type pressure sensing devices is also given as are outlines of some of the associated processing techniques.

Chapter 2

Capacitive Type Pressure Sensors

This chapter outlines the advantages that silicon presents over other materials as a material of construction for micro-machined sensors. Also, a description of the capacitive type silicon sensing device and the principle of operation are given.

2.1 Material of Construction

Silicon is possibly the most perfect mechanical material available. An added advantage is the vast amount of knowledge that has been acquired in studying silicon, and the enormous advances that have been made in the field of silicon processing. Silicon is the second-most abundantly available material (after oxygen) in the earth's crust, making up 25.7% of the crust by weight. It is present in a wide variety of materials including sand, clay, glass and bone.

The properties of single crystal silicon make it a unique material both electrically and mechanically; knowledge of the mechanical properties of this material have benefitted enormously from the tremendous amount of effort that has gone into the study of the electronic properties of silicon. Single crystal silicon has to be purified and made with special techniques; the electrical properties of the material are precisely controlled by introducing specific amounts of impurities into the melt from which the single crystal is formed. The strength-to-weight ratio of silicon is about five times higher than that of stainless-steel. The hardness of silicon is same as

that of quartz, its thermal conductivity is nearly as high as that of aluminium. It is readily machinable with a variety of chemical and electrochemical etchants as well as chemical/mechanical machining. Moreover, the ease with which the oxides, nitrides and carbides of silicon, i.e silicon dioxide, silicon nitride and silicon carbide, are produced from silicon, imparts it with a tremendous flexibility for fabricating mechanical devices and structures with silicon. These materials, if required, may be used to impart a very tough, hard, corrosion resistant coating, to enhance the performance of the device greatly. The table below gives some of the mechanical properties of silicon [1].

Yield Strength (10^{10}dynes/cm^2)	Young's Modulus (10^{12}dyne/cm^2)	Thermal Expansion (10^{-6}/°C)
7.0	1.9	2.33

Table 2.1: Mechanical Properties of Silicon[1]

Combining the mechanical properties outlined above with the electronic performance of silicon and adding its sensitivity to light, stress, magnetic fields, we get a material whose possible use has a range which is unparalleled by that of any other known material. The one property that needs further discussion is its brittleness; silicon fails when stressed beyond the yield point when it fails by fracturing, unlike steel which deforms plastically. Yet another point that becomes very pertinent to the user of silicon in micro-machines and like mechanical devices,

is the surface finish of silicon. The sharp features that are produced will cause stress concentration, which in turn limits the mechanical strength that these structures can possibly achieve. This fact has got to be considered whenever any structure that is being designed has sharp features. Abrupt corners and edges will have to be avoided by utilising smoothing techniques like wet isotropic etching, plasma etching or thermal oxidation (which smoothen corners).

The role that the insulators play in the type of devices that we are discussing, may

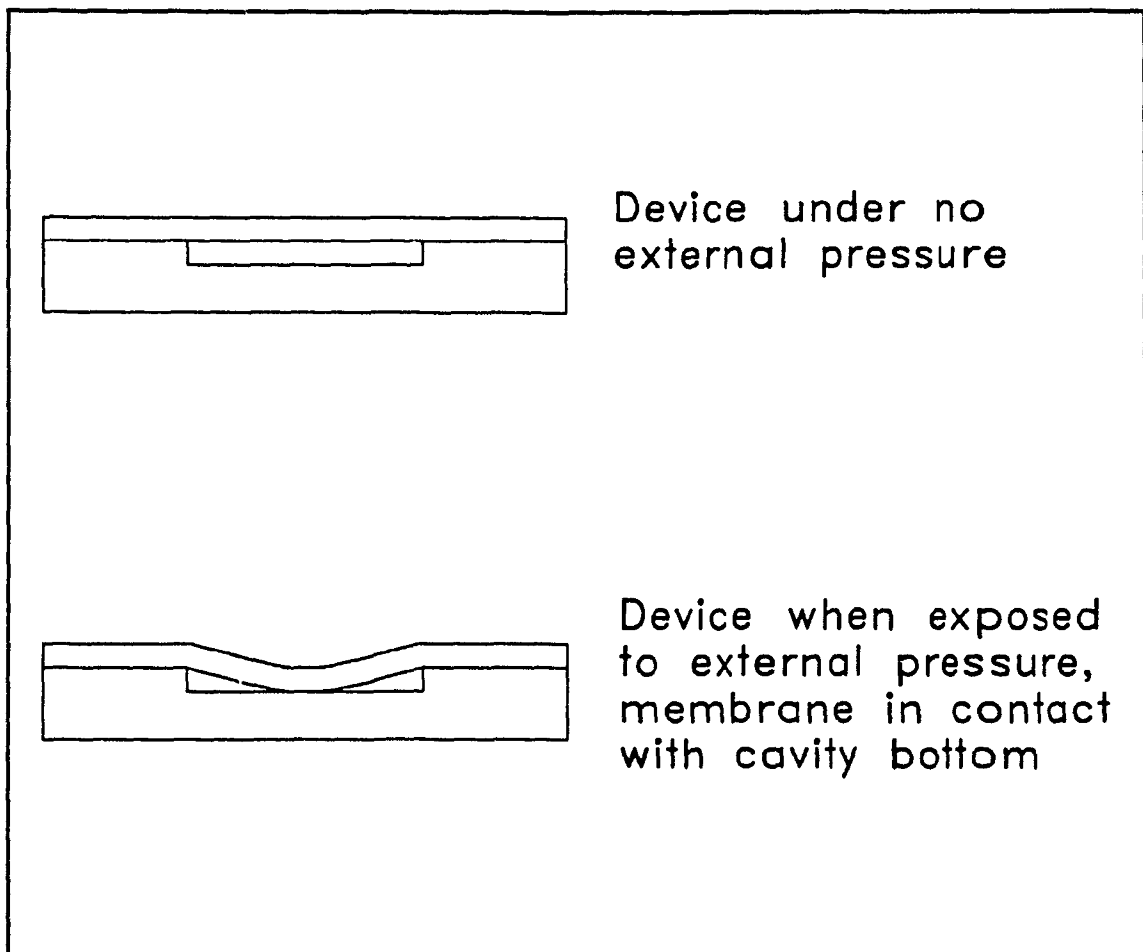

Figure 2.1: The operation of a Capacitive Type Pressure Sensing Device Under Uniform Load

be highlighted. Insulators are used to separate the various elements that are placed together to make these devices. Metal is separated from the silicon to prevent electrical shorting by using a layer of nitride or oxide of silicon. Insulators are also used as masking layers, such that the silicon can be selectively doped or etched into the desired electrical configuration or mechanical structure. The oxide or nitride insulator can also be used to have windows opened in them such that an opening can be made to the silicon lying under the layer. The fact that silicon has two such compounds which fit into the role of insulators, adds to the flexibility of the use of the material. Both are excellent insulators, and lend themselves to be patterned and etched as desired. The ease of forming a layer of either of the compound is a factor that favours the choice of silicon for such devices. The films of SiO_2 are easily controlled in thickness and uniformity. Silicon nitride has to be diffused into the silicon and grown like the oxide. Si_3N_4 is almost impervious to most impurities and all the silicon etchants.

2.2 Capacitive Type Silicon Sensing Devices

The survey of the literature reveals that there are two distinct types of pressure sensors being fabricated out of silicon using micro-machining techniques - the piezo-resistive type and the capacitive type. The design that is being described by this thesis is of the capacitive type. It should be mentioned here that silicon piezoresistive sensing devices are very popular, in fact there are more piezoresistive sensors being manufactured in volume and variety than the capacitive type. The piezoresistive sensors have been in existence in some form

or the other since the early 1950's. The capacitive sensors are however far newer in concept. The two methods have their own substantial advantages but there are no clear advantages of either over the other in a comparison of the two.

The principle of operation of the capacitive type sensing devices is simple. As shown in the figure 2.1, they usually have a diaphragm which bends when under pressure. The capacitance of the device depends upon the distance between the diaphragm and the cavity bottom - the greater the distance between the two, the lesser the capacitance. A layer of insulation, ie. silicon dioxide (SiO_2) or silicon nitride (Si_3N_4) is usually grown between the two parts so as to prevent the shorting of the two halves. The deflection of the top plate or the diaphragm is relative to the applied external pressure. This deflection causes the gap to reduce and thus increase the capacitance, which is therefore directly proportional to the pressure. Thus the capacitive sensor is a deflection sensor. As the deflection of the diaphragm is a measure of the pressure change, the change in capacitance is therefore a measure of the change in pressure. These sensors are relatively insensitive to temperature, the major effect of which is a relatively small change in dimension and a change in the elastic modulus of silicon. The capacitive sensors can be made to be more stable than piezoresistive sensor devices, keeping all other factors equal[1]. However, the use of capacitive pressure sensors may be restricted in moist air conditions, since the dielectric constant of the air will vary, thus upsetting the gauge configuration. Thus media compatibility is a shortcoming of such devices. To date the most successful commercial use of the

capacitive type sensors has been the manufacture of manifold absolute pressure sensors by Ford and Motorola. These are being produced in the millions. Apart from these, the capacitive type of silicon sensors have been used successfully in process control. However the dominance of the piezoresistive type will continue despite the progressive increase in the commercial applications of the capacitive type.

Many configurations can be envisaged for the parallel plate capacitive type pressure sensing device. The backing plate may be of glass or it could also be of silicon, which would eliminate any problems caused by the differing temperature coefficients. The cavity could have a vent connecting it to the outside, thus forming a gauge pressure sensing device. The diaphragm could also be made of a layer SiO_2 or even Si_3N_4 or even metals like tungsten. The diaphragm could be circular or square. The capacitive type pressure sensing devices are quite sensitive, and this sensitivity increases with the fourth power of the radius, decreases with the third power of the thickness of the diaphragm and is inversely proportional to the gap separating the two plates [10]. One problem that plagues the design is that the leads that connect the sensing device to the measuring instrument tend to exhibit stray capacitances which are of the same order as the device capacitance. This makes it necessary to integrate the electronic circuitry with the device to avoid such stray capacitances.

The linearity of the capacitive type pressure sensing device could be improved by having the diaphragm come in contact with the bottom of the reference chamber

or cavity [3]. Considering the bending of the diaphragm under an uniform load, we can say that the initial stage is when the diaphragm does not touch the bottom, i.e the deflection is not as large as the gap separating the two plates. This deflection can be described by the following equation [34] for circular diaphragms

$$w = \frac{P}{64\, D}(a^2 - r^2)^2$$

where

$$D = \frac{E\, h^3}{12\,(1 - \nu^2)}$$

and E is the modulus of elasticity of the material

h is the thickness of the plate

ν is the Poisson's ratio

W is the deflection

D is the flexural rigidity of the plate

The deflection after the contact is established between the two plates is given by the equation

$$w = C_1 + C_2 \log r + C_3\, r^2 + C_4\, r^2 \log r + \frac{p\, r^4}{64\, D}$$

where r is the distance of any point from the centre.

These equations will be dealt with in detail in the next chapter to arrive at relation between the pressure and the capacitance.

The circular diaphragms are very difficult to fabricate using micro-machining techniques as compared to the square diaphragms. This is because the <100> plane on being anisotropically etched will have the upright walls forming with the <111> planes and these will eventually form a square. (Figure 2.2 shows the important crystal planes in single-crystal silicon, also refer to the section 2.3.1.2). However, for the square diaphragms the stress concentrations at the edge cause ruptures at the edge. Another type of diaphragm that is in use is the ring structure [10]. For applications where small pressure differences have to be measured, the ring structure has some advantages. In such a diaphragm the centre part is not etched such that a small ring is obtained. The advantage is that the stresses induced in the diaphragm are due more from bending than stretching, which is a source of the non-linearity. The centre part can be used as one of the capacitive plates.

Having outlined the basic concepts and considerations that go into the design of the pressure sensing capacitive type device, the thesis will next look into the various processes that will be used to fabricate the sensor. It must be noted that this attempt at fabricating the device is being done within the constarints of the equipment available.

2.3 Description of the Processes

The capacitive type sensing device is made out of silicon using micro-machining

techniques. The following discussion is on some of the fabrication techniques and processes that have been used to fabricate the capacitive type pressure sensing device, concentrating only on those that have been actually used in the fabrication of the device. All these processes have been developed for the manufacture of semiconductor devices.

2.3.1 Etching of Crystalline Silicon

There are two types of etching - isotropic and anisotropic. The isotropic etching refers to an etching process which proceeds randomly at a uniform rate in all directions, whereas in the latter, (refer figure 2.3), the etch rate in the vertical direction is much greater than that in the transverse directions. The ratio of the lateral etch (or transverse etch) to the vertical etch defines the degree of isotropy which is influenced by many physical parameters.

2.3.1.2 Different Etchants for Silicon

Silicon belongs to the diamond cubic crystal structure; the crystallographic directions are perpendicular to the crystal planes. The three index planes most commonly used, the <100>, <110> and the <111>, are shown in the figure 2.2.

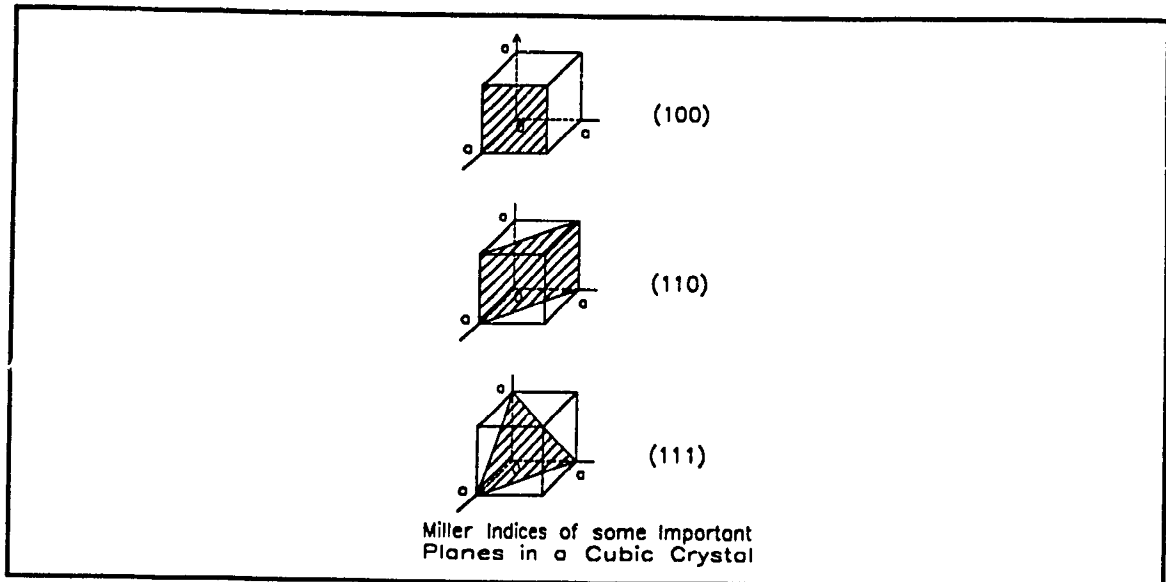

Figure 2.2: Miller Indices of Important Silicon Planes

The etch rates in these directions is affected by the atomic lattice packing density and the available bonds in the crystallographic planes. The <111> plane has avery high packing density, while in the <100> plane the packing density is considerably

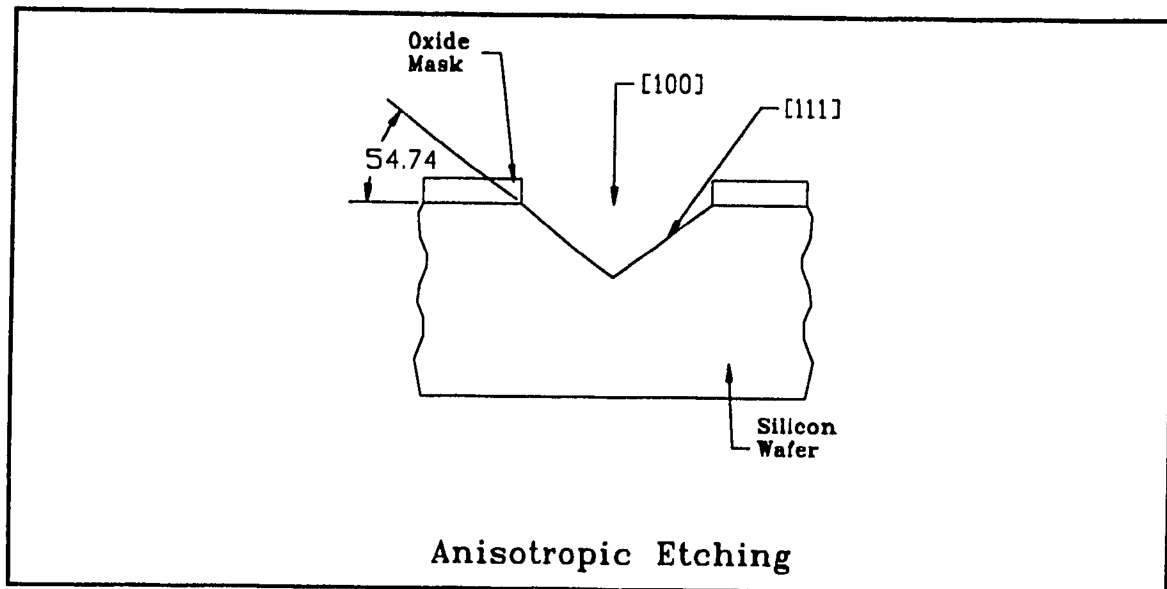

Figure 2.3: Anisotropic Etching of Silicon

lower. The packing density in the <110> plane is very low when compared to the <111> plane, thus the etch rates decrease as we move from the <110> to the <100> and then the <111> directions. Examining the crystal projection of the silicon <100> plane, the surface has four-fold symmetry. That is, the highly packed <111> planes are equidistantly spaced out from the <100> surface plane, at equal angles of 90° to each other. The <111> planes intersect at a steep angle of 54.74°, in the <110> directions. These are at 90° to the <100> surface plane.

Orientation dependant etchants have etch rates that are different in the different directions as mentioned earlier. For example, if we use a solution of potassium hydroxide (KOH), normal propanol and water, the etching in the <100> direction will proceed until the <111> plane is reached by the etch-front, the etch will then stop. The etch rates for <100> and <110> planes are attacked at rates approximately 200 and 400 times faster than the <111> surface in $KOH:H_2O$, according to Kendall [11], who suggests that the <111> surface is oxidised in the solution at a rate much faster than the other crystal surfaces thus passivating the surface against etching. This explanation is consistent with observed etch rates of <111> silicon and silicon dioxide (SiO_2) at temperatures around 85°C. However, it predicts <110>:<111> etch rates much greater than 1000 at 27°C, which is actually found to be around 400 at this temperature. Furthermore, the <110> surface is found to be the fastest oxidising surface rather than the <111> surface as predicted.

Another explanation put forward [35] for the differential etch rates is based on the

observation that the etch rate for silicon with KOH is maximum with the concentration of the KOH at around 22% by weight. The etch rate falls to zero at very high concentrations near the solubility level of KOH. The etch action of the alkaline solution may be described by the equation proposed by Palik *et al* [12].

$$Si + 2OH^- + 2H_2O \Rightarrow Si(OH)_2(O^-)_2 + 2H_2$$

From the above it is seen that the etch products are formed by the reaction which is a product of the OH^- ion and the free water molecule concentration. The former increases continuously with the concentration of the KOH in the H_2C but the latter actually decreases with the increase in the former. Thus the chemical activity of the water is decreased almost to zero as more and more free water molecules are created with the increase in the OH^- concentration. The saturation of the KOH is explained by the absence of any free water molecules to dissolve it, similarly at such high concentrations there are no free water molecules to etch the silicon.

Several ternary liquids have the ability to etch silicon at different rates in the principal crystal directions, as mentioned above. These consist of an oxidant, which oxidises silicon to hydrated silica, and a complexing agent to react with the silica and form a soluble complex ion and water. The latter functions as a catalyst by providing excess $(OH)^-$ ions for the oxidation step. Ethylene-diamine, potassium hydroxide and hydrazine all act as the oxidants, while iso-2-propyl alcohol (IPA) and pyro-catechol are the complexing agents.

The task at hand is to obtain a suitable etchant, which will provide the appropriate etch rates for the silicon and at the same time not affect the in-contact masking material, viz. the silicon dioxide, the etch also has to be done at a rate that provides ease of fabrication and also gives the adequate surface finish.

A study of relevant literature [13], has shown that there are a number of etchants that can be used for the etch that we have to make. For planar etches, i.e the etch rate being comparatively equal in all crystallographic directions, we can use an etch made up of hydrofluoric, nitric and acetic acids (~ 8% : 75% :17%). The etch rate for silicon with this etchant is approximately 5 μm/min. at 25°C. By changing the ratio of the etch rates in the different planar directions, it is possible to alter the overall etch rate. For example, by using 1 part hydrofluoric acid (HF), 15 parts nitric acid (HNO_3) and 15 parts acetic acid (CH_3COOH), the etch rate for ⟨100⟩ direction silicon is greatly reduced at 25°C to 0.20 μm/min., (approximately 1/25 of the planar etch rate). The etch rate for ⟨111⟩ silicon is also very small, ~0.15 μm/min. Yet another combination of the same materials will give us another etchant, this one somewhat orientation-dependant. This will etch ⟨100⟩ silicon at ~1300 Å/min. at 25°C and ⟨111⟩ silicon at 46 Å/min. This etches heavily doped silicon (p^+ or n^+ type greater than 5×10^{18}) much faster (~2.5 μm/min.) than lightly doped p- or n- type silicon. It is therefore dopant concentration-dependant. There are quite a few etchants that can be used to anisotropically etch silicon. These are the orientation dependent etchants like a solution of Potassium Hydroxide in de-ionised water with normal propanol (250 g: 800 g: 200 g). The mask here can be

of photo-resist for shallow etches, whereas for deep etches () 20 μm) the mask can be of a silicon-oxide or nitride film. The former etch is done at 25°C and the deep etch is at 80°C. The etch rate in the ⟨100⟩ direction is approximately one hundred times faster than the rate in the ⟨111⟩ direction, provided the mask is aligned properly. This etch attacks the oxide film at a rate of ~28Å/min.,whereas the nitride is not attacked in any appreciable amount (at 80°C). Yet another composition that has been noted is a mixture of KOH, propyl-alcohol and water (23.4% weight:13.3% weight:63.3% weight). This has an etch rate of 0.6 μm/min. for <100> and $6x10^{-3}$ for <111>. There are other orientation dependant etchants, like ethylenediamine (EDA), pyrocatechol and water (255 cm^3:45g:120 cm^3). This solution will etch ⟨100⟩ silicon at 1.1 μm/min. at 100°C and will etch SiO_2 at ~8Å/min. This etch is also concentration dependant as the etch rate is greatly reduced at a p^+ interface or junction. With hydrazine added to it, this etchant may also be used for ⟨110⟩ direction. The hydrazine will accelerate the etch-rate. In this direction the previous etchant mentioned, i.e KOH and water (~35 % by weight) at 80°C can also be used. The etch rate in the ⟨110⟩ direction is six hundred times faster than in the ⟨111⟩ direction, the mask being aligned at 35.26° off from the ⟨110⟩ flat. The ⟨110⟩ etch rate is 0.8 μm/min. and the SiO_2 rate is ~30 Å/min. Referring to another study by Lee[14] etch rates for etchant with hydrazine-Iso Propyl Alcohol-water mixture will increase with decreasing IPA content and is greatest when the mixture contains no IPA at all. According to that study, the IPA acts not as a complexing agent but as a moderator of the reaction. It shows that for this etchant if the boiling point is plotted against the composition, the boiling point will be highest for near 50% hydrazine, this composition giving the highest

etch rate, even at temperatures as low as 35°C. A deeper look into the rate controlling process involved in this etchant reveals that the hydrazine acts as a complexing agent as well as an oxidant. It suggests that with higher hydrazine concentration the etched surface will become flatter, i.e with fewer hillocks. The mixture of IPA, hydrazine and water is an anisotropic etchant and does not affect oxide masking films. Etch rates of 200 μm/hr. on the <100> oriented slices, at the boiling point of 120°C, have been reported with an equimolar mixture of N_2H_4 with water. This, according to Lee [14], will allow fine geometries to be etched with a high degree of accuracy. Here again the slowest etching plane is the <111> plane.

Anisotropic etching of silicon is possible [15] with yet another etchant. This is pyrocatechol and ethylene diamine with water. Here the etch rate increases in the order <100>, <110>, <111>. Contrast this with the sequence of increase for the KOH-IPA-water etch discussed earlier. Silicon dioxide is used here too as the mask material, noting its ease of deposition and the quality of the film. The thickness of the SiO_2 film usually varies from 0.5 μm to 0.2 μm. By accurately aligning the mask with the crystallographic planes, this etchant gives precise dimensional control over the geometry of the etched structure. The etch rates obtained with 4 m% (mol percent) pyrocatechol, 46.4 m% ethylene diamine and 49.4 m% water can give at a temperature of 118±1°C (i.e near its boiling point), in a non-oxidising atmosphere, are, 50, 30 and 1 μm/hr., for the <100>, <110> and the <111> planes respectively. This is compared to the etch rates for SiO_2 which is 150 Å/hr. and for Si_3N_4 it is 80 Å/hr. This in fact highlights the efficacy of the

choice of SiO_2 for the mask. The point to be noted here is that a high degree of cleanliness is required for the wafers and that native oxide is to be absent from the surface. Even a thin layer of the oxide will greatly reduce the etch rate. Increasing the concentration of the ethylene diamine gives a better surface finish, removing the hillocks. Lee [14] recommends the use of fresh solutions for better results.

An interesting experiment mentioned[14] is the fabrication of thin membranes out of silicon. This makes use of the fact that heavily doped p^+ Si has an etch resistance to this etchant. At impurity concentrations of $N_A \geq 10^{19}$ cm^{-3} the etch rate of silicon in this etchant drops sharply and reaches practically zero at $N_A \geq 7x10^{19}$ cm^{-3}. This gives an ideal tool for the fabrication of the free standing silicon membranes of thickness ranging from 1 μm to 10μm. The case being referred to here had a membrane of 3 μm thickness being fabricated out of <100> silicon. The mask was of SiO_2, thickness being between 1-2 μm; boron was the impurity (using a BBr_3 source), diffusion being done under conditions that resulted in a boron surface concentration close to its solubility limit in silicon. The thickness of the membrane was the area where the concentration of the boron was $N_A \geq 7x10^{19}$ cm^{-3}. The junction depth was at 8 μm. An earlier study had reported on the influence of boron doping on the etch rates for <100> silicon and found a constant etch rate of 50 μm/hr. for the resistivity range between 10^{-1} and 10^2ohm-cm, corresponding to boron concentrations from $2x10^{14}$ cm^{-3} to $5x10^{17}cm^{-3}$. Using a solution of 17ml. ethylene diamine, 8ml. water and 3g pyrocatechol, and a sample with the boron concentration decreasing from $5x10^{20}cm^{-3}$ at the surface, with a background doping

concentration of Arsenic of about $10^{17}cm^{-3}$, the etch time was kept at 10 minutes. The etch resulted in a sharp step on the bevel. The concentration profile was known, as was the distance of the step on the bevel from the un-attacked silicon surface; the critical concentration of electrically active boron atoms in silicon was estimated to about $7x10^{19}cm^{-3}$, corresponding to a resistivity of $1.7x10^{-3}$ohm-cm. Silicon with a higher boron concentration was reported to be completely un-attacked. The etching stopped at a depth of 4.8μm, almost 3μm above the junction, showing that the junction itself had no effect on the etch rate. Thus this etchant could be very appropriate for our use.

The steps involved in the lithography can be outlined as follows:

a) Cleaning the sample with the solvents in the sequence of Trichloroethane, Acetone and Propanol - there are more stringent cleaning processes involving the use of acids.

b) Spin-coating the wafer with a thin film of photo-resist. The thickness varies from 0.1 - 2μm, depending upon the speed and time of the spin. The speed used was 3000rpm and the for the spin was kept at 30 seconds.

c) Formation of the image of the mask on the resist by exposing the resist for the appropriate time through the mask in ultra-violet light.

d) Developing the resist by selectively dissolving away the exposed (for a positive resist) or unexposed (for a negative) regions of the resist film.

e) Baking the resist image by putting the wafer in an oven.

The process of lithography could be of several stages, progressively building up

the desired structure in a sequence that has been worked out in the device design process, this requiring several masks also. There are instances when the process is used to completely remove unwanted parts of the substrate.

2.3.2 Deposition of Metals

The deposition of metals is an integral part in the fabrication process of almost all devices. Usually metal films are formed mainly in areas that are to be used as interconnects, ohmic contacts and rectifying metal-semiconductor contacts. The term physical vapour deposition is used to describe those vacuum deposition techniques like evaporation, sputtering etc., where the metal that is to be deposited is passed into a vapour transport phase by a physical mechanism like evaporation, sublimation or ion bombardment. The deposition techniques in use in the industry range from Evaporation and Chemical Vapour Deposition to Sputtering and Molecular Beam Epitaxy. Physical vapour deposition methods are the most widely used means of depositing thin films and coatings of metallic contacts, dielectrics and semiconductors.

The advantages of the evaporation methods are the high deposition rates and the fact that the source material can be at a relatively simple form. This method is most effective for depositing low-melting point materials, even though it can be used for refractory materials, however such high temperatures make the method more difficult to execute. Aluminium is one of the most commonly used metals for deposition. This is a process of physical deposition where a source is used to

release the vapours of the metal to be deposited. By heating this source under special conditions the rate of release and hence deposition can be estimated. The source could be in the liquid or solid state, depending upon its vapour pressure relative to its melting point. The most common method of heating the source is resistive heating, either the source material itself or a support holding the material. Other methods used for heating are the use of a laser beam, an arc discharge or an electron beam. The evaporation process is carried out at a relatively low pressure, typically 10^{-5} to 10^{-6} Torr, such that the evaporated atoms undergo an essentially collisionless transport to the target substrate. It could be noted here that the mean free path of a gas particle is given by [16] $\lambda = \frac{5}{P_m}$ cm., where λ is mean free path and p_m is the pressure in mTorr. Thus at a pressure of 10^{-4} Torr, λ is of the order of 50cm and about equal to the size of a typical vacuum chamber. Another reason for the use of a low pressure is to avoid oxidising the source material which is being heated and the condensing coating. System cleanliness is required to reduce the pump-down period. The components and samples must be

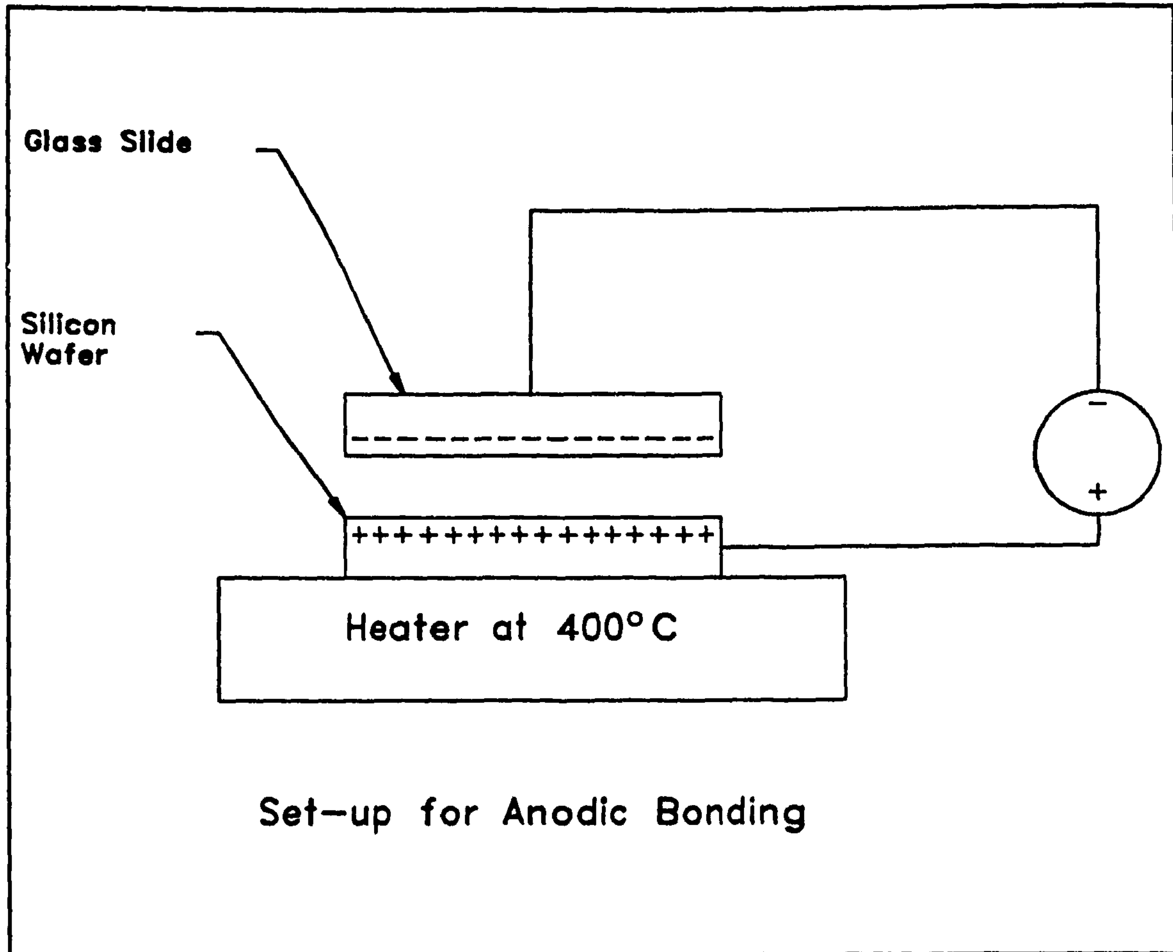

Figure 2.4: Field Assisted Glass-Silicon Bonding

chemically cleaned and then dried, and the interior film buildup must be reduced as far as possible. This is to remove a major source of trapped atmospheric gas. The vacuum system usually is of a two stage pumping configuration - the mechanical pump being the primary pumping followed by the diffusion pumping stage. The required pumping will depend upon the application, the deposition commencing after the chamber pressure reaches an empirically predetermined value. Here high pumping speeds are often equated with cleanliness of the inside surfaces and the components, and also their dryness since the pumping speed

depends upon many factors among which are the chamber volume, the chamber material, the contents of the chamber etc. The substrate are generally unbiased i.e they are electrically at ground potential.

The thickness of the deposited layer is monitored by a thickness indicator which shows the layer thickness in Angstroms. The source is usually in the form of a wire or it could be a foil. The support material of which the heating coil is made is usually of tungsten, molybdenum or tantalum. The resistance heated wire is cut into small pieces and hung from the coil such that the wire is directly heated when the coil has a current passing through it. The deposition rate of any material on the substrate during evaporation process depends upon the material that is being evaporated, the evaporation source type, the position and orientation of the substrate surface.

There are other source types, like the crucible sources, the sublimation sources, baffle type sources, Knudsen Cell sources and electron beam sources, etc. all of which have not been described here in detail.

2.3.3 Bonding Techniques

The fabrication of almost all micro-mechanical systems require the bonding of two silicon wafers or a wafer to a glass plate. The bonding techniques, like other procedures used in micro-machining, had been known for quite some time. The application of such techniques towards the fabrication of devices such as sensors and actuators is relatively recent, the increasing use has in turn brought about a

drastic increase in the types of structures that are now being devised. The following paragraphs outline the fundamental principles for the bonding techniques [35].

The driving force that causes the bonding results from the difference in free energy of two surfaces and the free energy of the bonded surfaces. Physical mechanisms - principally hydrogen bonding forces, but possibly including van der Waals forces - provide the energetic reduction in many circumstances. If the surfaces do not possess the flatness or the surface bonding configurations necessary, externally applied electrostatic forces across the gap in materials can supplement these attachment forces. Annealing can facilitate the formation of permanent chemical bonds between the surfaces, or an externally applied electric field can assist in electrochemical reactions at the interface. These phenomena, either in combination or separately, result in the bonding.

This crucial step is required to form the air-tight cavity for our device, and to mount the devices generally. A wide variety of techniques have been devised to achieve such bonds, and a general overview precedes the detailed discussion on the technique adopted for the fabrication of the sensor, i.e field assisted bonding or anodic bonding. Some of the most important methods that are being used in this field today are [17]:

i) Anodic bonding (Electrostatic Bonding, Field Assisted Glass Bonding)

ii) Silicon to Silicon Anodic Bonding

iii) Silicon to Silicon Fusion Bonding

iv) Fusion Bonding with Low Melting Temperature Glass

v) Field Assisted Fusion Bonding

vi) Eutectic Bonding

vii) Low Temperature Glass Bonding

viii) Anodic Bonding with Low Melting Temperature Glasses

ix) Epoxy bonding

x) Polyamide Bonding

xi) Thermocompression Metallic Bonding

xii) Ultrasonic Welding

xiii) Laser Welding

The field assisted bonding was first reported by Wallis and Pomerantz [18]. Different types of borosilicate glasses, including Pyrex 7740, soda lime 0800, potash soda 0120, aluminosilicate 1720, fused silica were bonded with metals like tantalum, titanium, Caver and semiconductors like silicon, germanium and gallium arsenide. Bonds between glass and thermally grown SiO_2 is also possible. Metals that have a large mismatch of thermal expansion v glass, such as aluminium, nickel, chromium, iron and boron could be bonded in thin-film form. Figure 2.4 outlines the procedure for anodic bonding. For a significant electric field to occur in the gap between the glass and the silicon surfaces, a space charge or polarisation region must develop in the glass. The electric field in the glass causes the drift of the positively charged tramp alkali (usually fluxing ions like Na^+), intermediates or related impurities [19], [20], [21], [22]. Heating the glass to a

temperature around 400°C enhances the mobility of these impurities and also reduces the time required for the space charge to form. These mobile impurities in turn leave behind relatively immobile negatively charged defects thus giving rise to the electrostatic field of the observed polarity. Studies show [22], [23], [24] that this space charge region exists for up to several micrometers into the glass. The electrostatic forces, according to Anthony [25], along with the viscous flow or elastic and inelastic deformation of the interface are sufficient to achieve intimate contact of the surfaces in the presence of some amount of surface roughness. The conclusion is that the thinner the material to be bonded, the lower the force necessary for the required mechanical deformation. The mechanical stresses arising during the bonding and the heat treatment process actually impose several restrictions on the use of this process. The use of thermal-expansion-matching glasses such as alkaline-earth aluminosilicates or lower softening temperature glasses which permit a room temperature bonding, are attempts at minimising the mechanical deformation. The substrate does not need to be a glass, as anodic bonding using sputtered glass systems have been reported by Brooks *et al.*, [26] and Esashi *et al.*[27]. However, the actual chemical reactions that are taking place at the interface to complete the bonding process are not well understood. Some authors [21] and [23] have suggested that some specific electrochemical reactions occurring between the glass and metal-oxides (presumably the native SiO_2 on the Silicon) including the electrochemical dissolution of the high points at the interface and transport of the reactants.

The result is the smooth transition from the glass through the metal oxides to the metal. The role of the temperature is also not very clearly understood. Joule heating at the interface due to the time-decaying current observed for the field assisted bonding has been shown to be unimportant in the glass-Silicon system by Kanda *et al.*[28]. There have been discussions and reports too of achieving bonds without the use of the electric field, since the application of the field poses some difficulty in certain cases. Higher temperatures may have to be resorted to. Esashi *et al.*[27] have mentioned in the paper quoted earlier, field-assisted bonding at room temperatur using lower softening temperature glass. Techniques of bonding without the use of the electric field have also been described. There have been reports of the use of intermediary layers of glass to assist the bonding between two dissimilar or similar materials. A study by Field and Muller [29] has shown the possibilities of using an intermediate layer of borosilicate glass to bond two silicon wafers. The glass was deposited on the silicon wafer by solid-source doping during the oxidation of the Silicon, and the bonding took place at a temperature of 450°C.

A common technique used to bond Silicon to Silicon is called Silicon Fusion Bonding (SFB), also called Atomic Bonding or even Thermal Bonding. This bonding technique allows the bonding of bare silicon wafers to similar wafers or to oxidised silicon wafers. This technique was not used in the fabrication process of the device being described in this thesis and therefore it is not being described in detail. However, as SFB has become a very important process in the field of

micro-devices and sensors, a brief discussion [35] is given. The first description of the technique was made in a patent (U.S Patent No. 3,288,656) issued in 1966 to T. Nakamura of NEC. The process eliminates the use of the electric field to assist in the bonding and relies on achieving intimate contact between the Silicon wafers. The wafers that are to be bonded together should be mirror-grade polished and the surfaces must be made hydrophillic prior to bonding since the key to the bonding is to achieve the proper chemical state of the surface. A study by Grundner and Jacob (1986) [30] shows that the Silicon surface that has been exposed to the oxidising ambient has at least a 1.5nm layer of native SiO_2 on it. The SiO_2 is terminated with a layer of silicon atoms (Iler, 1974) [31]. By proper preparation these silicon atoms can in turn, be terminated in silanol (Si-OH) bonds and such surfaces exhibit hydrophillic behaviour. Such surfaces can be prepared by using an oxidising etches such as (H_2O:H_2O_2:NH_4OH; 5:1:1, followed by H_2O:H_2O_2:HCl, 6:1:1), or the 'piranha etch' of (H_2O_2:H_2SO_4) or hot HNO_3, all of which leave the surface terminated with OH and include some amount of bound water molecules. For the hydrophillic surface, the water will wet the surface, giving a very low contact angle.

The process is in two steps - the first is when the two wafers are placed together at room temperature and weak bonds are established between the two at the interface. The next step is when the wafers are heated to a high temperature when the bonds are strengthened. The temperature to which the heating is carried out is usually around 1100°C, however there have been reports of bonding achieved

at lower temperatures [32]. A more detailed discussion of the silicon fusion bonding is not necessary here as the technique was not applied for this device.

In this chapter, the discussion was on the advantages of using a semi-conductor like Silicon as the material of construction for the sensor. The difference between silicon sensing devices of the capacitive type and those of the piezo-resistive type was discussed briefly. A description of the device that has been fabricated for this project is also given. This was followed by a discussion of some of the processes that have been used to fabricate the capacitive type sensing device. The next chapter will discuss the analytical design and simulation of the capacitive type pressure sensor.

Chapter 3

Analytical Design and Simulation of the Capacitive Type Pressure Sensor

3.1 Derivation of Relation Between Pressure and Capacitance

The capacitive type micro pressure transducer consists of essentially two circular plates separated by a gap. Of the two plates, the lower one is rigid while the upper one is clamped at the edge and is flexible. Thus under a uniformly distributed load the top plate is free to be deflected downwards until it touches the lower plate. The bending is considered to be axi-symmetric. The maximum deflection will be at the centre.

Capacitive type pressure sensors have been designed to operate in the region where the centre of the membrane does not touch the bottom of the cavity but approaches close to it, this is referred to as regime I. However, by further increasing the pressure the membrane will bend till it comes in contact with the cavity bottom. This is regime II. Here the membrane centre is in contact with the cavity bottom and any increase in the pressure causes an increase in the area of contact at the bottom. The area that is in contact has the insulation that is present on its bottom surface as the dielectric whereas, for the portion that is yet to get in contact, the dielectric is a combination of the air gap that separates the two plates and the insulation. thus there is a change in the capacitance with the change inthe pressure. We are interested in this second regime, since experimentation and simulation [3] show that it is here that the relation between the capacitance and

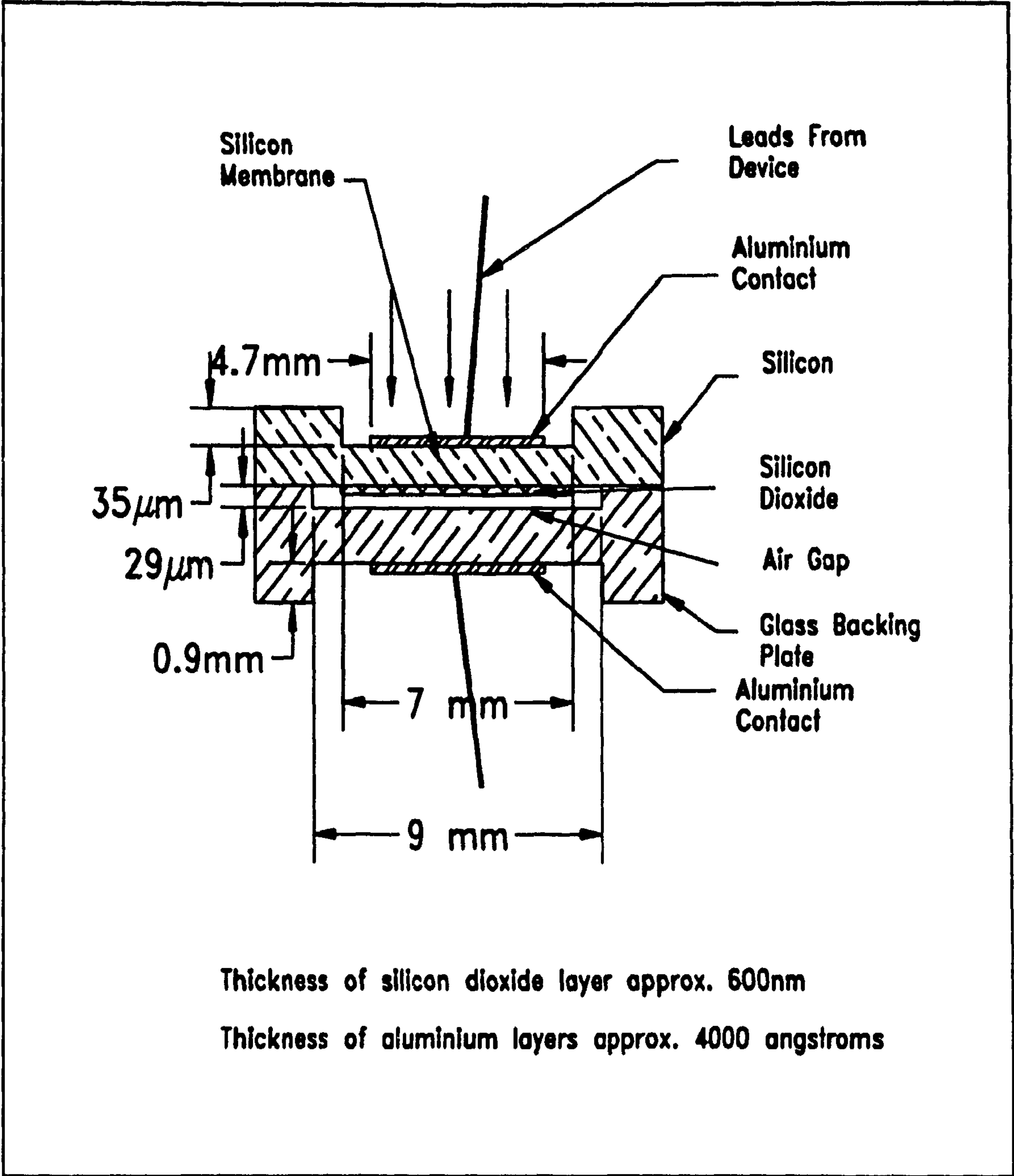

Figure 3.1: Detailed Structure of Device

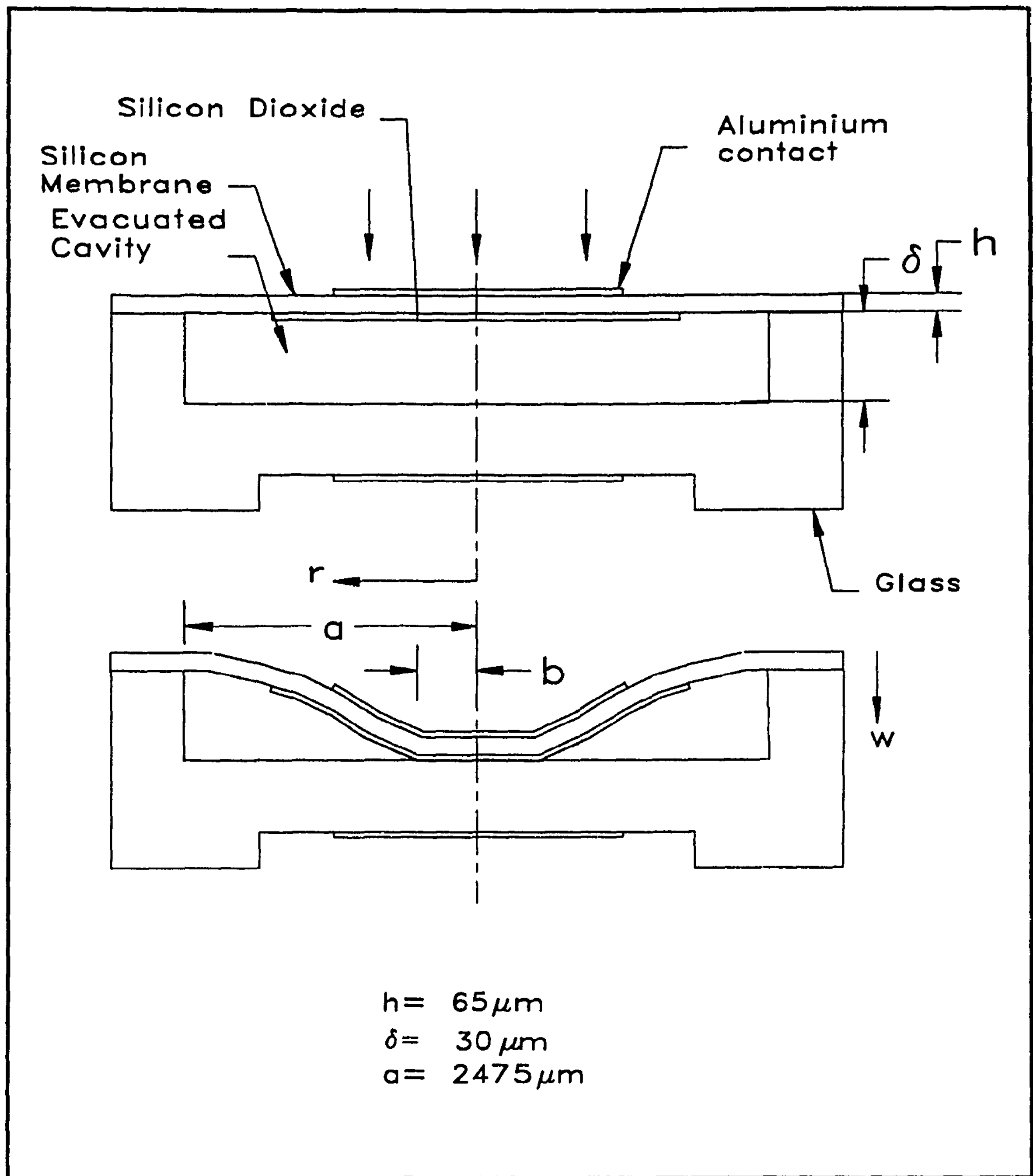

Figure 3.2: Behaviour of Parallel Plate Capacitive Sensor

the pressure is linear. One explanation for this is due to the increased stiffness of the centre of the membrane after contacting the cavity bottom. Another point that we should consider is the limiting pressure, i.e the threshold pressure when the top plate touches the cavity bottom. We are therefore more interested in those pressures that are above this threshold value. The pressure range for which the sensor is to be considered depends on a number of factors, the thickness of the plate that is being used as the sensing element, the gap between the two plates (i.e the distance for the top plate to travel before it touches the cavity bottom), the insulator thickness, the encapsulating temperature and pressure, etc. For example, by lowering the pressure at the time of encapsulation or sealing of the two halves of the sensor, the value of the threshold pressure can be lowered. A similar effect is obtained by sealing the two halves at a high temperature such that some of the air in the cavity is driven out before bonding is accomplished, some of the oxygen is also consumed to form an oxide layer. For our case, the simulation program considers the enclosed reference cavity to be devoid of any atmospheric air. Also, a number of dimensions for the sensor have been taken into consideration, the selection of the actual size and material have been influenced by factors, like ease of fabrication, availability of material, etc.

3.1.1 Behaviour of a Circular Plate Clamped at the Edge Under Uniform Loading

To understand the behaviour of the parallel plate capacitive type sensor, we should

first be in a position to analyze the response of the clamped top plate that is to bend under the uniform load that is to be sensed. The uniformly distributed loading that we consider for this analysis is static and the bending is axi-symmetric. As shown in figure 3.1, the top plate is clamped all along the edge and the bottom plate is at a certain distance from it. The top plate is part of the sensor that is exposed to the fluid whose pressure is to be sensed whereas the bottom plate is rigid. The point to be noted here is that the enclosed cavity that is formed by the two halves of the sensor is evacuated of air.

Referring again to figure 3.2, the deflection at any point at a radial distance r from the centre of the plate is given by [34].

$$w = \frac{P\,r^4}{64\,D} + \frac{c_1\,r^2}{4} + c_2 \log\frac{r}{a} + c_3 \qquad (1)$$

with

$$D = \frac{E\,h^3}{12\,(1 - \nu^2)}$$

where E is modulus of elasticity of the material

h is the thickness of the plate

ν is Poisson's ratio

w is the deflection and

and D is the flexural rigidity of the plate

Upon applying the boundary conditions

$w\big|_{r=0} = \delta$, which is the centre of the membrane

$$\left.\frac{dw}{dr}\right|_{r=0} = 0, \text{ and}$$

$$\left.\frac{dw}{dr}\right|_{r=a} = 0$$

the constants c_1, c_2 and c_3 are obtained as

$$c_1 = -\frac{Pa^2}{8D}, \; c_2 = 0 \text{ and}$$

$$c_3 = \frac{Pa^4}{64D}$$

The maximum deflection at the centre (i.e r=0) is given by

$$w_{max} = \frac{P\,a^4}{64\,D}$$

As explained earlier, the deflection of the plate may be divided into two different regimes, REGIME I and REGIME II, the first being described by the expression (1), where the upper plate bends without touching the lower plate.

The following expression describes the bending in the regime II [34],

$$w = K_1 + K_2 \log r + K_3 r^2 + K_4 r^2 \log r + \frac{p\, r^4}{64\, D} \qquad (2)$$

where r is the distance of any point on the plate from its centre.

The area of contact between the two plates has a radius of b, which will depend upon the following,

> δ the gap between the plates
>
> D the flexural rigidity of the plate material
>
> P the pressure being applied.

The constants of integration K_1, K_2, K_3, K_4 are obtained by applying the boundary conditions for the plate clamped at the edge, given by

$$w = 0 \text{ and } \left.\frac{dw}{dr}\right|_{r=a} = 0 \text{ at } r = a,$$

$$w = \delta \text{ and } \left.\frac{dw}{dr}\right|_{r=b} = 0 \text{ at } r = b, \text{ and}$$

$$M_r = 0 \text{ at } r = b.$$

To make the calculations easier, we can normalise the expression (2) by using the following:

$$\bar{r} = \frac{r}{a}$$

$$\bar{b} = \frac{b}{a}$$

$$\bar{\delta} = \frac{\delta\, D}{P_0\, a^4}$$

$$\bar{w} = \frac{w\, D}{P_0\, a^4}$$

$$\bar{P} = \frac{P}{P_0}\,,$$

where P_0 is the atmospheric pressure. Therefore, we get (2) as

$$\bar{w} = \frac{K_1\, D}{P_0\, a^4} + \frac{K_2\, D}{P_0\, a^4}\left[\log\left(\frac{r}{a}\right) + \log a\right] + \frac{K_3\, D}{P_0\, a^2}\left[\frac{r^2}{a^2}\right]$$

$$+ \frac{K_4\, D}{P_0\, a^2}\left[\frac{r^2}{a^2}\right]\left[\log\left(\frac{r}{a}\right) + \log a\right] + \frac{1}{64}\left[\frac{P}{P_0}\right]\left[\frac{r^4}{a^4}\right]$$

This can be written as

$$\bar{w}(\bar{r}) = C_1 + C_2 \log(\,\bar{r}\,) + C_3\, \bar{r}^{\,2} + C_4\, \bar{r}^{\,2} \log(\,\bar{r}\,) + \frac{\bar{r}^{\,4}\, \bar{P}}{64} \qquad (3)$$

Now, applying the boundary conditions

$$\bar{w}(1) = 0\,, \quad \bar{w}'(1) = 0$$

$$\bar{w}(\bar{b}) = \bar{\delta}\,, \quad \bar{w}'(\bar{b}) = 0$$

and $\overline{M}_r(\overline{b}) = 0$ where $\overline{M}_r = (\overline{w}'' + \frac{\nu}{\overline{r}}\overline{w}')$ we get the constants as

$$C_1 + C_3 = -\frac{\overline{P}}{64} \tag{4}$$

$$C_2 + 2C_3 + C_4 = -\frac{\overline{P}}{16} \tag{5}$$

$$C_1 + C_2 \log\overline{b} + C_3\overline{b}^2 + C_4\overline{b}^2\log\overline{b} = -\frac{\overline{b}^4}{64}(\overline{P}) + \overline{\delta} \tag{6}$$

$$\frac{C_2}{\overline{b}} + 2C_3\overline{b} + C_4\overline{b}(2\log\overline{b} + 1) = -\frac{\overline{b}^3}{16}(\overline{P}) \tag{7}$$

and

$$\frac{C_2(\nu - 1)}{\overline{b}^2} + 2C_3(\nu+1) + C_4(3 + 2\log\overline{b} + 2\nu\log\overline{b} + \nu) = -\overline{P}\frac{\overline{b}^2}{16}(3 + \nu) \tag{8}$$

The values of C_1, C_2, C_3, and C_4 are obtained numerically. A relation between $\overline{P}$ and $\overline{b}$ is therefore established.

This allows us to know the pressure at which the upper plate comes into contact with the bottom plate.

3.1.2 Stress calculations

It is necessary that the stress values are obtained so as to ensure that the stresses, both radial and tangential, do not exceed the permissible limits at any point on the flexing plate.

The following are the expressions for the radial and tangential components of the bending moments at the plate

$$M_r = -D\left(\frac{d^2w}{dr^2} + \frac{\nu}{r}\frac{dw}{dr}\right)$$

$$M_t = -D\left(\frac{1}{r}\frac{dw}{dr} + \nu\frac{d^2w}{dr^2}\right)$$

where M is the moment per unit length.

Let δ be the length of an element in the plate, and if z is the section modulus,

$$z = \frac{\delta h^3}{12}$$

The maximum stress is obtained as

$$\sigma_{max} = \frac{M\,\delta}{z}\left(\frac{h}{2}\right) = \frac{6\ M}{h^2},$$

this occurs at a distance of h/2 from the middle plane.

Substituting for M, the maximum stress is

$$\sigma_{max} = \frac{6}{h^2} D \left(\frac{d^2w}{dr^2} + \frac{\nu}{r}\frac{dw}{dr}\right)$$

Substituting the value of $D = \dfrac{E\,h^3}{12\,(1 - \nu^2)}$, we get

$$\sigma_{r_{max}} = \frac{E\,h}{2\,(1 - \nu^2)} \left[\frac{d^2w}{dr^2} + \frac{\nu}{r}\,\frac{dw}{dr}\right]$$

To normalise this expression, we write

$$\sigma_r = -\frac{E\,h}{2(1 - \nu^2)} \left[\frac{P_0\,a^4}{D\,a^2}\right] \left[\frac{d^2\,\bar{w}}{d\,\bar{r}^2} + \frac{\nu}{r}\,\frac{d\,\bar{w}}{d\,\bar{r}}\right]$$

where

$$\bar{\sigma}_r = \left[\frac{d^2\bar{w}}{d\bar{r}^2} + \frac{\nu}{\bar{r}}\,\frac{d\bar{w}}{d\bar{r}}\right]$$

Similarly

$$\bar{\sigma}_t = \left[\,\frac{1}{\bar{r}}\,\frac{d\bar{w}}{d\bar{r}} + \nu\,\frac{d^2\bar{w}}{d\bar{r}^2}\,\right]$$

$$r = a\,\bar{r}$$

$$\frac{d}{dr} = \frac{1}{a}\frac{d}{d\bar{r}}$$

$$\frac{d^2}{dr^2} = \frac{1}{a^2}\frac{d^2}{d\bar{r}^2}$$

$$\frac{d^2w}{dr^2} + \frac{\nu}{r}\frac{dw}{dr} = \frac{1}{a^2}\left(\frac{d^2w}{d\bar{r}^2} + \frac{\nu}{\bar{r}}\frac{dw}{d\bar{r}}\right)$$

$$\overline{\sigma_r} = \left[\frac{h^2}{6\,P_0\,a^2}\right]\sigma$$

This gives a normalised expression for the stress. To obtain the value of the actual bending and the associated stresses we can multiply by the corresponding normalising factors.

3.1.3 Capacitance Calculations

The device can be considered to be a combination of capacitances, as shown in the figure 3.2. The aim of this section is to obtain an expression for the equivalent capacitance.

The expression for the capacitance is given by $C = 2\pi\varepsilon_0\varepsilon_r\int_{r=0}^{r=a}\frac{rdr}{\delta}$, [38]

where ε_0 is the vacuum permittivity

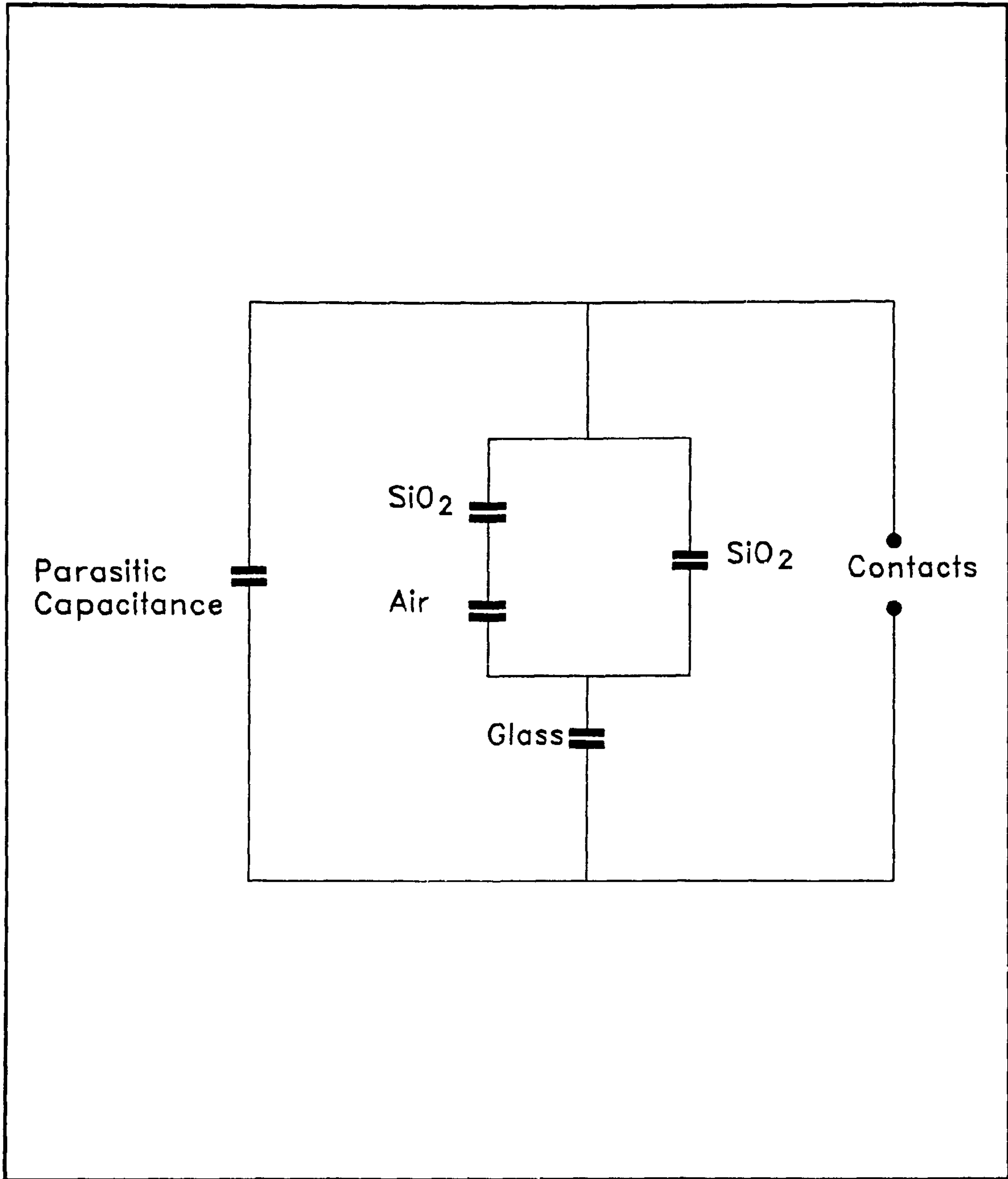

Figure 3.3: Equivalent Circuit

and ε_r, the relative permittivity = $\frac{\varepsilon_{material}}{\varepsilon_0}$

For the area of the plate which is not in contact the capacitance is to be obtained by summing up of two capacitances - one where the air is the dielectric and the other with the insulation as the dielectric. These two capacitances are in series:

- for the air gap $C_{air} = 2\pi\varepsilon_0\varepsilon_{air}\int\frac{rdr}{d - w(r) - t}$

- for the insulation $C_{insulation} = 2\pi\varepsilon_0\varepsilon_r\int\frac{r\,dr}{t} = \frac{\pi\varepsilon_0\varepsilon_r}{t}(a^2 - R^2)$

where **R** is the radius of the area in contact and **t** is the thickness of the insulation layer, r varying from 0 to a.

The effective capacitance of this area is given by

$$C_2 = \frac{C_{insl} \times C_{air}}{C_{insl.} + C_{air}}$$

For the area in contact the capacitance is given by

$$C_1 = 2\pi\varepsilon_0\varepsilon_r\int\frac{rdr}{t} = \frac{\pi\varepsilon_0\varepsilon_r R^2}{t}$$

The capacitances of the two regions C_1 and C_2, that is of the area in contact and the area not in contact, are in parallel. The total effective capacitance is therefore

$$C_{eq} = C_1 + C_2$$

The third dielectric is the glass, whose capacitance C_{gl} is in series with the above equivalent capacitance. Therefore, the total capacitance of the device including that of the glass is

$$C_{total} = \frac{C_{gl} \times C_{eq}}{C_{gl} + C_{eq}}$$

3.2 Simulation Program

In the program listed in the appendix, the first step is to set the physical parameters of the sensor by fixing values for the diameter of the membrane, its thickness, and the gap between the two plates, the thickness of the insulating material. Values for the Young's Modulus the relative permittivity for the insulation, and other such necessary constants are fed in after deciding on the materials for the membrane, the insulation between the two plates, etc. The program first calculates the bending of the clamped plate by using the expression as given in equation (2), the stresses are then obtained and compared with the limiting values for the material being considered. If these stresses exceed the acceptable amount of stress there is a notification of the possibility of failure of the membrane. The next step in the program is the estimation of the capacitance using the formulae discussed above. For a fixed set of physical dimensions for the sensor, we can therefore estimate and hence plot graphically, the values of deflection at different points of the top plate under different loads. Similarly, plots are obtained for the

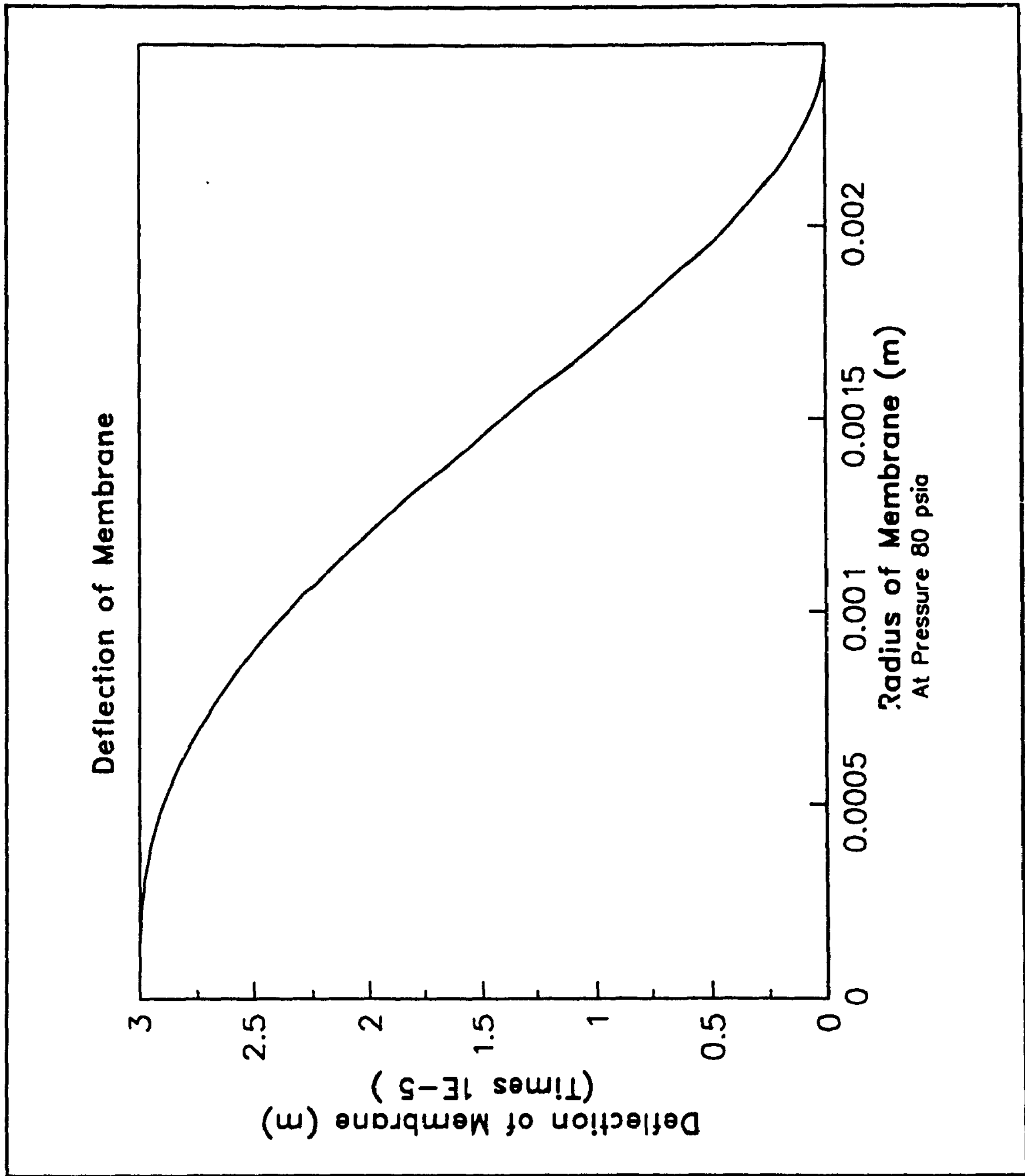

Figure 3.4: Deflection of Membrane under Uniform Load

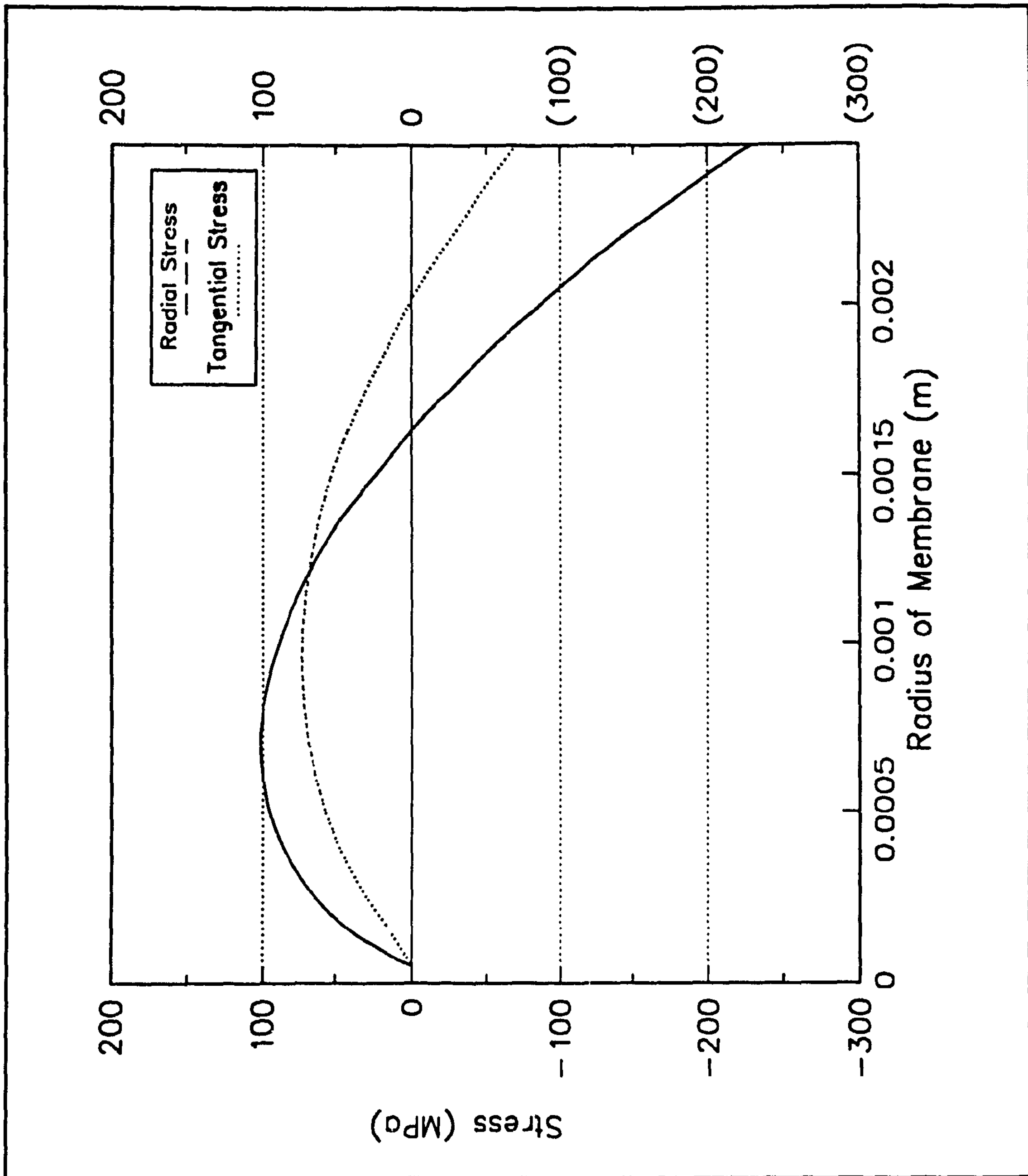

Figure 3.5: Stress Distribution in Membrane under Uniform Load

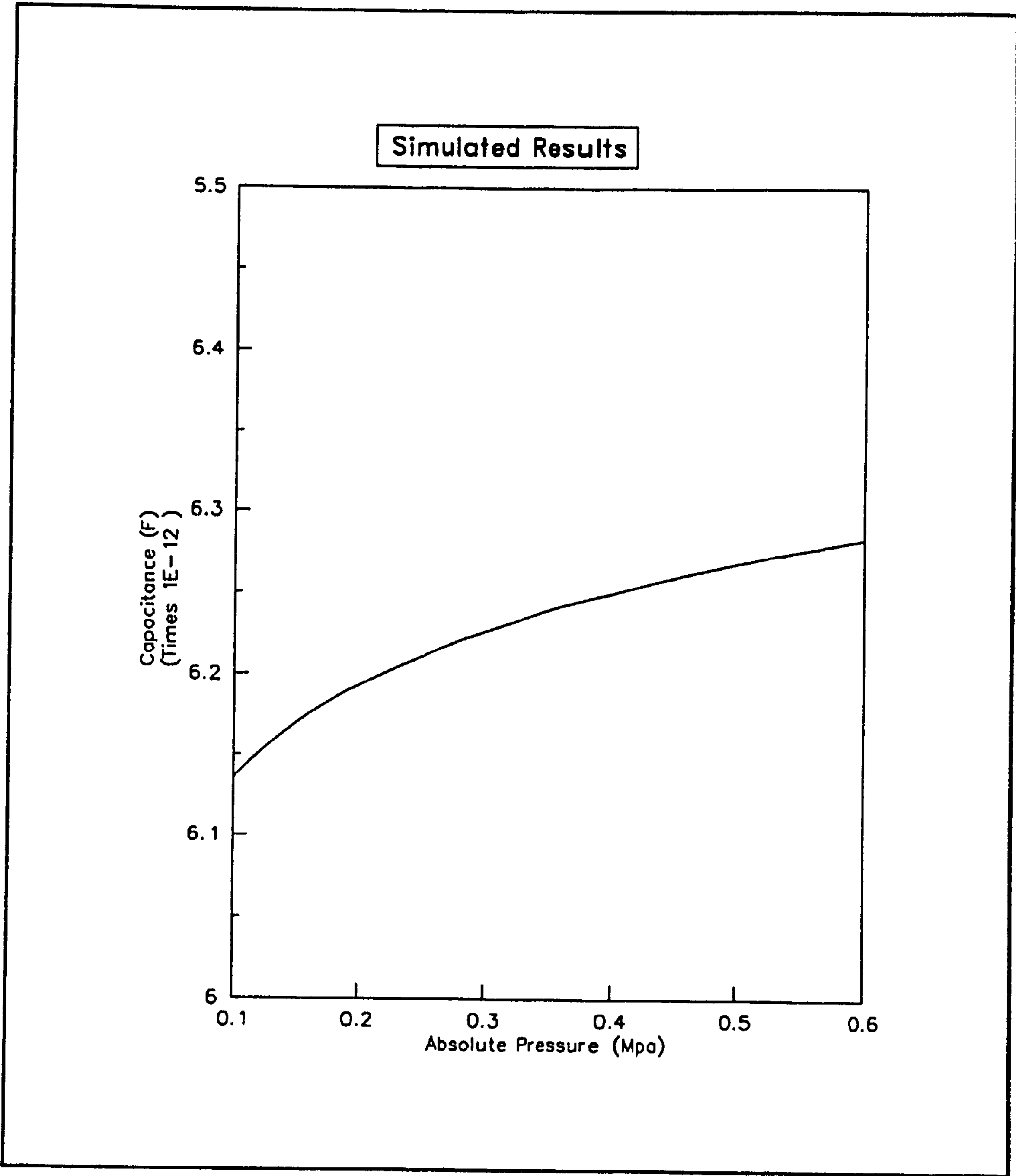

Figure 3.6: Capacitance Variation under Uniform Load

stresses and also the capacitance values against the pressure. These calculations have been done for a large number of combinations for the physical dimensions of the sensor. An examination of the variation of the capacitance with the change of the pressure illustrates the dependence of capacitance on the pressure.

The figures 3.4, 3.5 and 3.6 show the different results obtained for the device of size as detailed:

Membrane diameter = 4950μm

Membrane thickness = 65μm

Gap between the two halves = 30μm

Thickness of the SiO_2 layer = 0.05μm

Glass backing plate thickness = 960μm

The figure 3.4 shows the deflection in the membrane when under a uniform load. The contact takes place with the bottom of the cavity at approximately 15psi. Figure 3.5 shows the stresses induced in the membrane during the bending process. The purpose of this calculation is to ensure that the silicon membrane does not faol during the bending process.

The figure 3.6 shows the variation of the capacitance with the pressure. The pressure variation is shown from 20 psi since the calculation of the capacitance is carried out from the pressure when the top plate comes in contact with the bottom of the cavity. This is because the program that has been written for the simulation of the response starts the capacitance calculation only in regimeII. As this happens at approximately 15psi, the first calculated value for the total

capacitance obtained is for 20psi. With an increase in the contact area, the capacitance of the device changes as shown in figure 3.6. The change is noted to be in two stages. To summarise this chapter, a relation has been established between the pressure variation and the capacitance change. The analysis takes into consideration the stress levels that the silicon membrane can withstand when under different uniform loads. A program has been written which can calculate the pressure at which the membrane comes into contact with the bottom of the cavity, and also the total capacitance of the device under specific pressure values. The next chapter will discuss the fabrication aspects of the sensor.

Chapter 4

Fabrication of The Capacitive Type Silicon Pressure Sensor

This chapter describes the device structure and the different processes used for its fabrication. It discusses the anisotropic etching process for silicon, where different explanations for the anisotropic character of the etch are given. This chapter also describes the actual fabrication steps for the devices that were made. Three different sets of devices were fabricated to accommodate changes in the design that had to be incorporated so as to eliminate certain shortcomings perceived in the earlier device and thus upgrade the performance. The bonding process and the deposition of metals were discussed in detail in the second chapter where there was a discussion on the etching of silicon. In this chapter, after first describing the crystalline structure of silicon, the etching process is discussed in further detail. A comparison of some of the other anisotropic etchants is also given, as is a survey of the published reports on the etching of silicon in KOH. The bonding processes and the deposition are described.

4.1 Description of the Pressure sensor

The sensor has two parts, a sensing diaphragm and a backing plate that is rigid. The diaphragm will bend under pressure and come in contact with the backing plate. The diaphragm and the backing plate together form a sealed cavity which is partially evacuated during the sealing/bonding process. There is a layer of SiO_2

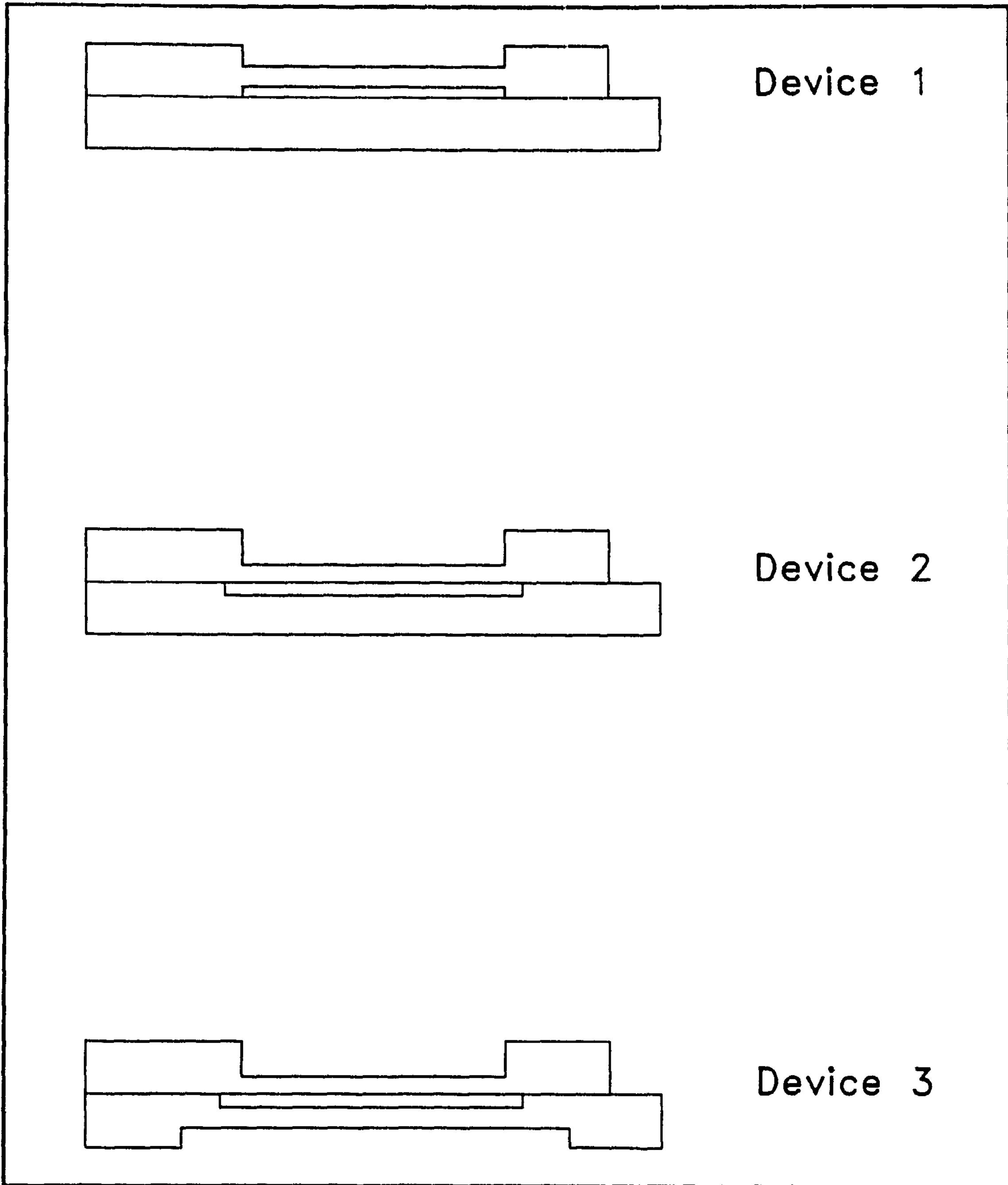

Figure 4.1: Three Devices Fabricated

grown on the bottom surface of the diaphragm, which is primarily used to prevent a short-circuit between the two capacitor plates when they come in contact. The thickness of the diaphragm and the distance through which the diaphragm deflects before contact is made are the two parameters that need to be predetermined as accurately as possible.

The membrane for the sensor is etched out of p type silicon. The etchant used is potassium hydroxide which is an anisotropic etchant for silicon. The actual set-up used for the etching process will be described later. The thickness of the membrane is determined by controlling the etch rate and the time for the etch. Here it should be noted that, the etch rate depends upon the concentration of the potassium hydroxide and also the temperature at which the etch is carried out. The three versions of the device fabricated are described below. The first device had the membrane etched out of the silicon wafer, which was then bonded to the backing plate which was a normal glass slide. The second device had a n type silicon wafer acting as the backing plate. The third device had the backing plate made of a special glass slide, the silicon wafer with the membrane being anodically bonded to the glass. Figure 4.1 shows the three devices.

The need for making the three different devices is discussed here briefly. The first device had the membrane etched out of the silicon wafer while the cavity was also etched from the other side of the same wafer. The etch time for the two etches were different. This wafer was then bonded to the glass backing plate by using a glue. As the cavity thus formed was not evacuated of the air that was trapped

inside, the sensitivity of the device suffered greatly. Therefore the bonding process with the glue could not be utilised. The second version had the membrane etched out of the *p* type 100μm silicon wafer used earlier, while the cavity was etched out of another silicon wafer. The two were bonded by 'welding' them with a layer of aluminium that was deposited on the two mating surfaces. As the glass being used earlier could not be heated to a temperature around 700°C, (the melting point of aluminium being 660°C) the glass had therefore to be replaced by the silicon. The problem faced with this second version was that the aluminium diffused through the layer of silicon dioxide that was grown on the silicon as an insulator. This caused the resistance of the device to break down and thus become unusable as a sensor. The requirement was to have the two halves of the device bonded by a process that involved heating to a fairly high temperature which would drive out the air from the cavity. This was achieved by using anodic bonding, where the silicon wafer was bonded to a glass slide, which had the cavity etched into it, at a temperature of 400°C. This temperature was sufficiently high for the chamber to be evacuated of the air. The special glass used had a thermal coefficient of expansion near that of the silicon since after the bonding was done it had to cool without cracking.

Of the three versions of the device that have been made, the first two did not perform successfully. The problems encountered in these two were overcome in the third whose tests are satisfactory and form the basis of this thesis.

The figures 4.2, 4.3, 4.4 give the process sequence for the three versions of the device. In the first attempt for fabrication of the sensor, i.e for the Device 1, the membrane was obtained by etching both sides of the 100µm wafer, where the first etch determined the gap for the cavity for the capacitor and the second etch actually reduced the thickness of the wafer to the desired value and so obtained the membrane. For the second device, Device 2, there were two wafers used, as shown in the figure, the first of 100µm thickness which was etched to obtain the membrane, and the other of 500µm thickness which was etched to give the desired gap for the cavity. In case of the third and final version i.e Device 3, the membrane is obtained by etching the 100µm thick wafer to the desired depth, but the etching is done after the bonding step because the heating during the bonding process causes the membrane to crack. The glass backing plate is first etched with Hydrofluoric acid (HF) to form the cavity.

After the etches had been done to satisfaction, the deposition of Aluminium was done on the wafer which had the membrane, for the first and second version. This wafer was then bonded to a glass slide in the case of the first version, which also had a layer of Aluminium deposited on it. The two metal layers were the plates of the capacitor. These two were separated by the gap as defined by the first etch. For the final version of the device the deposition was done last, i.e after the etch was done in the silicon wafer. The aluminium conducting layers were deposited on the membrane and the glass in two different processes.

The two parts of the sensor were bonded in the first version of the device by

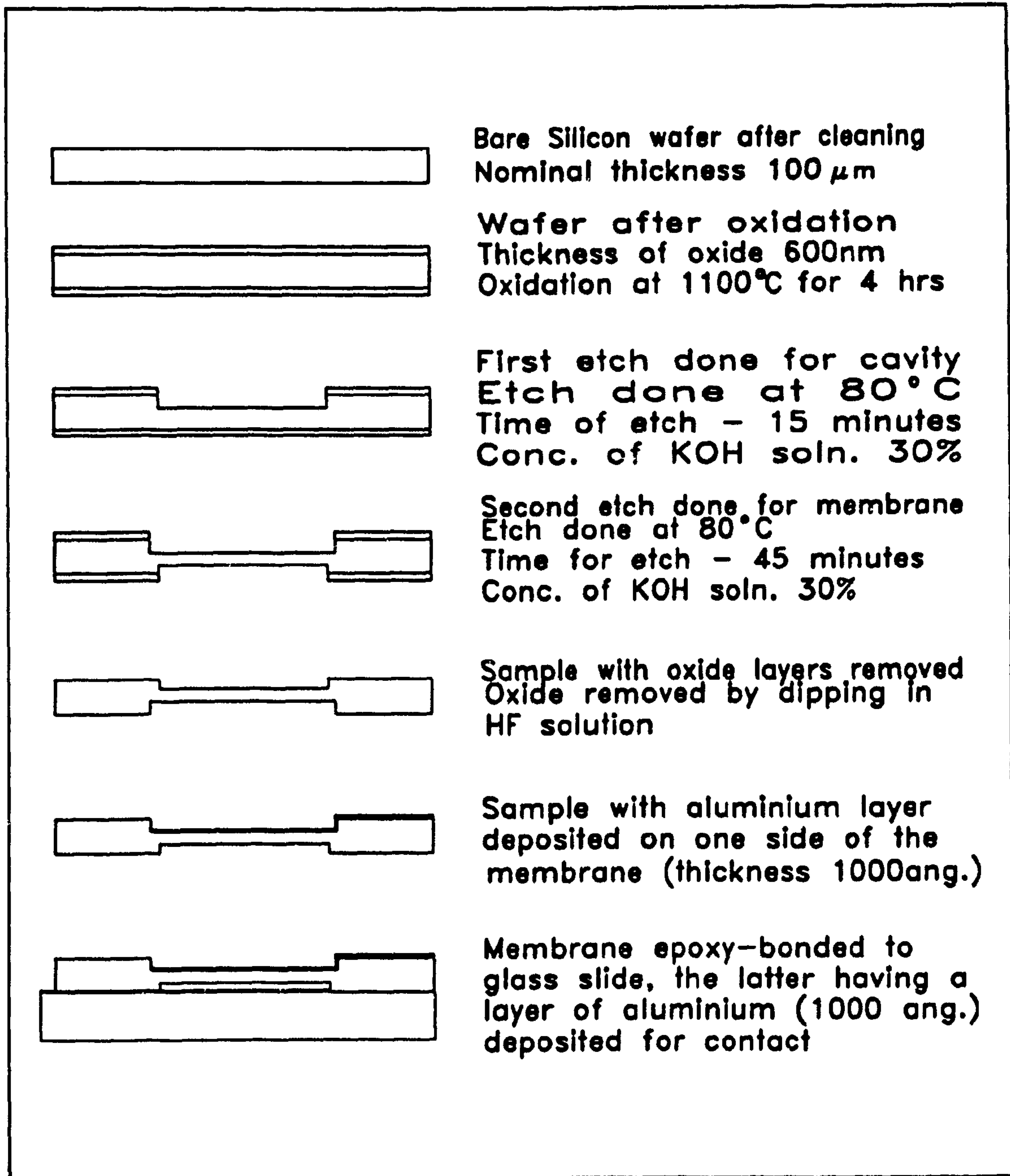

Figure 4.2: Fabrication sequence for Device1

epoxy, in the second by fusion of the adjacent layers of aluminium. The second version of the device was different from the first in that this had aluminium deposited on both sides of the wafer. The aluminium melted when heated above its melting point melted and when the assembly was cooled down the two parts were bonded together. The heating also helped to drive out some of the air inside the cavity, thus causing a small evacuation in the enclosed space. This was how this device was different from the first. Another difference is that in the first device the two halves of the sensor were separated by the layer of epoxy resin which being non-conductive, acted as the insulating layer. This insulation was replaced by a film of Silicon dioxide in the second device. The oxide was grown before the etches were carried out. The layer of oxide also helped to keep the surface of the wafers clean and unaffected by the small amounts of potassium hydroxide that normally leaked out through the o-ring in the teflon cell used for the special etching process to be described later. For the final version the bonding was done by anodic bonding. The process will be described in detail later. The bonding process required the device to be heated which caused the air in the cavity to be driven out. Figures 4.2, 4.3 and 4.4 show the steps followed in the fabrication of the three versions of the device. The allignment of the two halves of the device in the second version was done manually; this being an approximate method proper allignment was ensured by making the membrane diameter slightly larger than the cavity diameter.

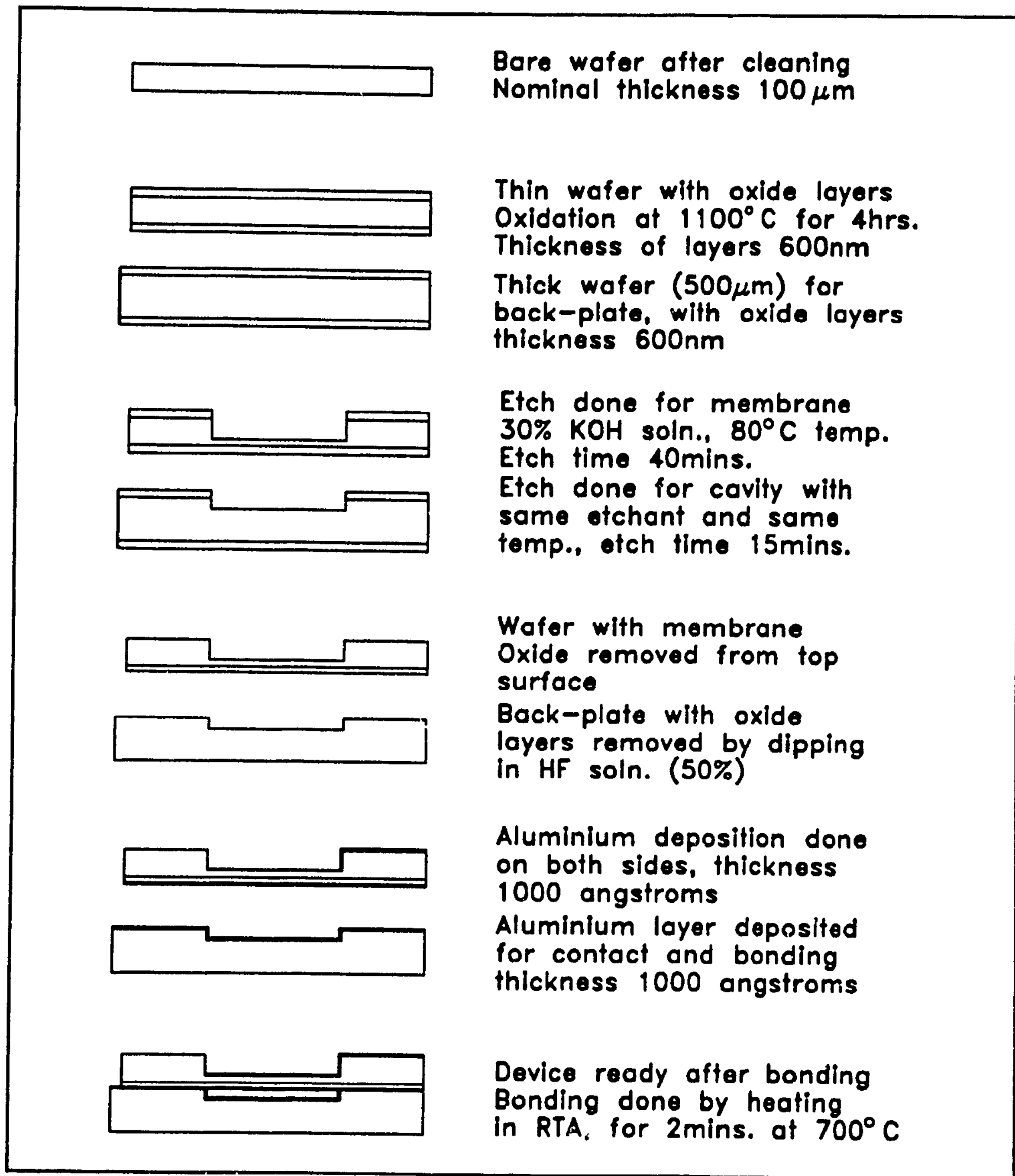

Figure 4.3: Fabrication Sequence for Device2

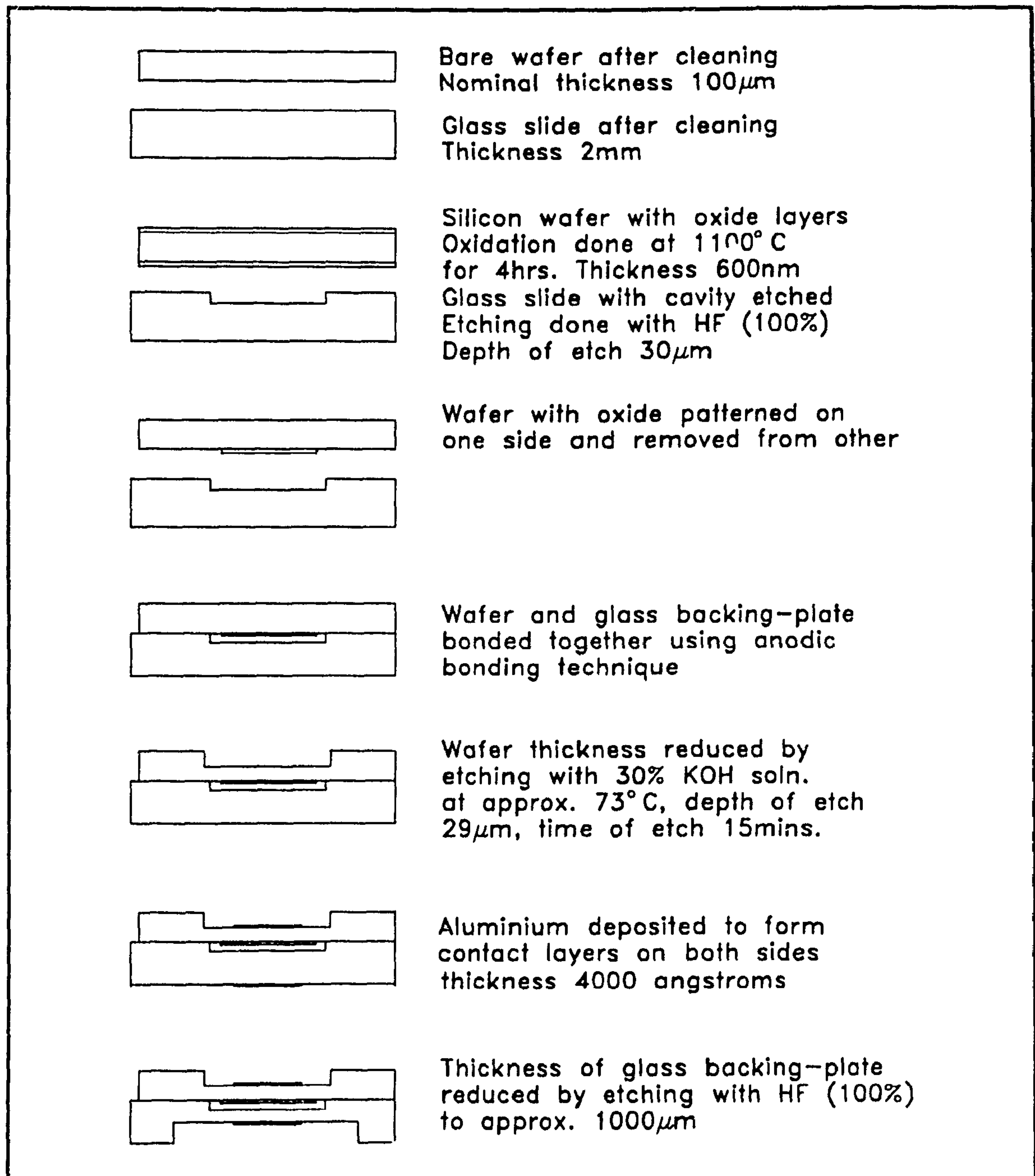

Figure 4.4: Fabrication Sequence for Device 3, the final device

4.2 Description of the Process of Fabrication

One of the major steps in the fabrication of the device was the etching of the silicon wafer to get the membrane. The etchant chosen was an anisotropic etchant - potassium hydroxide (KOH). The bonding of the two halves of the sensor, and deposition of the conductive layers of aluminium were the other major steps. The second device had an oxidation step before the etching was done, and also the bonding process was somewhat different from that of the first device. In case of the third device, the etching of the glass backing plate was done before the bonding and the etching of the silicon wafer to get the membrane was done later. The deposition of the conducting layers of aluminium was done last.

Diameter	4 inches
Type	p
Orientation	<100>
Thickness	2.95 - 4.92 mils.
Resisitivity	1 - 2 ohmcm

Table 4.1: Details of wafer used for membrane fabrication

4.2.1 The etching of Silicon

The etching of the silicon wafer of thickness 100μm was done with potassium hydroxide (KOH) so as to realize the membrane. The details of the wafers used are given in the preceding table. This wafer was used after the characterization of

the etching process was completed. For the characterization of the etchant a p-type silicon wafer was used with a thickness of 500μm. These samples were patterned by using a lithographic process.

The etching of silicon with the KOH is termed as *anisotropic.* Anisotropic etching is defined as that etch which proceeds at a much faster rate in one particular crystal plane than the other planes. Potassium hydroxide (KOH) shows a doping dependence, with the etch rate slowing down considerably as the silicon becomes more than $3x10^{19}$ cm^{-3} *p*-type with boron doping. The rate slows down to a point where such dopant levels are used as effective etch stops. The device that is being described in this thesis was initially designed to be fabricated with such an etch stop. However, due to the difficulties encountered with the diffusion process and the impracticality of implantation of the dopant at required concentrations and depths, it was decided to do without the etch stop. As a result of the above difficulties, the etch rate had to be monitored in a way such that it would be possible to fabricate the membrane without the presence of an etch-stop. This meant that the etch would have to be timed for a specific depth of penetration.

4.2.2 Characterization of the Etchant

The objective is to etch the silicon until we obtain a membrane of the required thickness. The etchant that was chosen was KOH-H_2O solution, this choice was made primarily for its property of anisotropic etching of silicon, easy availability, the

ease of use and also the fact that it attacks the silicon dioxide at a very low rate. The aim was to achieve an etch that goes up to a precise depth, leaving behind the membrane of silicon. To achieve this we could make use of an etch-stop as mentioned earlier, where a dopant that has been diffused into the wafer acted as the stopping layer, bringing the etch rate down to an almost negligible value. This depth of the etch can be therefore pre-determined by diffusion of the impurity up to a calculated depth from the reverse surface of the wafer. The initial attempts at the membrane fabrication had used such an etch-stop, employing an impurity concentration going above the value as mentioned earlier. The dopant diffusion was done at 1100°C for one hour, as a survey of the literature for the dopant had shown that at this temperature a penetration of 3μm would be possible. The dopant used was Boron, in the form of a Borosilicate paint. The mask used had squares and circles of 100μm in diameter. This was patterned on a thermally grown oxide layer by photo-lithography. The impurity, borosilicate, was painted on some samples and spun onto some others, this was done so as to ascertain the most effective method for applying the borosilicate.

The etch rate was studied in detail such that the etching process itself could be controlled. The literature studied [33] had shown the etch rates of the KOH varied as per the temperature and concentration. At a temperature of 80°C, the etch rate was quoted at 79μm/hour for 30% concentration of KOH, and for 20% concentration the rate was 86μm/hour. The table 4.2 gives the rates. The rates of etch for silicon dioxide varies according to the temperature and concentration of the KOH, like that of the silicon.

For example at 20% concentration, the rate is 0.3μm/hr at 80°C while for 42% concentration it is 0.5μm/hr.

% KOH	Temperature °C								
	20	30	40	50	60	70	80	90	100
10	1.49	3.2	6.7	13.3	25.2	46	82	140	233
15	1.56	3.4	7.0	14.0	26.5	49	86	147	245
20	1.57	3.4	7.1	14.0	26.7	49	86	148	246
25	1.53	3.3	6.9	13.6	25.9	47	84	144	239
30	1.44	3.1	6.5	12.8	24.4	45	79	135	225
35	1.32	2.9	5.9	11.8	22.3	41	72	124	206
40	1.17	2.5	5.3	10.5	19.9	36	64	110	184
45	1.01	2.2	4.6	9.0	17.1	31	55	95	158
50	0.84	1.8	3.8	7.5	14.2	26	46	79	131
55	0.66	1.4	3.0	5.9	11.2	21	36	62	104
60	0.50	1.1	2.2	4.4	8.4	15	27	47	78

Table 4.2: Etch Rates in μm/hr. for Silicon with KOH[33]

This meant that with a wafer of thickness 500μm the etch would have to continue for five hours, thus the SiO_2 mask be thick enough. An oxide mask thickness of

well over one micron would be required. The thickness of this oxide mask would be a factor which would have to be taken into consideration when the ultimate process was actually selected. A factor that could have an effect on the etching process was the way in which the etch was being carried out. As the etch progressed the hydrogen that was being generated came out as bubbles which clung to the surface of the sample. These bubbles caused the flow of the etchant along the surface that was being etched to be broken up. Therefore, a method had to be devised for these bubbles to be carried away as soon as they were generated.

The first set of samples to be used for the characterization had been diffused for one hour at 1100°C. This diffusion should have resulted in a penetration depth of 3μm according to the literature provided by the manufacturers of the borosilicate paint. The samples were allowed to float in the etchant during the etch. The results obtained from the etch using 20% potassium hydroxide solution at 80°C were not very satisfactory. The surface of the silicon at the bottom of the etch was very uneven and rough and certain areas had been etched through. The membrane thus obtained was not acceptable for our purpose. The possible explanation for this was that the diffusion process had resulted in a very uneven distribution of the dopant. This was repeated for another set of similar samples, with the same result being obtained.

The next batch of samples had the diffusion done for a longer period of time, at 1250°C for four hours. This should have resulted in a depth of penetration for the impurities of approximately 20μm. Different concentrations of the KOH etchant

were also tried out, 20, 25, 30% and 35%. The temperature was also varied between 70°C to 80°C. The results from all were similar in that the etched surfaces of the membranes obtained were not very smooth.

The results from the numerous etches done as described above gave an insight into a few aspects of the process. Firstly the diffusion process was not proceeding as per the literature from the manufacturer of the borosilica material that was used as the dopant. The depths of penetration achieved were not as predicted. Moreover the distribution of the impurity was not even. It was therefore becoming apparent that this approach would not give very good surfaces for the membrane. The possible alternative to the above diffusion process could be the use of implantation of the dopant. The results from implantation would be very precise, in that the desired concentration could be attained at the correct depth. This should, atleast theoretically, result in a smooth surface for the membrane, moreover the membrane thickness could be more correctly predicted.

The second conclusion that was arrived at was on the etch rates for the silicon with the potassium hydroxide etchant being used. The rates that were published were found to be slightly higher than the ones that were obtained by the above experiments. For example the rate obtained for 30% KOH at 80°C was 66μm/hr whereas the published rates were higher at 79μm/hr.

The table 4.3 compares the etch rates obtained with those published.

	Etch Rates (μm/hr) for Silicon at 80°C	
Concentration of KOH, (g per 100ml. of DI water)	Published	Obtained
35	72	63
30	79	69
25	84	75

Table 4.3: Comparision of experimentally obtained and published etch rates

Another fact that was observed was that it would be impossible to obtain circular shapes for the membrane, especially if the etch was to be carried out for long periods. The etch proceeds along the <100> plane, the sides being defined by the <111> planes, this results in the circles being converted to straight-edged shapes within about 45 - 50 minutes of the start of the etch. These ultimately become squares within two hours of etching. Thus the etch time had to be limited to a maximum of one hour if circular membranes of 100μm in diameter, were to be obtained. An experiment was carried out where the diameter of the etched area was increased to 1mm, 2mm and then 4mm. The etches showed that there was a change in the shape from the circular towards square but the change took place much later, more so in the largest diameter. Thus, it became apparent that the etch could not be carried out for such long periods of time, and that the size of the membrane would have to be much larger, preferably in the region of a few

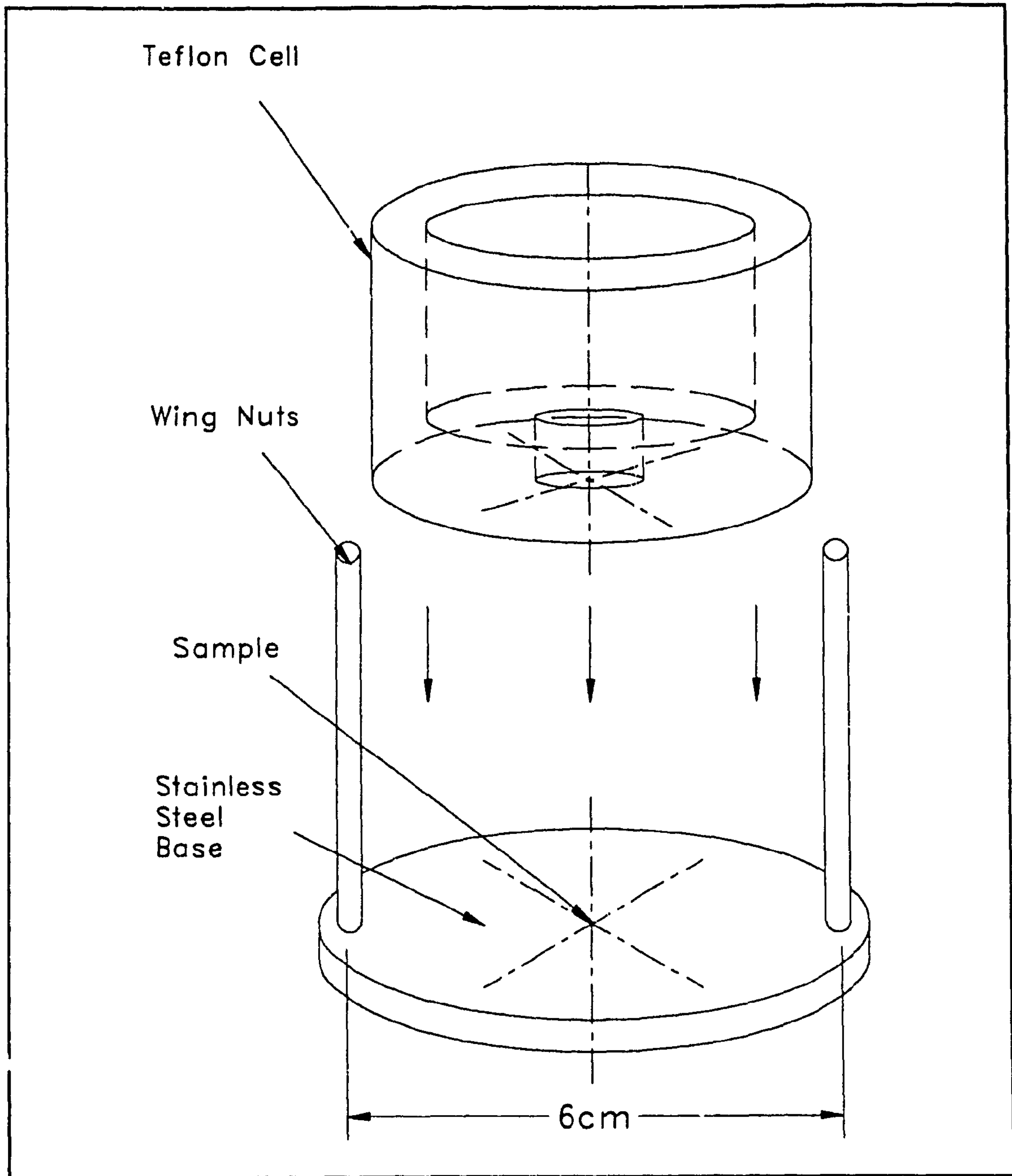

Figure 4.5: Teflon Cell used for Etching

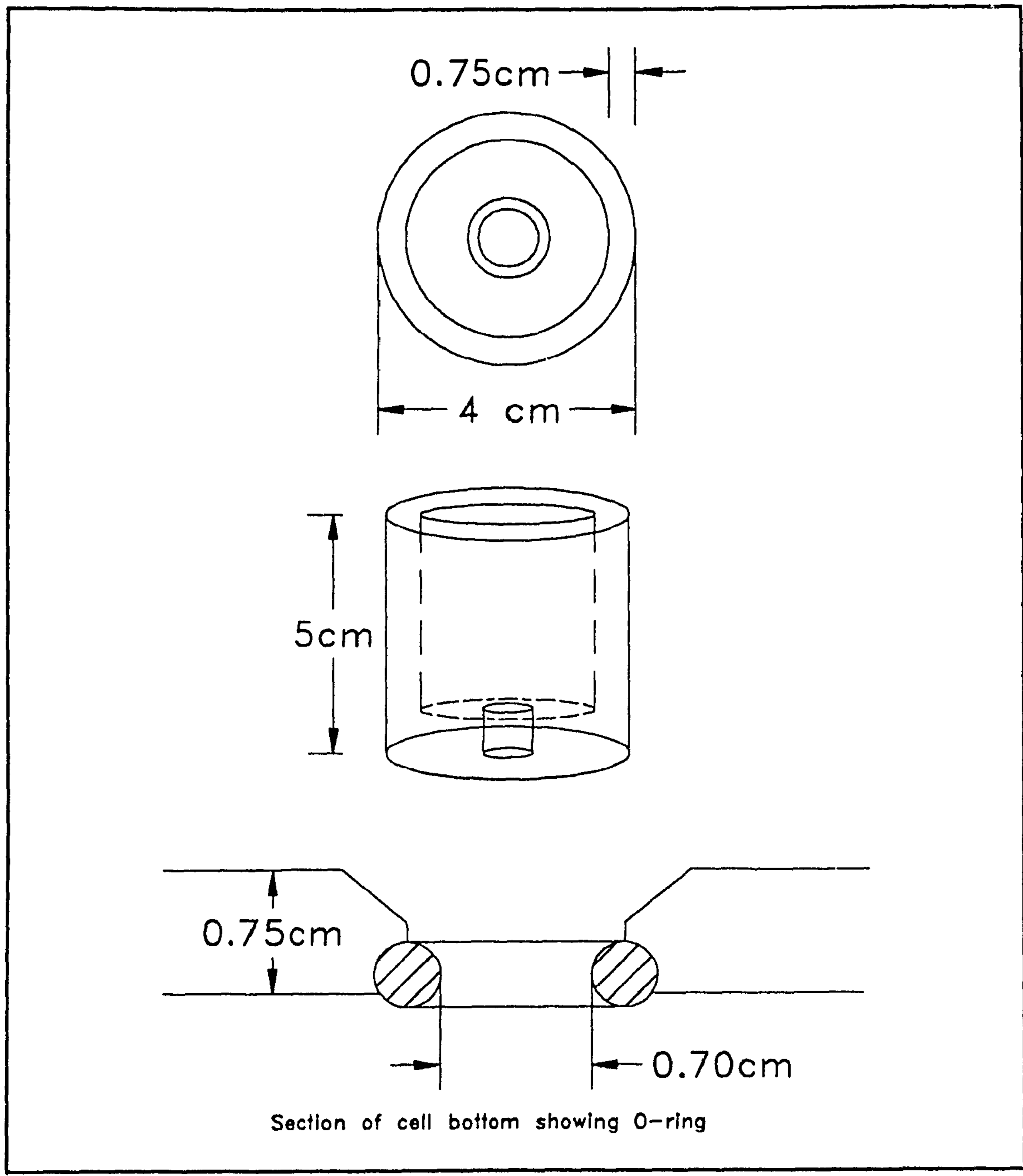

Figure 4.6: Details of Teflon Cell

millimetres.

4.2.3 Fabrication of the Membrane

To eliminate some of the problems described in the previous section, it was decided to use a thinner wafer for the fabrication of the membrane. This would reduce the time required for the etch. A novel method was devised for the etch itself. The etch was carried out in a cell made up of teflon. The figure 4.5 shows the teflon cell with the stainless-steel base. The teflon cell was made from a piece of partially hollowed out teflon bar, approximately two inches in diameter. The cavity that was made had a small hole drilled at its bottom, the diameter of this hole being the desired diameter of the membrane. This cell had to be placed on the wafer, with the cavity filled with potassium hydroxide. The etchant was prevented from leaking out of the cavity by means of an O-ring that was pressed onto the wafer when the cell was tightened down by means of an arrangement of screws on the two upright rods on either side of the cell. The arrangement, once set and filled with the etchant, could be placed in a bath whose temperature could be set at the desired level. The screws which hold down the cell are not shown in the figure. The advantage of this method was that it eliminated the problems faced earlier. Since the teflon was acting as the mask, the need for photo-lithography was eliminated altogether and there was no requirement for lengthy oxidation processes, thus reducing the processing time greatly. Also, since the sample was being held down by the cell, removal of the bubbles generated during the etch

process would be possible by directing a stream of etchant at the surface of the area being etched, which would cause the bubbles to be swept away. However, there were limitations on the minimum sizes for the holes in the cavity bottom, that would restrict the minimum size of the devices that could be made with this arrangement. As discussed earlier, the sizes that were experimented with earlier had been fairly large, as much as 4mm in diameter. With this new cell, the holes that could be used for the etch were restricted by the size of the O-ring; the first few cells had holes of the sizes - 5mm, 7mm, 12mm, and 37mm.

The experiments carried out with this teflon cell were very satisfactory. The etched surface was found to be very smooth, almost mirror like to the naked eye. Asthe diameter of the membranes being etched were large, the change in shape of the circle to the square was not observed. The etchant concentration was kept at 30% and the temperature for the bath at 80°C. Since the etchant was contained inside the teflon cell, the temperature at which the etch was carried out was less than that of the bath by several degrees. Thus, the temperature of the water bath had to be higher than the temperature of the etchant in the cell. These experiments were being carried out with wafers whose thickness was nominally 100μm. This allowed the time for the etch to be reduced drastically. Therefore, by carefully controlling the temperature and the time of the etch, the use of a stopping layer for the fabrication of the membrane could be eliminated altogether. This method, with some further modifications to the cell and to the process, holds the promise of better results.

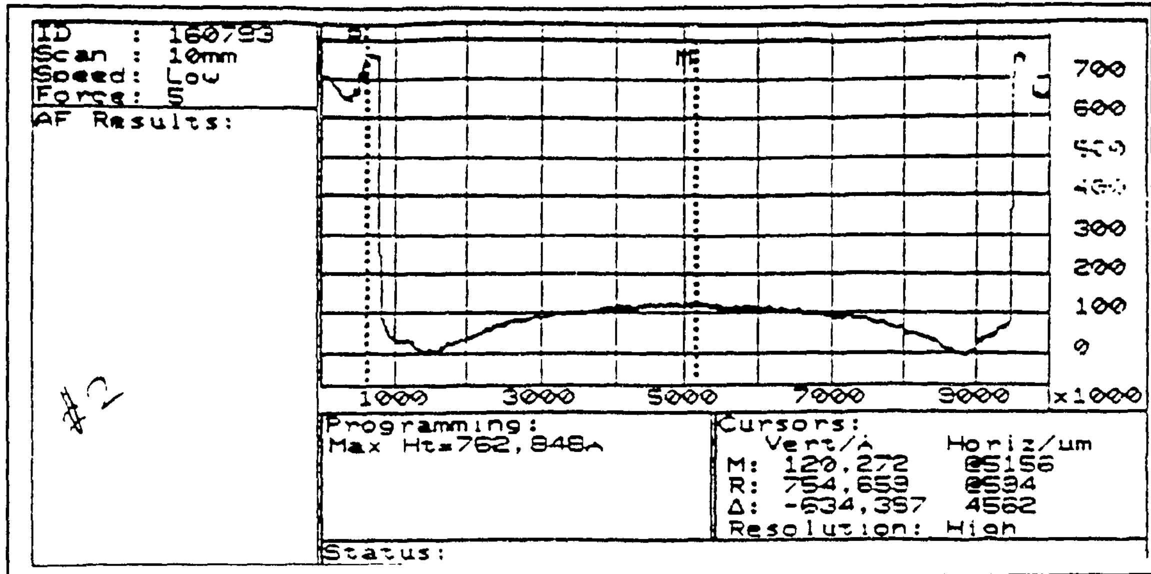

Figure 4.7: DEKTAK printout showing depth of etch

The above method was utilised to fabricate the membranes for the different versions of the sensor that were made. As mentioned earlier, for the first device, the etch was done on the 100μm thick wafer from two sides, one etch to define the

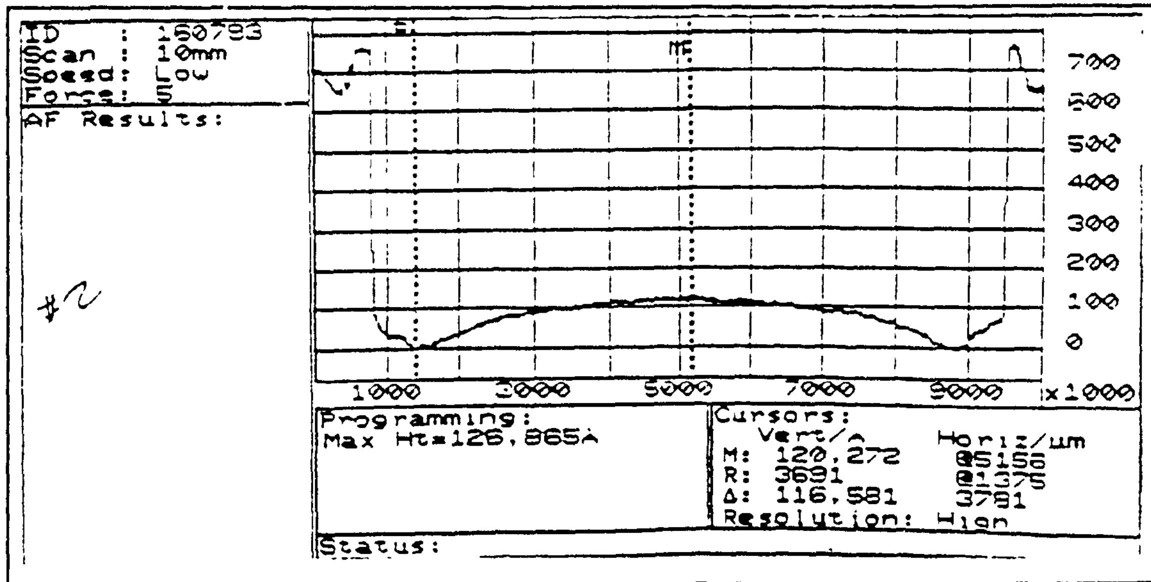

Figure 4.8: DEKTAK printout showing surface finish

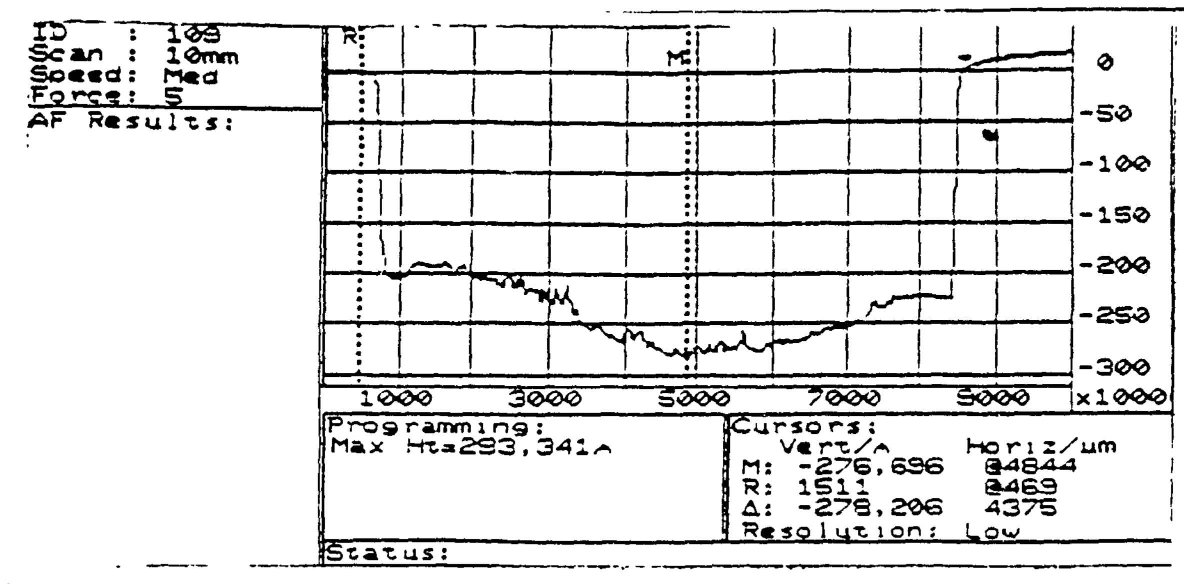

Figure 4.9: DEKTAK printout for membrane for Device3

cavity and the other to thin down the wafer thickness to the desired value for themembrane. The results of these etches can be seen from the DEKTAK printouts shown in figures 4.7 and 4.8. The etched surface was always very smooth, this smoothness could have been due to the fact that the substrate being held down unlike the experiments conducted earlier where the samples were left to float in the etchant. Note the difference in the etch depth at the edge of the membrane (figure 4.9). The etch rates being established, and the etching system tried out successfully, the membranes required for the devices were etched out of silicon. For the Device1 the etch that was done to define the cavity was for ten to fifteen minutes, the reverse side of the wafer was then etched for forty to forty five minutes. The resulting membranes were of a thickness of approximately 15 to 20μm. For the Device2 the etch made on the first wafer, which was 100μm thick to start with, was for a period of 50 minutes, resulting in a membrane thickness of

approximately 10 to 15μm. Examining the DEKTAK printout (figure 4.8), it is apparent that the surface of the etched membrane was not absolutely flat. The membranes had been etched more at the edge than the centres, the etch being deeper at the edge by approximately 15 to 20μm. This difference could be have two explanations. The first, due to the heating of the liquid KOH in the well, the KOH rose in the central region and descended along the sides of the well, very much like the convection current, this causing the edges to be etched faster than the centre. Another reason could be the fact that the wafer was stressed along the edges by the cell which was forced down on it by the arrangement of screws. This the resulted in the edge being stressed more than the central region, which in turn resulted in the etch rate being larger in the edge[37].

For the third device, the etching for the membrane was done after the bonding of the two halves was over. The reason for this was that during the bonding process the wafer and glass assembly had to be heated to a temperature slightly above 400°C. This heating process raised stresses on the membrane which resulted in the membrane cracking, as in the first attempted device. The etching of the wafer, after the bonding was complete, was carried out with the same cell as used earlier. However, the etch rates for these samples were somewhat higher. The etch was done for a period of fifteen minutes which resulted in an etched depth of approximately 29μm (see DEKTAK printout of figure 4.9).

The temperature of the water bath in which the assembled cell was placed for all

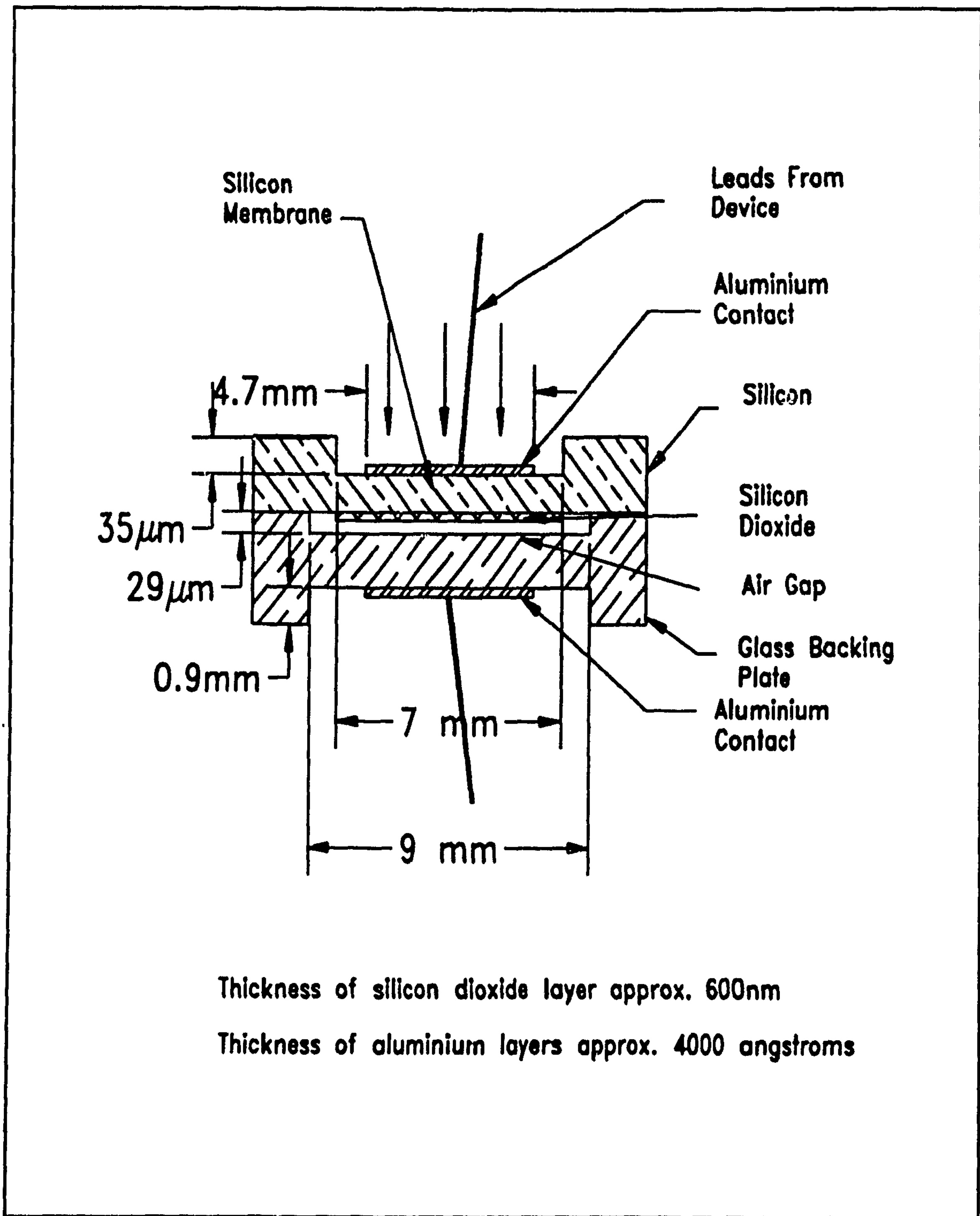

Figure 4.10: Detailed Structure of Device 3

the above etches, was maintained at around 90°C, the temperature of the KOH inside the cell varying between 68 to 73°C. The temperature had to be noted every five minutes and the adjustments made so as to have the temperature within the desired range. There was no need to stir the etchant as the quantity of the KOH was small and the circulation inside the cell was adequate for it to be at a uniform temperature. The bubbles that were being emitted were carried to the top of the etchant surface. Sometimes the bubbles covered the entire top of the hole and on such occasions they had to be dislodged. The temperature inside the hole when this happened rose to above 85°C. The etch was timed accurately, care being taken to keep the etch going on only for the desired time. After the etch was complete, the wafer was taken out of the assembly and carefully washed with de-ionised water and dried. The etch was then measured using a DEKTAK surface profile measurement system.

The etchant, KOH leaked along the edge of the O-ring, especially if the ring happened to be one that was not new. The leaking KOH affected the surface of the silicon, leaving behind a discoloured area wherever the reaction had taken place. To reduce the effects of the leaking KOH and to have near flawless surfaces, the second device had a layer of oxide thermally grown on the wafer surfaces prior to the etch. This oxide layer was to prevent the silicon surface from being affected by the leaking KOH and thus leave the surface clear. The other reason for the layer of oxide was to have a layer of insulation between the two halves of the device when it was bonded using the aluminium welding technique. The thickness of this layer of oxide was approximately 600 - 700 nanometres. The

surfaces of the samples after the etches were completed were very clean. The oxide had been etched away at some places by the leaking KOH, however sufficient oxide was left behind to form a complete insulation layer.

The membranes were fabricated as described above.

4.3 Bonding of the two parts of the Device

As the discussed in chapter 2, the use of Anodic bonding allows the bonding of two dissimilar materials. This technique was used to bond the two parts of the final device. However, the anodic bonding method was tried out after epoxy bonding and the thermal 'welding' with aluminium were proven to be impractical.

The first device consisted of one silicon wafer which has the membrane bonded with epoxy resin to the glass slide. The cavity could not be evacuated of the air that caused the device to be somewhat insensitive to the external pressure and thus the device had very little effectiveness as a sensor.

The attempt to overcome this problem was made in the next device, where the bonding was done with a layer of aluminium being deposited between the two silicon wafers which constituted the sensor. This layer was melted by heating the assembly to 700°C, above the melting point of aluminium at 660°C. On cooling, the two halves were bonded together. This heating had driven out some of the air in the cavity and thus overcame the problem encountered in the first device. However, it gave rise to another more serious problem. When these devices were tested, it showed that the insulation between the two halves had broken down, in

effect there was no capacitance in the device. The aluminium had diffused through the insulation layer during the heating process which was done in a Rapid Thermal Annealing (RTA). This caused the resistance to break down.

To overcome the above problems anodic bonding process was adopted. This required a basic change in the design of the device necessitating the use of dissimilar materials for bonding while the membrane was still of silicon. The bottom plate was to be a glass slide, a special glass PYREX 7740, refer to figure 4.10. The cavity was etched in this glass using Hydrofluoric acid. The etch was done for one minute in the first case, and two minutes and finally five minutes in the third sample. The first sample had a cavity of approximately 10μm, for the second the cavity depth was 15μm while for the third the depth was 29μm.

The anodic bonding was done with all three. A small circular patch of oxide was left on the underside of the wafer such that this oxide would be directly above the cavity bottom. The purpose of this layer is to prevent that area from also being bonded to the glass surface. Published reports have mentioned that surfaces that had oxide coatings would not bond. In the first device the silicon membrane that was bonded had cracked during the process.

The second attempt was made without the wafer being etched prior to the bonding so as to eliminate the chances of the membrane cracking. This second attempt was also unsuccessful since the wafer was sucked into the cavity and was bonded. This was in spite of the oxide layer that was present in that area. The

third sample had the cavity depth increased to 30μm, as mentioned earlier. The oxide layer was also increased in thickness. These steps were taken so as to decrease the possibilities of the wafer being sucked in like in the second attempt. This third attempt was successful in bonding the wafer to the glass slide.

This third device had the etching done on the silicon after the bonding of the glass and silicon was done .

4.4 Deposition of Aluminium

The deposition process was described in chapter 2. There were two depositions of aluminium done, one each for the two conductive plates of the capacitive type pressure sensor. The thickness of the metal deposited, one on the glass and the other on the silicon, was approximately 4000Å each.

The deposition of metal was the final step in the fabrication of the device. It was now ready for the testing which is described in the next chapter.

Chapter 5

Testing and Results

This chapter discusses the testing of the pressure sensor and the results obtained. The set-up for the testing is described and then the actual test procedure. The results are then discussed in detail. The tests were carried out on Device3. The first two versions had been tested, as mentioned earlier, however the results were not satisfactory.

The first device was found to be insensitive to pressure. This was explained by the fact that the air, trapped in the cavity between the membrane and the bottom half of the device, was being compressed when the device was exposed to pressure, thus preventing the membrane from being deflected adequately. The second device did not register any significant capacitance. There was a break down of the insulation between the two halves of the device; this was due to the diffusion of aluminium through the layer of silicon dioxide during the bonding process. For this reason, the device3, as shown in Figure 5.1, was chosen as the final design.

The device dimensions are as follows:

Membrane diameter = 9mm

Membrane thickness (initial) = 100μm

Membrane thickness (final) = 65μm

Gap between two parts of device = 29μm

Glass backing plate thickness (initial) = 1700μm

Glass backing plate thickness (final) = 1100μm

The membrane and the glass plate were reduced in thickness after being tested.

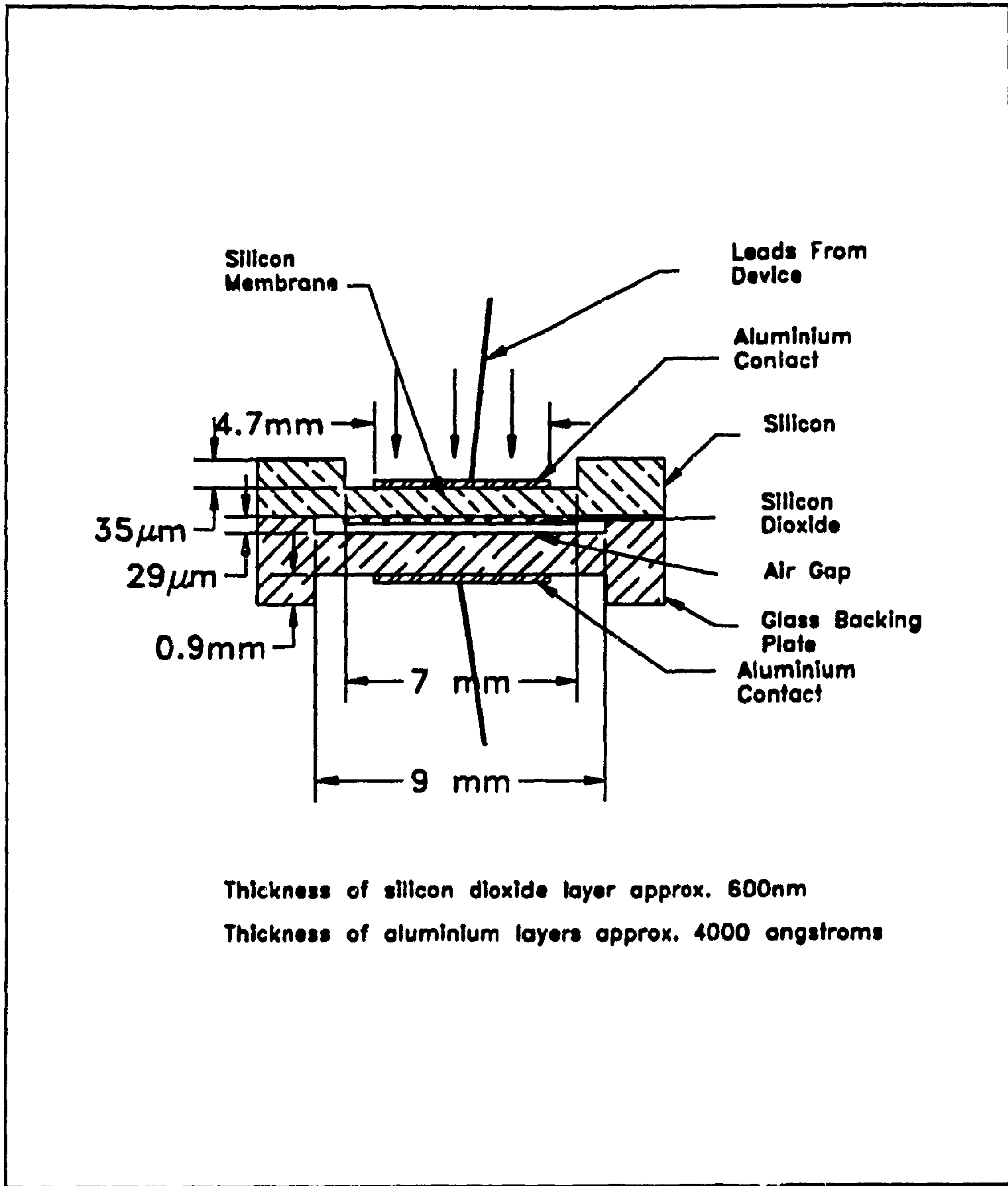

Figure 5.1: Detailed Structure of final Device 3

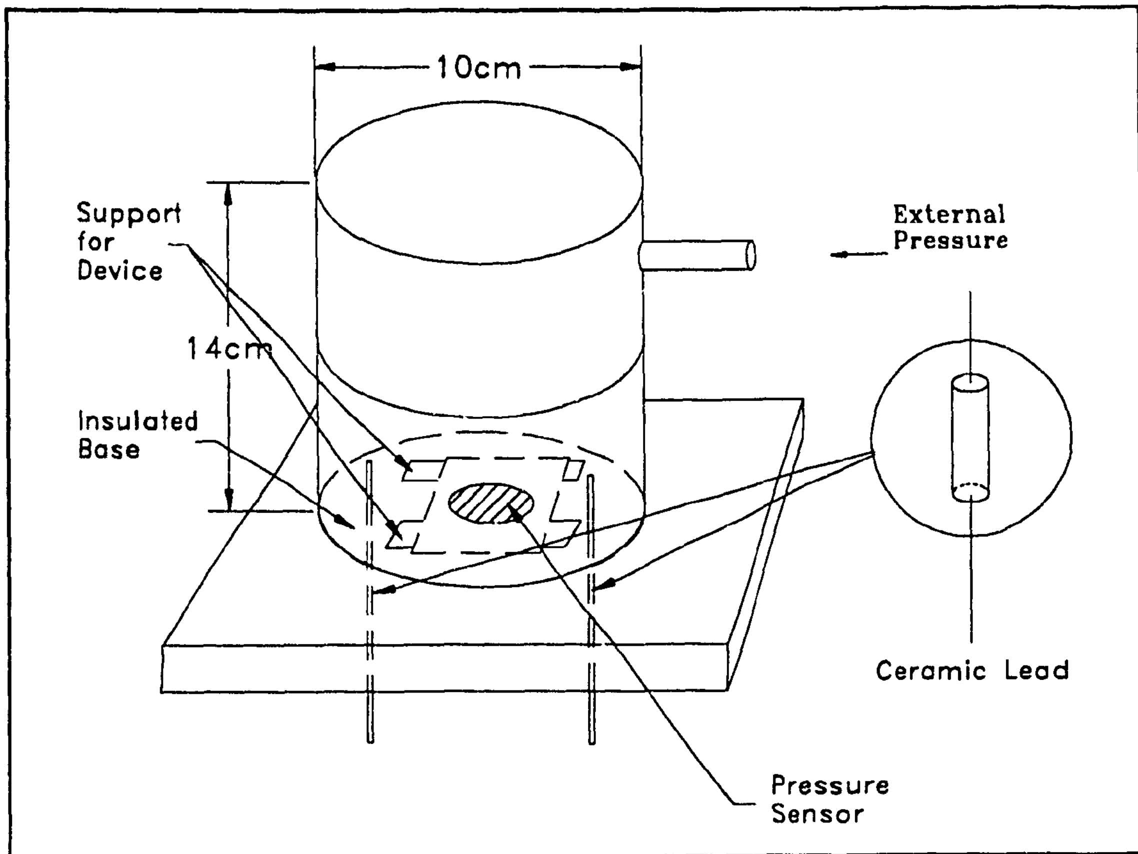

Figure 5.2: Details of the Pressure Chamber

5.1 The Test Set-up

To test the pressure sensor under different pressures a chamber was designed. This chamber, which was constructed out of steel, was connected to a cylinder of nitrogen by means of Teflon tubing. The pressure inside the chamber could be regulated and measured by means of a pressure gauge and regulator. The pressure chamber was designed to have the signals from the device placed inside it to be brought out by means of two leads as shown in figures 5.2 and 5.3 and connected to the measuring instrument by means of BNC connectors and shielded cables so as to minimise the effects of external fields.

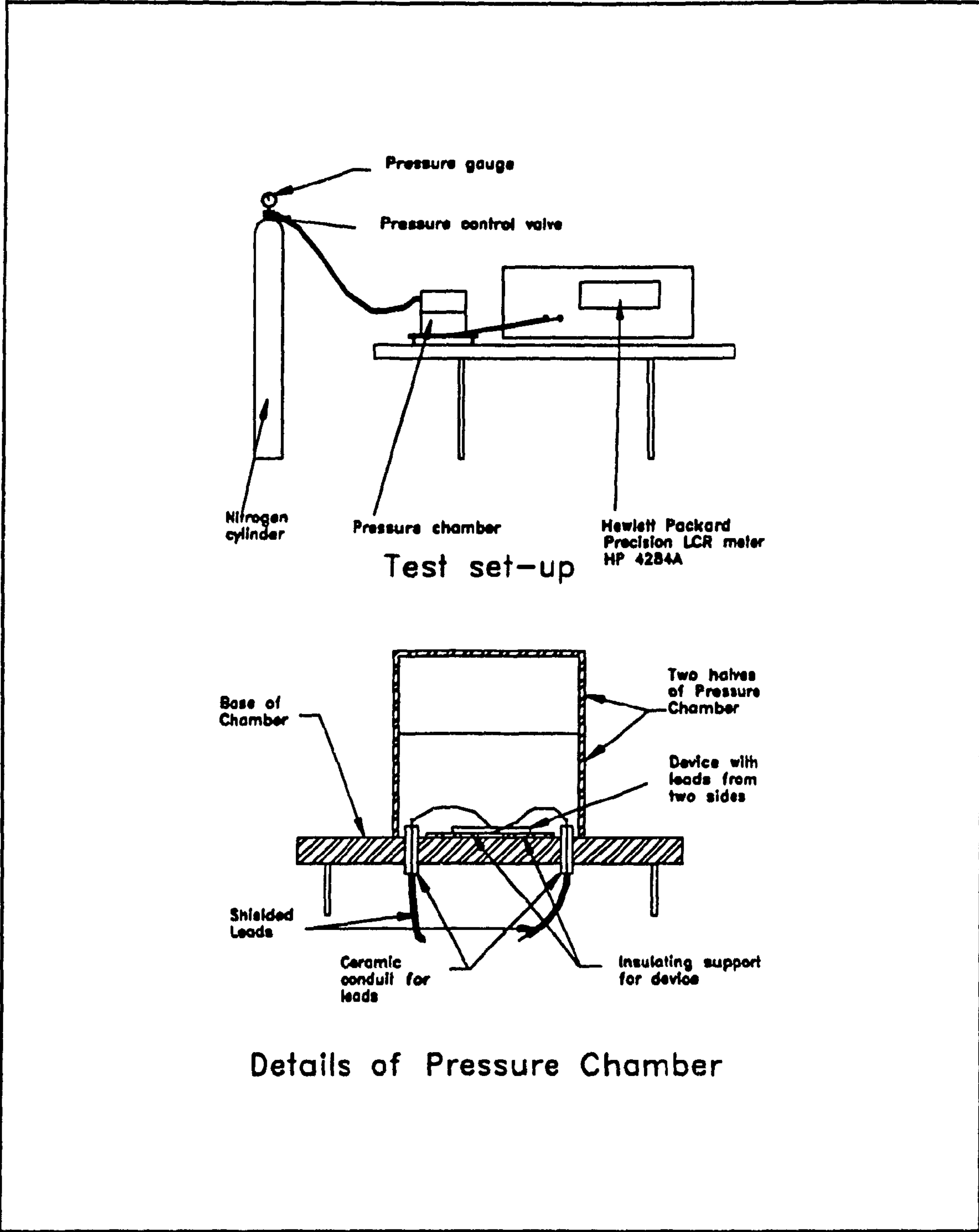

Figure 5.3: The Test Set-up

It would have been more appropriate for this chamber to have been made with a probe station and a pair of probes inside it, however this could not be done. In the absence of such probes, the device had to be connected by means of leads which were connected onto the conducting aluminium layers on either side of the device by means of conductive silver paste.

The instrument used to measure the capacitance of the device and the change in the capacitance value when under changing pressure, was the Hewlett Packard Precision LCRmeter HP 4284A (20Hz to 1MHz). This was connected to the device by means of shielded cables with BNC connectors. Such connections had to be used so as to eliminate the fluctuations. The fluctuations in the capacitance readings of the device during the first few attempts at testing made with normal connectors, were very high. The readings did not keep at a steady value, the variation was in the range of tens of pico farads and no credible readings could be taken. This fluctuation was nearly eliminated when the BNC connectors were used with the shielded cables, the fluctuation now being a few femto farads. Another factor that affected the measurements was the presence of light. This effect was observed when the device was tested first under light, and then under no lights. There was a small difference of approximately 1-3% in the device response under the two conditions.

5.2 The Test Procedure

5.2.1 Characterization of the Pressure Sensor:

The testing of the device was preceded by its characterization. This involved

checking its response to input voltages at different frequencies so as to define the most stable operating frequency and amplitude range. This was done by using the whole range of signal frequency available with the instrument, from 20Hz to 1MHz. These experiments were done without any external pressure being imposed inside the chamber, however some of these readings were taken with a pressure of 50psi inside the chamber as a control. The amplitude of the sinusoidal signal was also varied in another sequence of experiments, from 20mV to 1V, however, only two values were used for detailed examination, 20mV and 1V. The effect of the bias on these readings was also tested by first using no bias and then varying the DC bias to -10V, -1V, 1V and 10V. The discussion will be on the selection of the operating frequency range for the device. This will help us designate a region where the change in the device capacitance can only be from the change in the pressure. It is to be noted here that the capacitance readings of the device fluctuated greatly at low frequencies of the measuring signal. This variation in the capacitance readings of the device decreased with the increase in the signal frequency. For frequencies above 800kHz the fluctuation reduced greatly, and for the frequency value of 1MHz there were no fluctuations at all.

The figures 5.4 and 5.5 show the variation in the readings of the device for a signal amplitude of 1V, with no DC bias and 10V DC bias respectively. The variation of the capacitance with the frequency shows that the readings above 800kHz had stabilised. Below a value of 300kHz for the frequency, the readings were very erratic. The above experiment was carried out for two different input

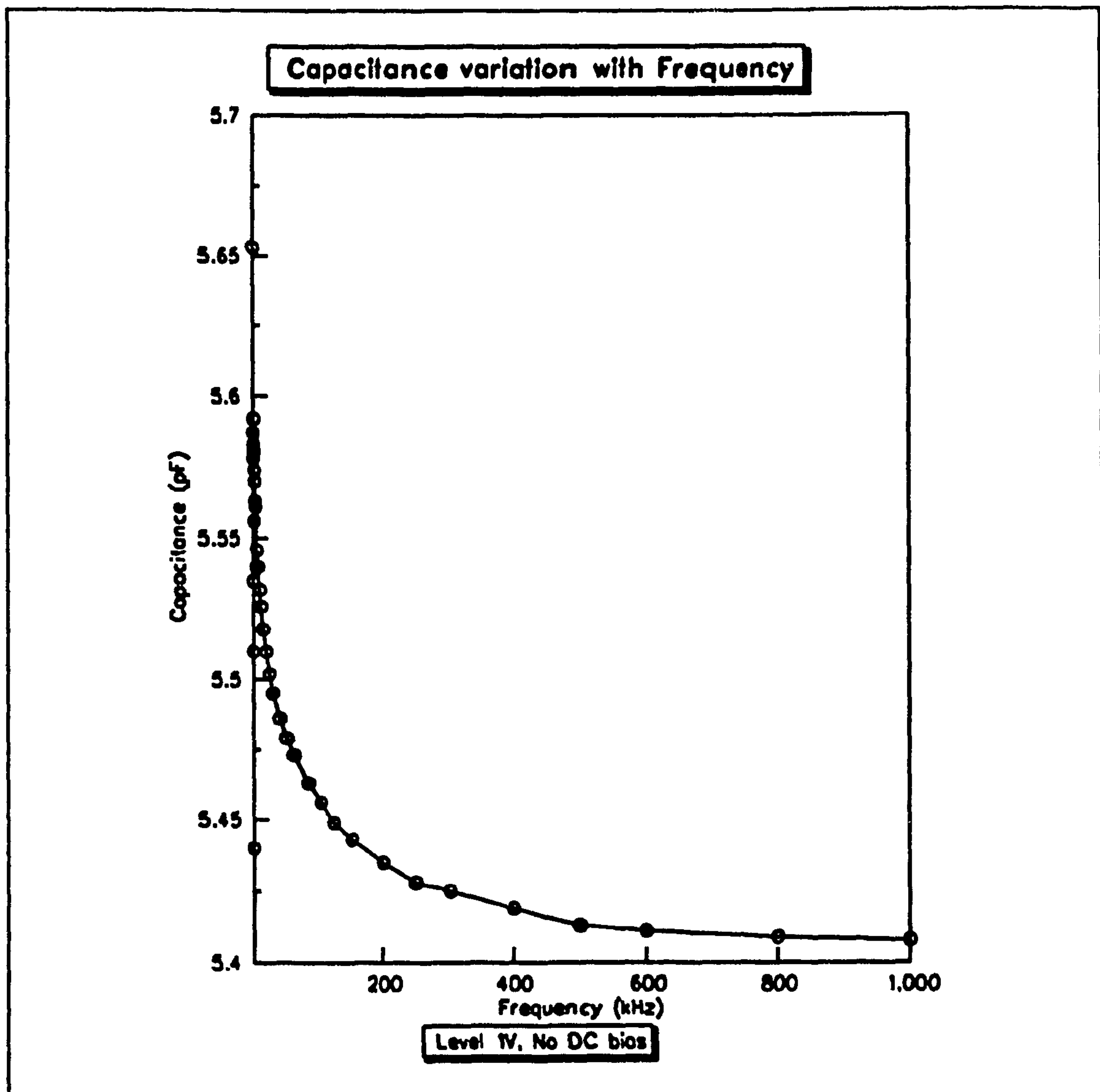

Figure 5.4: Capacitance Variation with Frequency

signal amplitude values, 1V and 20mV. For each of these amplitudes the DC bias was also changed, from -10V to 10V. The effects of this change were not very great - the steady capacitance values were obtained only for frequency values above the 800kHz range. As before, the capacitance readings were very erratic for frequencies under 300kHz. For the frequency range between 800kHz and

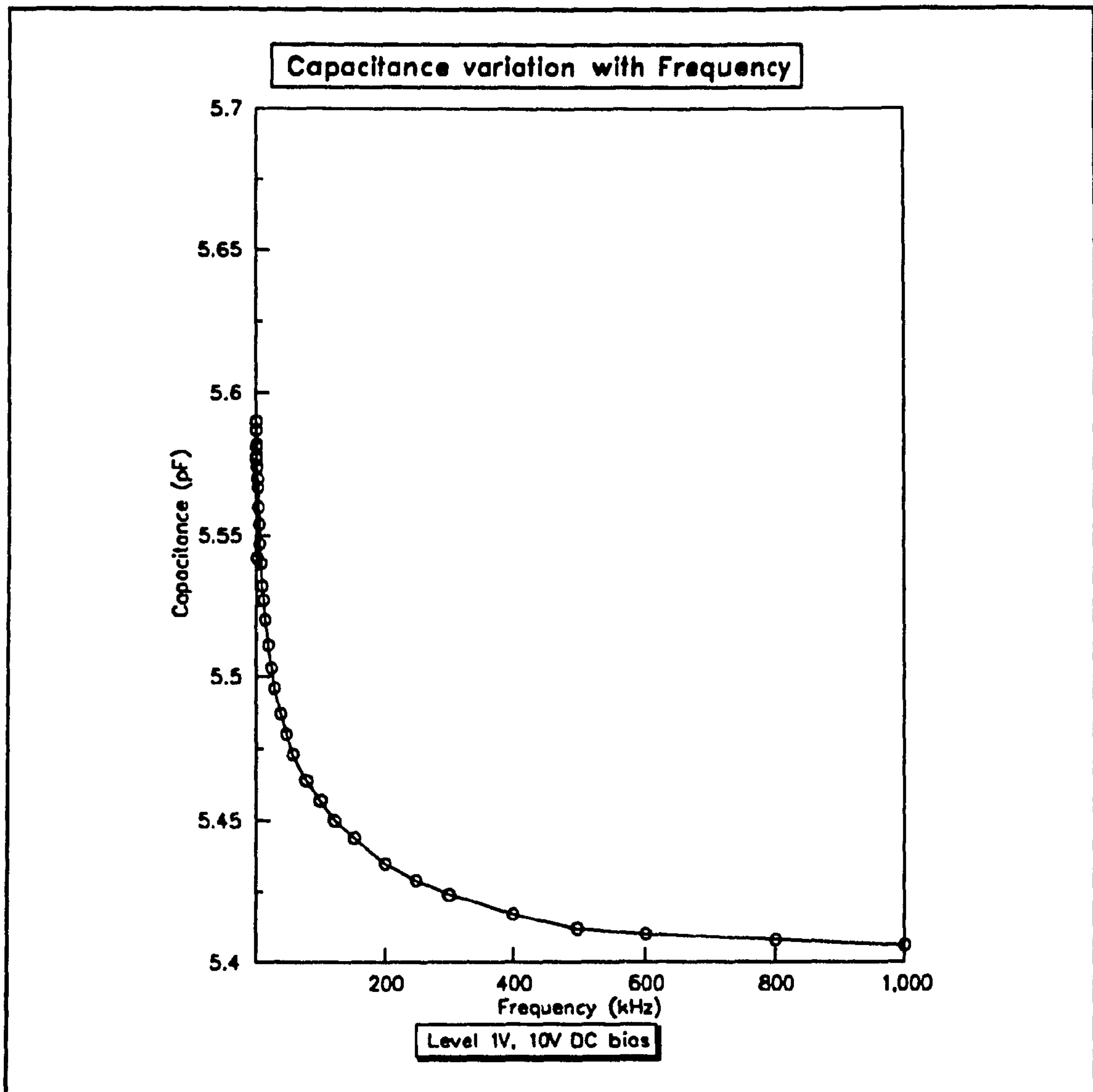

Figure 5.5: Capacitance Variation with Frequency

300kHz, the fluctuations were large, the readings not being steady. Thus it becomes obvious that the range of frequencies at which this device can operate effectively lies above 800kHz.

To summarise, the results obtained by changing the signal frequency and noting down the capacitance value, show that the capacitance readings given by the

device were steady for the higher frequencies. As the frequency was brought down, the capacitance value for the device began fluctuating. The fluctuations were less for frequency values above 800kHz, being in the range of a few femto farads; they increased greatly as the frequency of the signal was decreased below 600kHz to within tens of pico farads. For frequencies below 300kHz, the capacitance readings shown by the instrument fluctuated greatly. There were no effects of the DC bias, the readings being almost identical. The same was true for the two different signal amplitudes.

From the above results, it becomes apparent that the device should be used at signal frequencies above 800kHz since the capacitance readings were more stable for frequencies above 800kHz, and thus all experimentation was done at a signal frequency of 1MHz. The amplitude of this signal was kept at 1V.

5.2.2: The Effect of DC Bias on the Capacitance Variation with Change in Pressure

The effect of the bias on the device response was also examined. As mentioned in the preceding section, the following DC bias levels were applied to the device: 10V, 1V, -1V and -10V. Two examples of the output are shown in the figures 5.4 and 5.5 The readings obtained were virtually identical, as were the readings for the tests with the other bias levels. The DC bias therefore, did not have any noticeable effect, neither did the change in the amplitude of the input signal.

5.3 The Effect of Pressure Change on the Capacitance of the Device

The device was next tested in the chamber for changes in capacitances with changes in the applied pressure. The connections were made as described earlier and shown in the figure 5.3; the signal frequency and amplitude of the instrument were set at 1MHz and 1V respectively. The chamber lid was bolted down tight so as to prevent any leakage of the nitrogen gas. The pressure chamber and the plastic tubing connecting the gas cylinder to the chamber were first tested for leaks. The pressure was then raised by allowing the gas to flow in to the chamber through the plastic tubing, the regulator allowed the pressure to be held at a steady value while the capacitance readings were taken. As soon as the gas was introduced to the chamber there was an immediate change in the capacitance. The change was steady as long as the pressure was held at that level. The pressure was increased in steps, with increments of 10psi to a maximum of 80psi. After reaching the maximum, the readings were repeated as the pressure was reduced in similar steps of 10psi. These were to check for any hysteresis effects in the device. It may be noted here that the simulation had shown that the membrane comes in contact with the cavity bottom at a pressure of approximately 15psi, (1psi = 0.007MPa).

The following figures show the effect of the pressure change on the capacitance. For these tests, the frequency of the signal was kept steady at 1MHz.

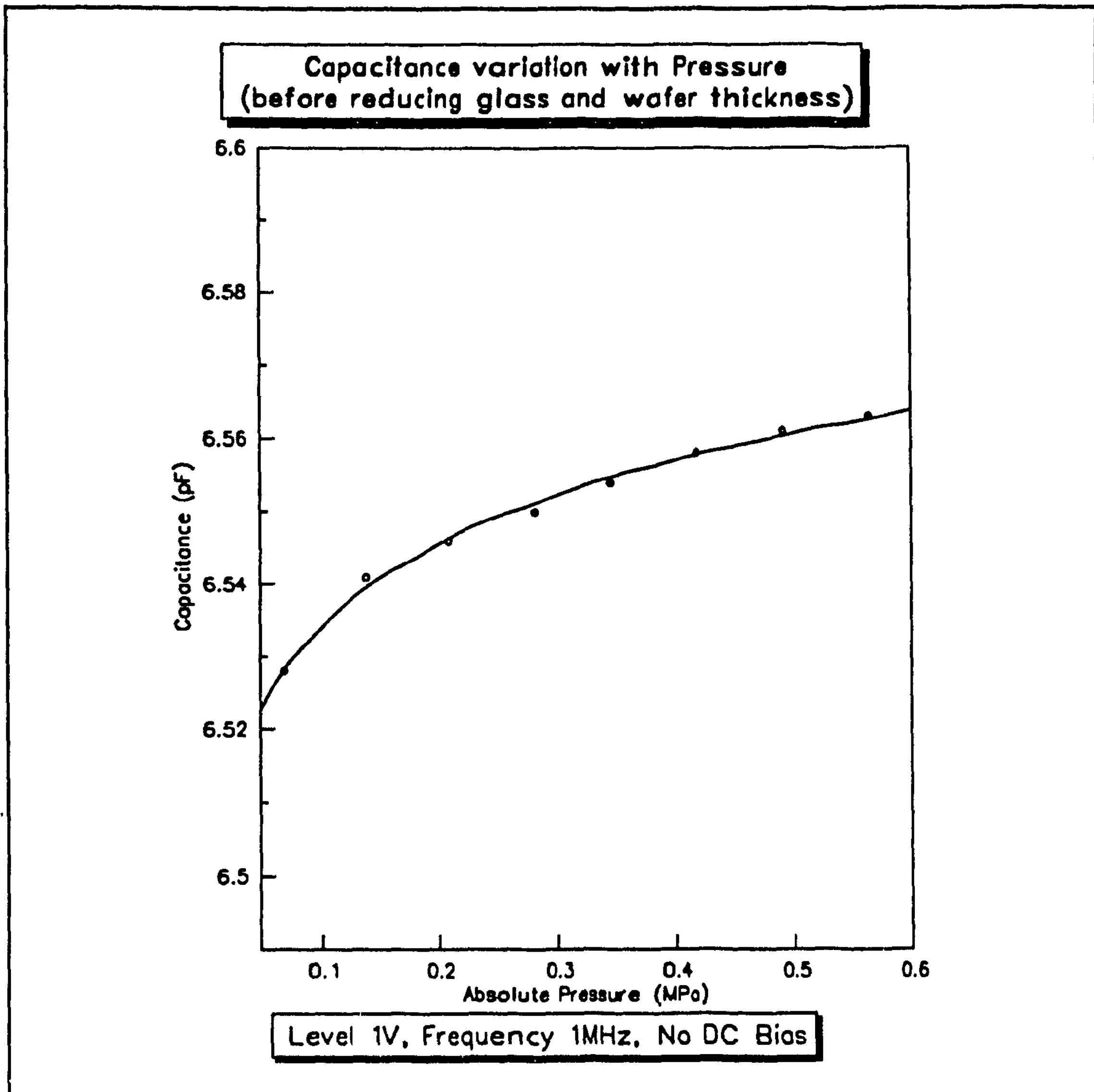

Figure 5.6: Capacitance Variation with Pressure

In the figure 5.6 the effect of the pressure change on the capacitance of the device3 is shown. There was no DC bias applied on the device, the amplitude of the signal was kept at 1V and the frequency of the signal was 1MHz. There are two stages in the capacitance increase, one up to a pressure of 0.105MPa, (i.e regime I) and the other beyond that pressure.

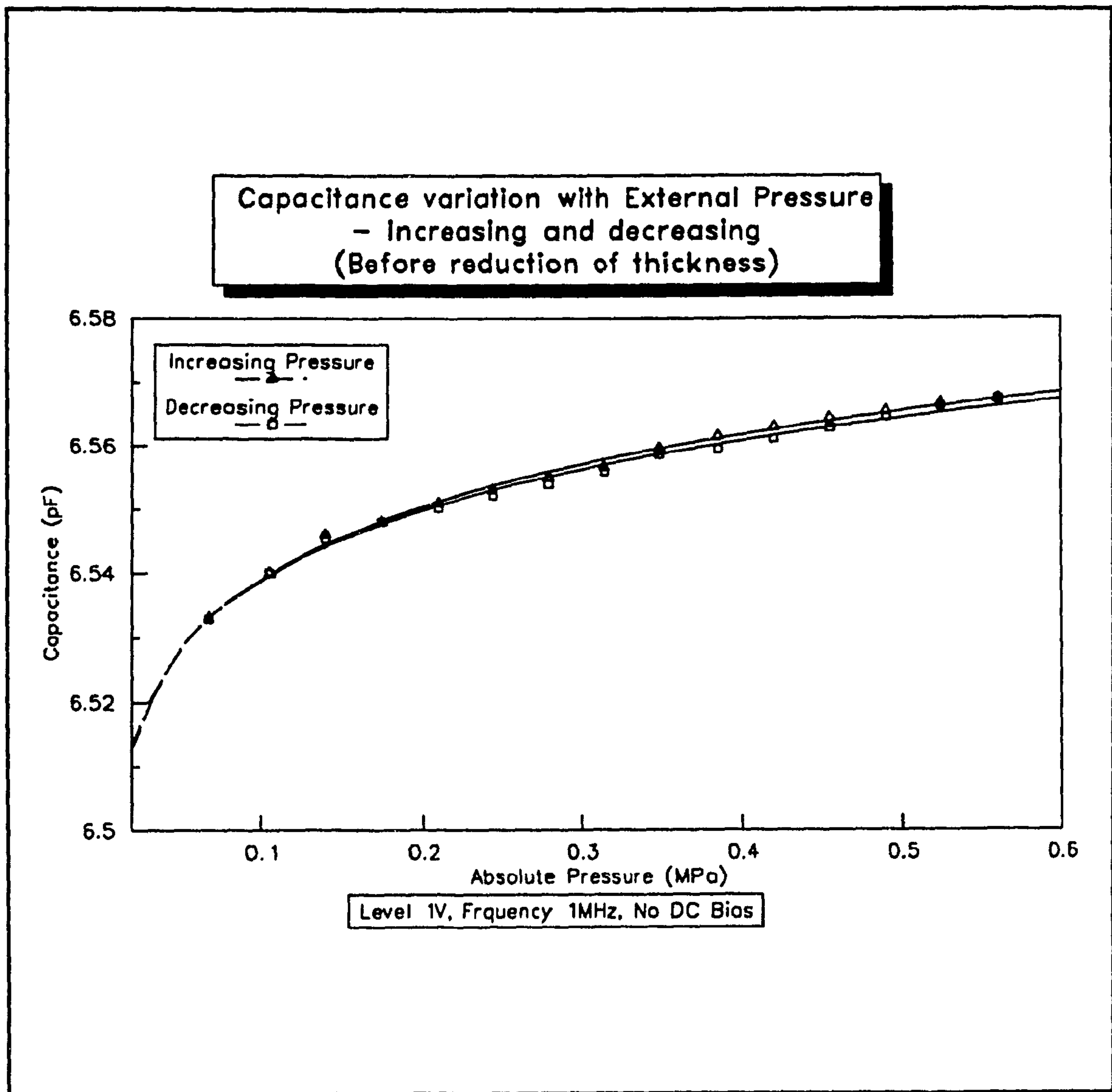

Figure 5.7: Capacitance Variation with Pressure - full cycle

The figure 5.7 shows the capacitance variation for a full cycle where the pressure was increased to 80psi (0.56MPa) and then decreased to the starting point in steps of 10 psi (0.07MPa). This experiment was performed every time the pressure on the device was varied. The hysteresis was found to be minimal.

The above results show that the variation of the external pressure causes the

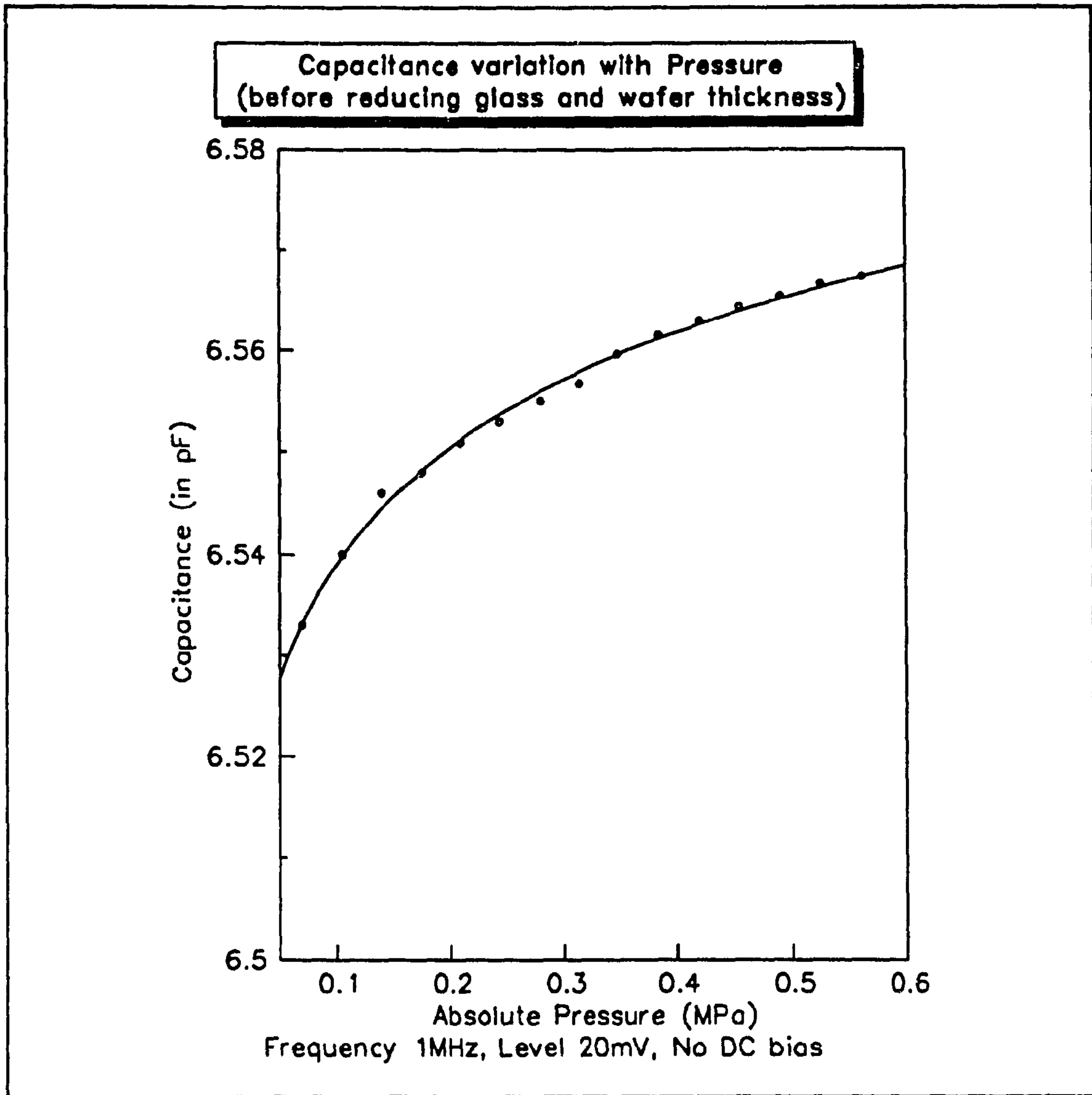

Figure 5.8: Capacitance Variation with Pressure

capacitance to change immediately. Thus the device is very sensitive to such pressure changes and can be very effectively used as a pressure sensor. Figure 5.8 shows the variation in the capacitance of the device with pressure change for a signal amplitude of 20mV. It is apparent from a comparison of Figures 5.6 and 5.8 that the capacitance change from 20psi (0.14MPa) to 80psi pressure, is

virtually identical. For the first case, the increase in the capacitance is 0.022pF whereas for the next it is 0.021pF. This shows that the change in the input signal amplitude has no effect on the response of the device. The default signal amplitude for the subsequent tests was kept at 1V.

5.4 The Effect of the Glass Thickness and the Membrane Thickness on the Device Capacitance

As described earlier in chapter 3, the capacitance of the device is actually a combination of different capacitances. Barring the parasitic capacitances, there are three dielectrics in the device between the two conducting layers of aluminium - the first being the insulation of silicon dioxide, the second being the air gap between the two plates and third the glass backing plate. Ideally, this glass plate should be as thin as possible. The glass plate has the dominating capacitance as all three capacitances are in series, and with a thick glass dielectric the resulting capacitance is very small when compared to the capacitances of the oxide and the air gap. Therefore, any changes in the device capacitance with pressure is actually being masked by the glass capacitance.

The next step in the testing was to examine the effects of the glass and the membrane thicknesses on the device sensitivity. This was done by first etching the glass from the reverse side and then reducing the membrane thickness also by etching the wafer for 20 minutes with KOH. The glass which was 1.7mm thick for the initial tests, was reduced to 1mm and the membrane from 100μm to 65μm.

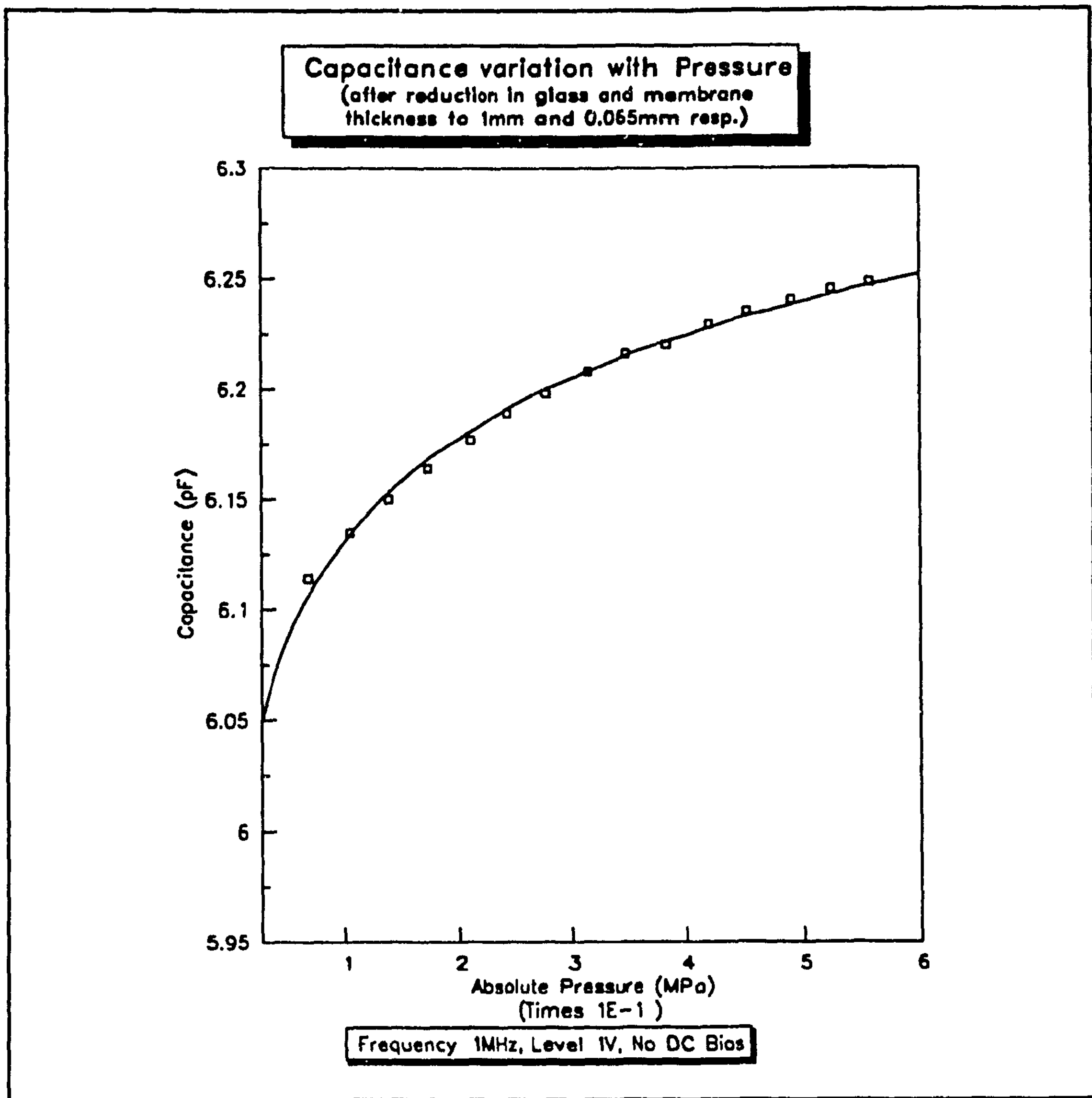

Figure 5.9: Capacitance Variation with Pressure

shown in the equivalent circuit of figure 5.11. The figure 5.9 shows the change in the capacitance with the change in the pressure after the device had been further etched to reduce the thickness of the membrane and the glass backing plate. Comparing the results with those of figure 5.6, it is seen that there is a small difference in the capacitance value of the device at the start. This difference could

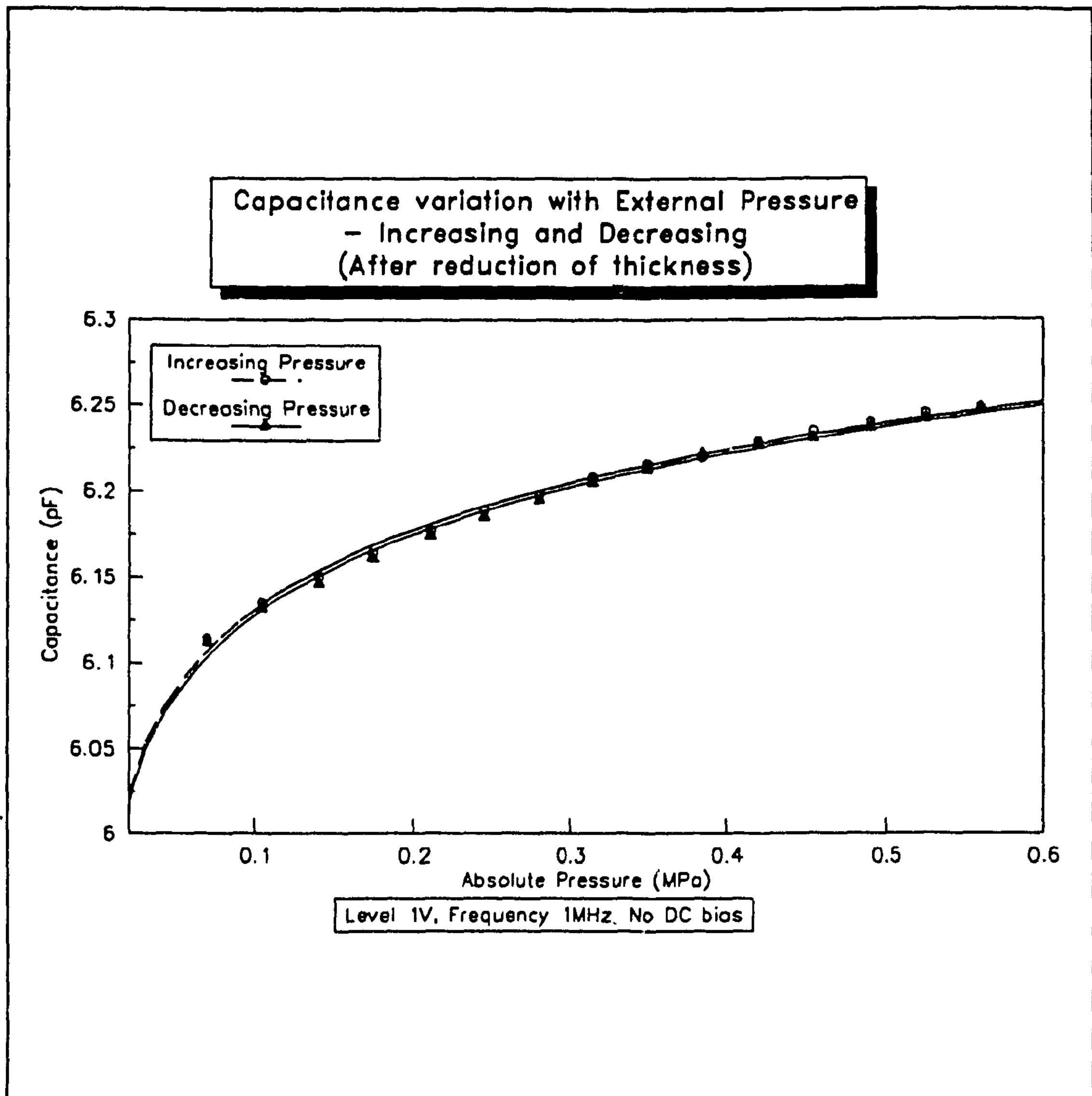

Figure 5.10: Capacitance Variation with Pressure - full cycle

be attributed to the parasitic capacitances as shown in the equivalent circuit of figure 5.11. The figure 5.10 shows that the change in the pressure over a complete cycle. However, when compared to the change shown in the figure 5.7, the change in this device is of greater magnitude. For the un-thinned device, the same set of signal amplitudes and frequencies showed a change in the capacitance of

0.0503pF, while the change is now seen to be 0.240pF, i.e 4.77 times the previous value. Thus, these results show that the attempt at making the device more sensitive by thinning was very successful. The change in the capacitance can be taken to be in two parts - one where the increase is much steeper, i.e up to 15psi, and the next where it is more gradual. The slopes for the increase in the capacitance for these two regions are as shown in table 5.1.

	0-15psi external pressure, pF/psi	20-80 psi external pressure, pF/psi
Before reduction of thickness	0.00135	0.00037
After reduction of thickness	0.00870	0.00160

Table 5.1: Rate of change of Capacitance with Pressure

5.4.1 The Effect of Parasitic Capacitance

The capacitance being measured by the instrument can be considered to be the combination of the capacitance of the device and the parasitic capacitances from the silver paste used for the connection, the leads and also the connecting cables. The figure 5.11 shows this equivalent circuit, with the parasitic capacitance shown in parallel to the device.

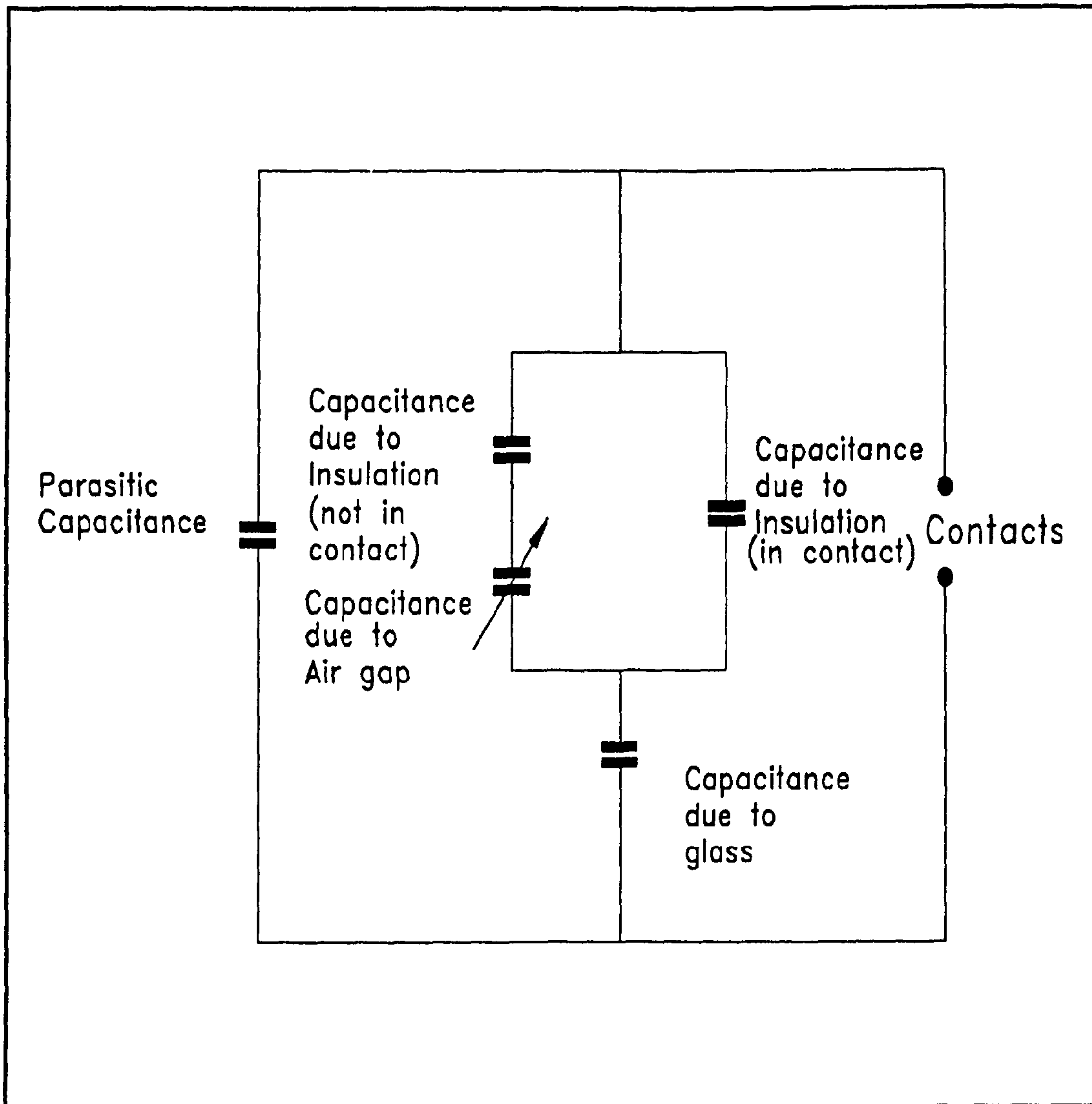

Figure 5.11: Equivalent Circuit showing Parasitic Capacitances

Having established the role of the parasitic capacitance in the measurement of the absolute capacitance levels, the relative variations in the capacitance can now be considered.

The figure 5.12 shows the device response for a signal frequency and amplitude same as that for figure5.9, i.e 1MHz and 1V respectively.

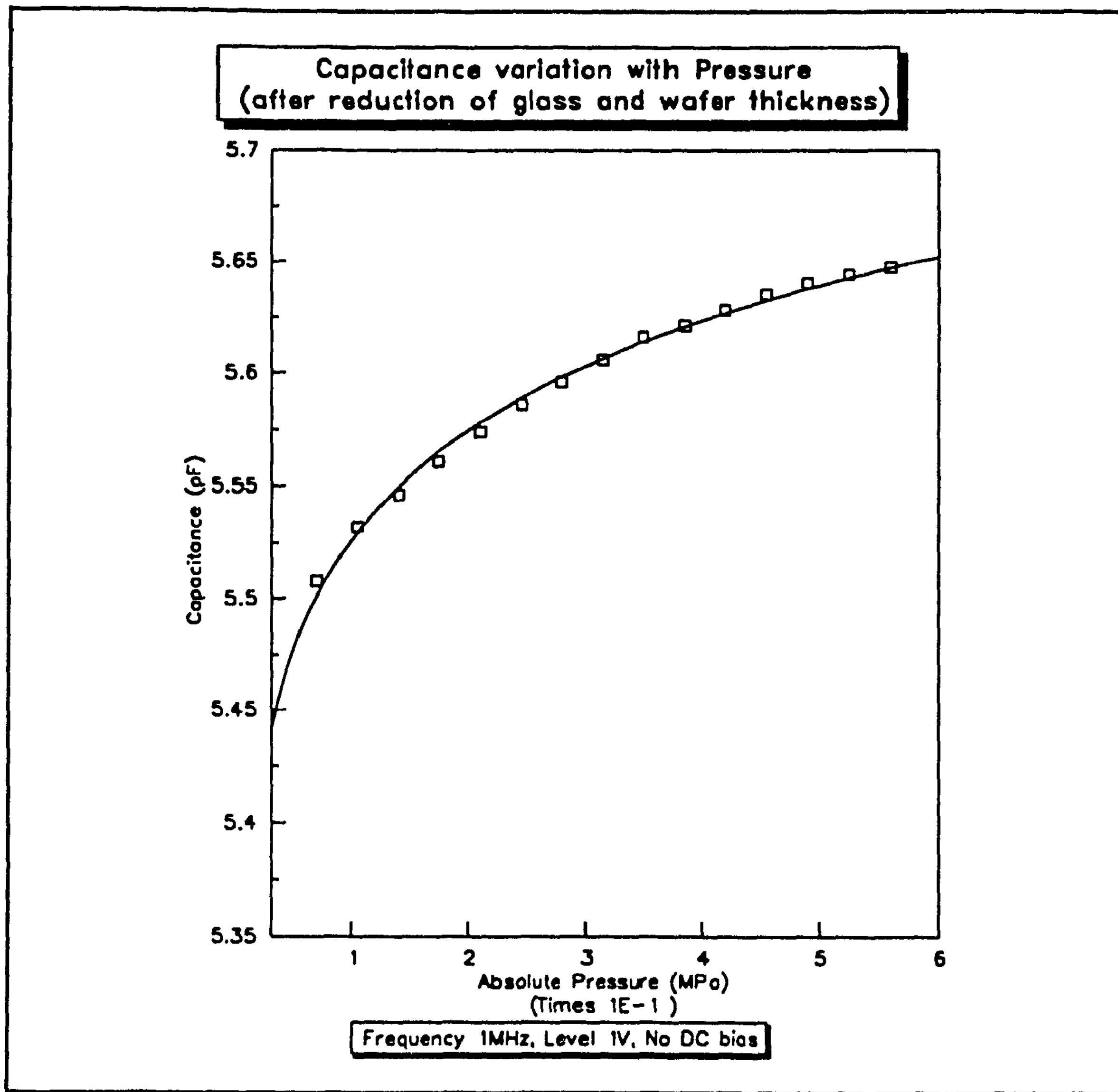

Figure 5.12: Capacitnace Variation with Pressure

The results show that the capacitance for the device starts at a value of 5.406pF whereas in the previous case the first value was 6.008pF. This offset could be atrributed to the parasitic capacitances, which change along with a change in the setting of the device. The fact that the change in the capacitnace was almost identical in every test however confirms that such changes were actually due to

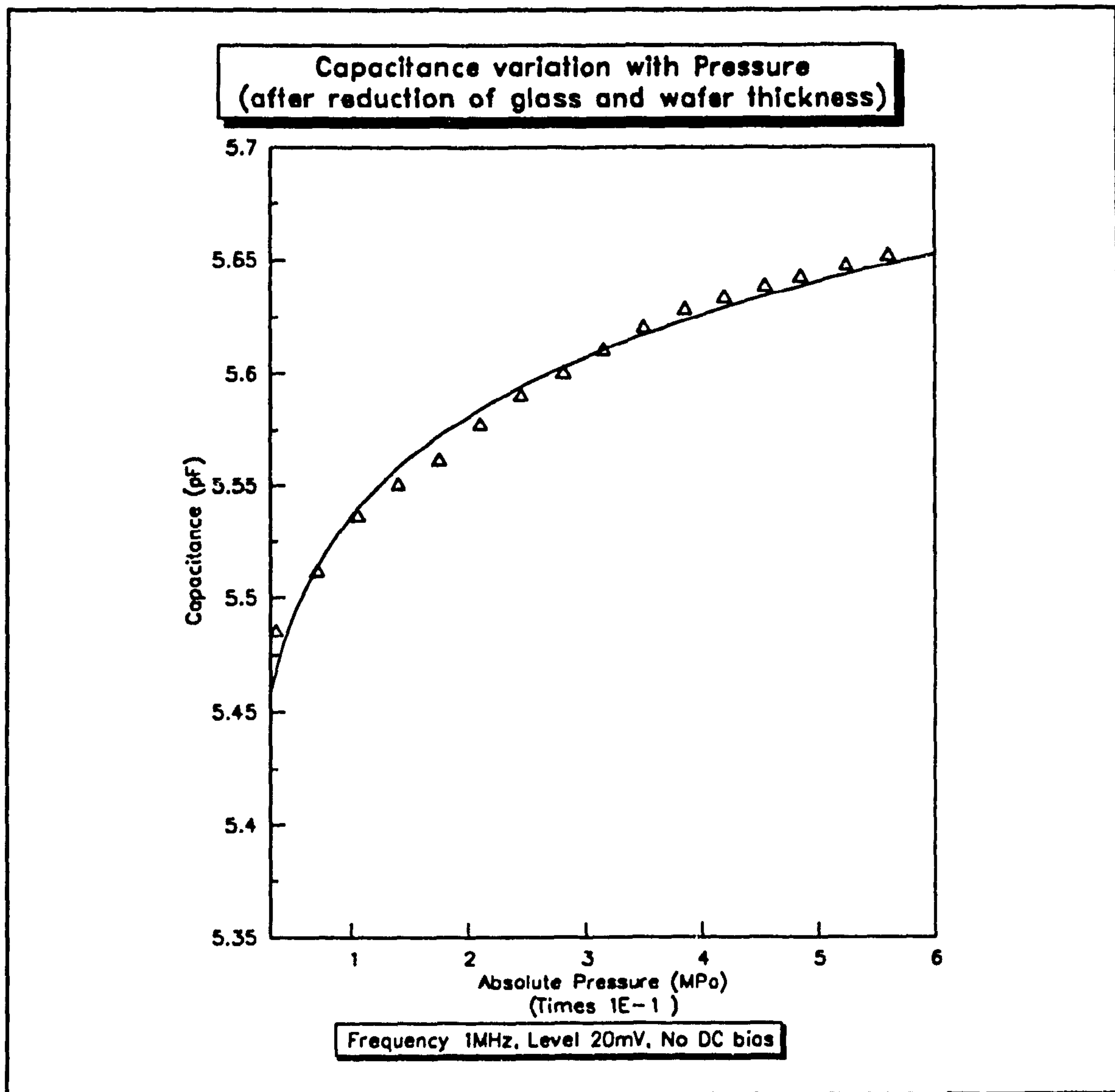

Figure 5.13: Capacitance Variation with Pressure

the device capacitance changing and not other extraneous capacitances. The figure 5.13 shows the variation of the capacitance for a signal amplitude of 20mV. From the results it is apparent that the change in the signal amplitude has no effect on the device response. The change in the device capacitance for pressure change of 80psi (0.56MPa), was 0.241pF in both cases, i.e figures 5.9 and 5.13.

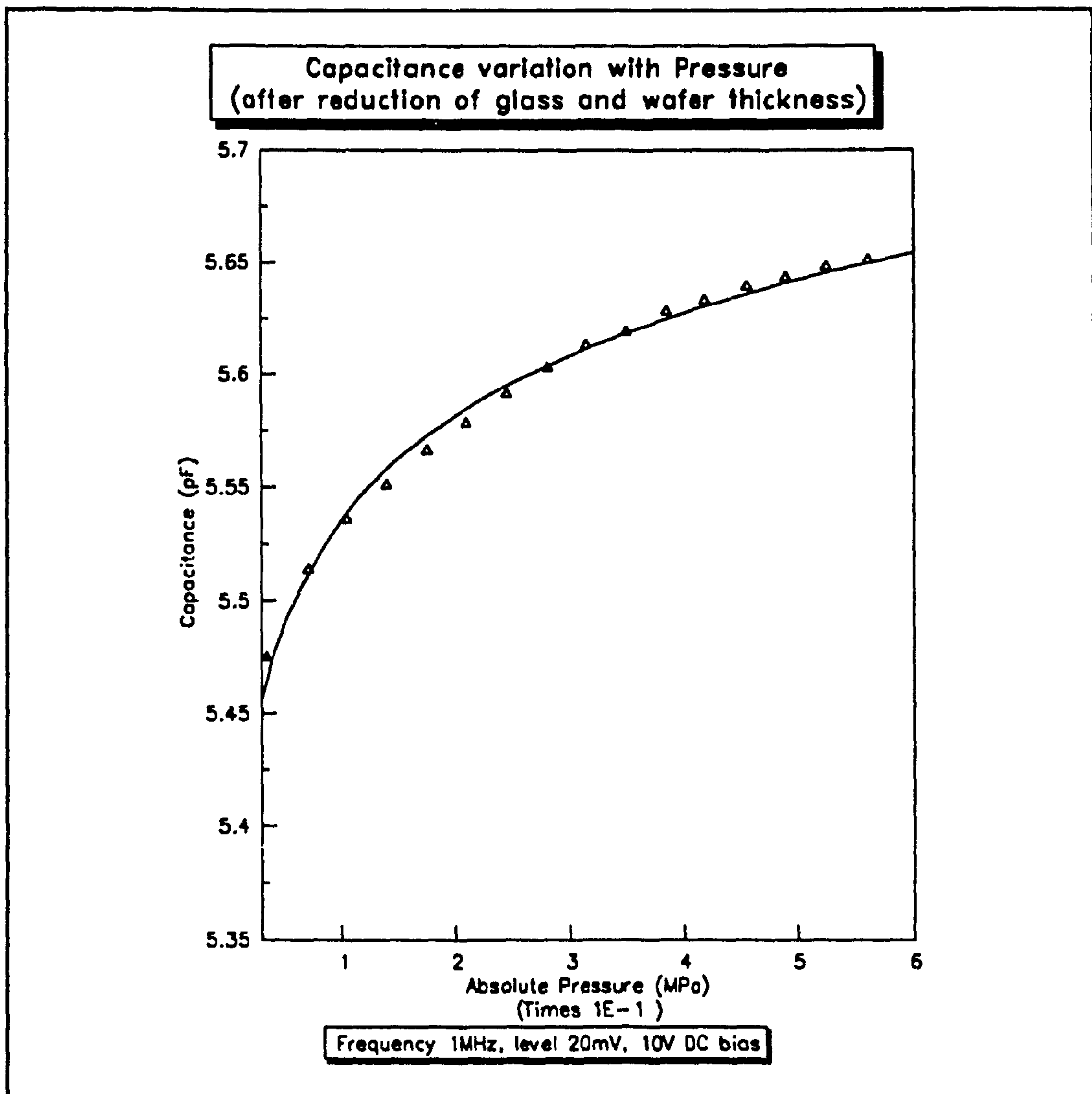

Figure 5.14: Capacitance Variation with Pressure

The figure 5.14 shows the effect of changing the DC bias on the device. Comparing these results with those of figures 5.9, 5.12 and 5.13, it is apparent that the change in the DC bias on the device does not have any effect on its response to an external pressure change.

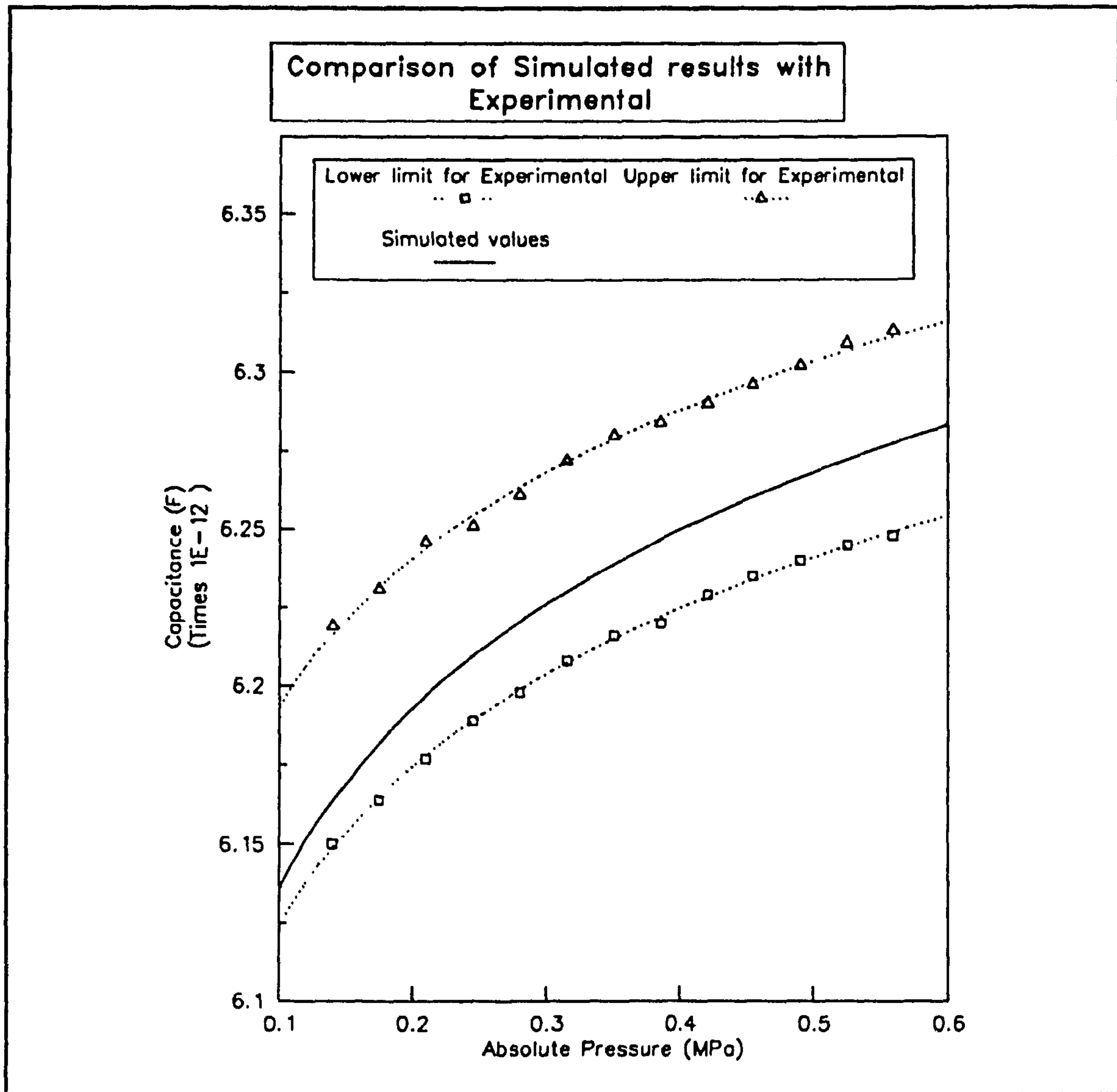

Figure 5.15: Comparison of Simulated Results with Experimental

5.4.2 Comparision of the Simulated Results with Experimental Results

The figure 5.15 shows the comparision of the actual experimental results with the simulated values obtained previously in chapter 3. The experimental values shown in this figure had been the results obtained after the reduction in the thicknesses

of the membrane and the glass backing plate. The signal frequency was 1MHz and the amplitude was 1V. There was no DC bias applied for these readings. The two sets of experimental values shown indicate the maximum variation observed in the readings during one sequence of experimentation.

It was calculated that for the device parameters as considered, the top plate of the device which is the membrane, comes into contact with the backing plate at a pressure of approximately 1.02 times the atmospheric pressure, that is 15psi (0.105MPa). The simulation values shown are from 20psi (0.14MPa) pressure onwards corresponding to the start of regime II, where the top plate comes in contact with the cavity bottom. Hence the first capacitance value that is obtained is at 20psi. Simulation results agree well with those obtained experimentally.

.A sensitivity analysis of the mathematical model was done. The mathematical model for the device takes into account the different physical parameters of the device that affect the output. For example, the area of the membrane, the gap between the two parts of the device and thickness of both the membrane and the glass backing plate are parameters that dramatically affect the device capacitance. Changes could be made on each parameter separately or in combinations of parameters. The simulation program was run with such changes being made in these parameters and the results obtained from them are outlined in the following paragraph.

The first dimension that was changed was the area of the membrane. For a change in the diameter of the membrane from 8000μm to 9000μm, the simulated

capacitance of the device increased by a factor of 12.1%; for this simulation the glass backing plate thickness was kept constant at 900μm and the gap at 28μm, the thickness of the SiO_2 layer at 0.05μm. For another simulation, the thickness of the glass backing plate was decreased from 1000μm to 900μm to produce a 10.4% increase in the device capacitance. Here the diameter was kept constant at 8000μm and the other parameters like the gap between the two parts of the device and the thickness of the SiO_2 layer were the same as mentioned before. The effect of change in the gap between the two halves of the device on its output capacitance was examined by similarly changing its value in the simulation program. For a change in the gap from 30μm to 20μm the capacitance of the device was shown to increase by 2.1%, the other parameters being kept constant - the diameter of the membrane being 4950μm, the thickness of the glass backing plate 960μm, and the thickness of the SiO_2 being 0.05μm. Similar simulations were done for the effect of the thickness of the membrane, keeping the diameter of the membrane at 4950μm, the glass backing plate thickness at 960μm, and the gap at 30μm. The membrane thickness was varied from 60μm to 70μm, and the change in the device capacitance was found to be 9.4%, the capacitance being reduced. For the change in the thickness of the SiO_2 layer, a change from 0.05μm to 0.10μm was found to have a negligible effect on the device capacitance, i.e. below a fraction of a percent. This series of simulations provided an insight into the behaviour of the device. It was seen that the area of the membrane and the thickness of the glass backing plate are the two parameters that affected the device output significantly, whereas neither the membrane thickness nor the gap

between the two halves did have as dramatic an effect on the results.

The results from the above simulations were compiled and studied to arrive at a combination of parameters that could provide a simulated result which would be compatible with the actual results obtained.

This procedure resulted in the dimensions of the device being set at:

Diameter of Membrane: 4950μm

Thickness of glass backing plate: 960μm

Thickness of Membrane: 65μm

Gap between the two halves of the device: 30μm

Thickness of SiO_2 layer: 0.05μm

The simulation program was run with these dimensions and the results were compared as shown in figure 5.15, with the experimental values.

The difference in the absolute capacitance values for the two cases could be explained by considering factors like the parasitic capacitances and errors in the measurements. Measurements of the thicknesses of the glass backing plate, the silicon membrane thickness, the layer of SiO_2 and even the gap would be affecting the calculated value of the capacitance. The parasitic capacitnaces, as explained earlier, would arise from the leads, cables and silver paste used to connect the measuring instrument to the device. All of these have capacitances which ultimately affect the end results. The difference between the actual results and the simulation results can therefore be considered to be due to such discrepancies.

5.5 Summary of Results

To conclude, the Device 3 has been tested and found to perform satisfactorily. The change in the capacitance when an external pressure is applied is instantaneous. The consistency of the results was examined by carrying out the tests repeatedly, and the device was found to give same results each time. The feature that stands out is the fact that the increase in the capacitance is always the same. It was shown that the sensor would be most effectively used with the signal frequency being kept at 1MHz, lower frequencies causing the readings to fluctuate.

The device sensitivity was improved greatly by reducing the glass thickness and also the membrane thickness. Further improvements would be possible by using a glass backing plate of even lower thickness which would reduce the effect of the capacitance due to the glass and substantially enhance the device sensitivity. Reduction of the membrane thickness will also result in greater sensitivity. As the membrane diameter used for this device was fairly large, a smaller diameter would be very effective with thinner membranes. This would allow the use of higher pressures for testing. A comparison with the simulation results showed remarkable conformity. The sensor could not be tested at higher pressures as it was not possible to increase the external pressure above 80psi with the system being used, since the plastic tubing used to connect the nitrogen cylinder to the chamber does not stand much higher pressures.

Chapter 6

Conclusions and Recommendations for Future Work

6.1 Conclusions

This thesis is on the design, analysis, fabrication and testing of a Capacitive type Silicon Pressure Sensor using Micro-machining techniques. The material used was silicon with a glass slide acting as its backing plate. The sensor design was first analyzed and its performance simulated. The simulations were carried out for different pressure ranges. Due to the limitations of the facilities available, the design was altered by increasing the size of the device, the concept remaining the same.

The device consists of a silicon wafer bonded to a glass slide. The glass slide has a small cavity etched in it, whose depth was measured using a DEKTAK 3030 surface profile measurement system. The bonding of the glass to the silicon wafer was done by using a technique known as Anodic Bonding. This bonding technique uses an electric field to assist the bonding process where the two pieces being bonded are heated to a temperature of 400°C. The wafer was then etched from the top so as to reduce the thickness at the region above the cavity. This etch was carried out using Potassium Hydroxide which anisotropically etches silicon. A novel technique was employed to carry out this etch. This technique eliminated the use of photolithography altogether. The technique used a teflon cell designed to etch the wafer that is placed in it. The wafer is exposed to the etchant only in the area

that is to be etched. This allows for faster processing. The glass thickness was reduced from the bottom so as to reduce the effect of the capacitance due to the glass.

The device was first characterised by finding out a range of signal frequencies where the device output would remain stable. The tests showed that the sensor would have to be tested at frequencies higher than 800kHz. The effect of DC bias was also studied, it was found that the bias had no noticeable effect on its performance. The testing of the device was done from external pressures ranging from 0 to 80 psi. The changes in the capacitance value of the device was noted and later plotted against the pressure. This experimental variation was compared to the simulated variation. The increase in the capacitance with the increase in pressure may be divided into two stages, the first till a pressure of 15psi and the next beyond 15psi. The difference between these two stages is the linearity, the second stage having a more linear relation between the capacitance and the pressure. The simulation had shown that the membrane comes into contact with the bottom of the cavity at a pressure of 15psi. Previous work carried out [3] had shown a similar increase in linearity after the threshold pressure where the membrane deflects and touches the bottom plate.

It can be said here that the device sensitivity can be greatly increased by reducing the thickness of the glass backing plate. When the thickness of the glass backing plate is compared to the air-gap thickness and the insulation thickness, all three

of which act as dielectrics in series, it is seen that the glass thickness is by far the largest of all three. Therefore, the capacitance due to this glass dielectric is the dominant capacitance. It is thus obvious that the glass thickness has to be reduced in order to give prominence to the air-gap capacitance, as we are attempting to measure the change in just that capacitance value. Moreover, since it is the actual change that we are interested in and not the absolute value of the capacitance, it becomes all the more important that the glass thickness be reduced. This was shown by actually reducing the glass backing plate thickness by approximately 700μms. The capacitance change after the reduction was four times greater than that before the reduction. Another parameter that can be reduced is the thickness of the silicon sensing membrane. This will also increase the sensitivity of the device. However, reductions in the thickness will have to be accompanied with reductions in the diameter of the membrane.

The results of the tests show that the device is very sensitive to pressure changes. The readings are also very consistent and repeatable. This proves that the design of the sensor was conceptually correct and viable. A comparison with experimental results published elsewhere, corroborates this conclusion. The main conclusions may be listed as follows:

1. The pressure variation causes a deflection in the membrane of the device and this deflection brings about a change in the device capacitance.

2. The capacitance change is linear to the change in pressure, and this

linearity is increased after the bottom plate comes in contact with the membrane.

3. The sensitivity of the device is greatly increased by reducing the thickness of the glass backing plate.

6.2 Recommendations for Future Work

The work described by this thesis has illustrated the possibilities of the design that has been presented. As regards immediate improvements of the device presented in this thesis, the first step would be to reduce the diameter of the membrane along with the thickness. This would require a thinner backing plate to be used, which would also help in reducing the glass capacitance and thus increase the response of the device to pressure changes.

The device is of a very simple design which has the added advantage of being made from different materials. By varying the different parameters of the device, like the thickness of the membrane, the gap that separates the two halves of the device, the diameter of the membrane and also the material being used for the membrane, there can be large number of devices made for different pressure ranges and for different fluids. The inclusion of the capacitance measurement and related processing circuitry on the same chip as the device will increase its versatility. This will be possible if the glass backing plate is replaced with a silicon backing plate, which would necessitate using a different bonding technique.

A large number of small sensing devices can be arranged on a single chip in an array by using lithography. This along with the related circuitry could be used as a tactile sensing device for imaging of pressure. Thinner membranes could be made from depositions of materials like tungsten on a sacrificial substrate which on being etched away would leave behind the free standing membrane. Such a technique could be used to have very precisely controlled thicknesses for the membranes. This method could also allow the use of composite layers of materials, to increase the strength of the membrane. The design could also be used as a pressure switch.

References

[1] Brysek,J., Petersen,K., Mallon,J.R, Christel,L., Pourahmadi,F., - "Silicon Sensors and Micro-structures" Brysek,J., Petersen,K., Mallon,J.R, Christel,L., Pourahmadi,F., - NOVASENSOR, Fremont, September 1991

[2] Middelhoek, S., Audet, S.A., - "Silicon Sensors", Academic Press, London, New York, 1990

[3] Lars Rosengren, Jan Soderkvist, Leif Smith "Micromachined sensor structures with linear capacitive response" - Sensors and Actuators, vol 31, No. 1-3 March 1992, pp 200-205

[4] Chau, H.L., Wise, K.D., "An Ultraminiature Solid-State Pressure Sensor for Cardiovascular Catheter", - IEEE Transactions Electron Devices, Dec. 1988, Vol. 35, no. 12, pp 2355-2362

[5] Chun, K.J., Wise, K.D., "A Capacitive Silicon Tactile Imaging Array" - Rec. of the 3rd. Intl. Conf. on Solid State Sensors and Actuators, 1985, pp. 22-25

[6] Roylance, L.M., Agnell, J.B, "A batch-fabricated silicon Accelerometer", - IEEE Transactions on Electron Devices, ED-26, Dec. 1979, p1911

[7] Allen, H.V, "Silicon-Based Micromechanical Switches for Industrial Applications" - IEEE Micro Robots and Teleoperators Workshop, Hyannis, Massachusetts, Nov. 1987

[8] Matsumoto Y., Shoji S., Esashi M., " Absolute Pressure Sensors by Air-tight Electrical Feed Through Structure"- (Abstracts from 22nd. Conference on Solid

State Devices and Materials, Sendai, Japan, 1990), Sensors and Actuators, Vol.23, No. 1-3, April 1990, pp 1048-1052

[9] Ko, W.H, "Solid State Capacitive Pressure Transducers" - Sensors and Actuators, Vol.10, 1986, pp 303-320,

[10] Ko, W.H., Bao, M.H., Hong, Y.D., "A High Sensitivity Integrated Circuit Capacitive Pressure Transducer" - IEEE Trabsactions Electron Devices, Vol. 29, 1982, pp 48-56

[11] Kendall, D.L., "Dopant Selective HF Anodic Etching of Silicon (For the Realization of Low-doped Monocrystalline Silicon Microstructures", - Applied Physics Letters, Vol. 26, 1975, p 195

[12] Palik,E.D., Bermudez,V.M., Glembocki,O.J. "Ellipsometric Study of the Etch-Stop Mechanism in Heavily Doped Silicon", - Journal of Electrochemical Society, Vol.132, 1985, pp 135-141

[13] Bean,K.E., "Anisotropic Etching of Silicon" - IEEE Transactions on Electron Devices ED-25, 1978, pp 1185 - 1192

[14] Lee, D.B, "Anisotropic Etching of Silicon" - Journal of Applied Physics, Vol. 40, October 1969, pp 4569-4574

[15] Bassous, E., "Fabrication of Novel Three Dimensional Micro-structures by the Anisotropic Etching of (100) and (110) Silicon"- IEEE Transactions on Electron Devices, ED-25, 1978, pp 1178-1184

[16] "Semiconductor Materials and Process Technology Handbook" ed. McGuire, G.E., Noyes Publication, p 336

[17] Hanneborg, A., "Silicon Wafer Bonding Techniques for Assembly of Micromechanical Elements" - IEEE Proceedings of MEMS. 1991, p 92

[18] Wallis, G., Pomerantz, D.I., "Field Assisted Glass-Metal Sealing", - Journal of Applied Physics, Vol.40, No. 10, Sept. 1969, pp 3946-3949

[19] Wallis, G., "Field Assisted Glass-Sealing", - Electrocomponents Science and Technology, Vol.2, No.1, 1975, pp 45-53

[20] P.M Sutton, "Space Charge and Electrode Polarization in Glass" - Journal of American Ceramic Society, Vol.47, 1964, pp 188- 194, pp 219-230

[21] Anthony, T.R "Dielectric Isolation of Silicon by Anodic Bonding" - Journal Applied Physics, Vol. 58(3), May 1983, pp 1240-1247

[22] Wallis, G., "Direct-Current Polarisation During Field-assisted Glass-Metal Sealing", - Journal American Ceramic Society, Vol. 53, No.10, October 1970, pp 563-567

[23] Borom, M.P., "Electron Microprobe Study of Field Assisted Bonding of Glasses to Metals" - Journal of American Ceramic Society, Vol. 56, May 1973, pp 254-257

[24] Gossink, R.G., "Sims Analysis of Aqueous Corrosion Profiles in Soda-lime-Silica Glass" - Journal of American Ceramic Society, Vol.62, No. 12, Jan-Feb 1978, pp 4-9

[25] Anthony, T.R., "Anodic Bonding of Imperfect Surfaces" - Journal of Applied Physics, Vol. 54, No. 5, May 1983, pp 2419-2428

[26] Donovan, R.P., Hardesty, C.A., Brooks, A.D., "Silicon to Silicon Seals using Sputtered Borosilicate Glass" - Journal of Electrochemical Society, Vol.119, 1972,

p 545

[27] Esashi, M., Nakano, A, Shoji, S., Hebiguchi H., "Low Temperature Silicon to Silicon Anodic Bonding with Intermediate Low Melting-Point Glass" - Sensors and Actuators, Vol. A21-A22, 1990, pp 931-934

[28] Kanda, Y., Matsuda, R.S., Murayama, C., Sugaya, J., "Mechanism of Field Assisted Silicon-Glass Bonding" - Sensors and Actuators, Tranducers'89,Vol.23, No. 1-3, April 1990, pp 939-943

[29] Grundner, M., Jacob, H., "Investigations on Hydrophilic and Hydrphobic Silicon (100) Wafer Surfaces by X-Ray Photoelectron and High Resolution Electron Energy Loss Spectroscopy" - Applied Physics, Vol. A39, Feb.1986, pp 73-82

[30] Field, L.A., Muller, R.S., "Fusing Silicon Wafers with Low Melting Temperature Glass" - Sensors and Actuators, Vol. A21-A23, No. 1-3, pp 935-938, 1990

[31] Iller, R.K., - The Chemistry of Silica, Wiley -New York, 1974, Wiley

[32] Muller, B., Stoffel A., "Vertically Structured Silicon Membranes by Electrochemical Etching" - (MME'90 Technical Digest), - Sensors and Actuators, Vol. 23, No. 1-3, April 1990, pp 899-903

[33]Lee, K.C, "The Fabrication of Thin, Freestanding, Single-Crystal, Semiconductor Membranes", - Journal of Electrochemical Society, Vol.137, 1990, pp 2556-2574

[34] S. Timoshenko and S. Woinowsky-Kreiger - "Theory of Plates and Shells", Wiley, New York, 1968

[35] Kendall, D.L., Fleddermann, C.B., Malloy, K.J., - "The Mechanical Properties

of Semiconductors and Semimetals", Vol. 37, Academic Press, London, New York, 1992

[36] Bohg, A. "Ethylene Diamine-Pyrocatechol-Water Mixture Shows Etching Anomaly in Boron-doped Silicon", - Journal of Electrochemical Society, Vol. 118, No.2, 1971, pp 401

[37] Stiharu, I., Bhat, R.B., Kahrizi, M., Landsberger, L., - "The Influence of The Stress State in Silicon on the Anisotropic Etching Process", - #2045-41, SPIE'93, Quebec

[38] Sze, S.M. -"Semiconductor Devices - Physics and Technology", - John Wiley & Sons, New York, 1985

Appendix

```
c   CALCULATION OF DEFLECTION OF PLATE
    PROGRAM FREQEQUATION
    IMPLICIT DOUBLE PRECISION (A-H,O-Z)
    COMMON/CONS/C1,C2,C3,C4
    DIMENSION A(4), B(4), C(4), D(4), E(4)
    COMMON/CONS/AC1(100), AC2(100),AC3(100), AC4(100)
    open(unit=6,file='devx.OUT',status='new')
    open(unit=12,file='SPIN2',status='new')
    PBAR=0.15D0
 1010   IF (PBAR.GT.5.5)GOTO 1100
    BBAR=0.0D0
    DLBAR=DELBAR(ETUNG,H,XNU,DFR,DELTA,ARE,PNOT)
    A(1) = 1.0 D0
    A(2) = 0.0 D0
    A(3) = 1.0 D0
    A(4) = 0.0 D0
    B(1) = 0.0 D0
    B(2) = 1.0 D0
    C(1) = 1.0 D0
```

```
      C(2) = 2.0 D0
      D(1) = 0.0 D0
      D(2) = 1.0 D0
      E(1) = -(PBAR)/64.0D0
      E(2) = -(PBAR)/16.0D0
    1 DBBAR=0.01
      NFLG1=0
      NFLG2=0
    2 BBAR=BBAR+DBBAR
*
      B(3) = DLOG(BBAR)
      B(4) = 1.0D0/BBAR
      C(3) = BBAR*BBAR
      C(4) = 2.0D0*BBAR
      D(3) = BBAR*BBAR*DLOG(BBAR)
      D(4) = BBAR*2.0D0*DLOG(BBAR) + BBAR
      E(3) = DLBAR-(BBAR**4)*PBAR/64.0D0
      E(4) = -(BBAR**3)*PBAR/16.0D0
*
      DENOM = DET(A,B,C,D)
      IF (DENOM.EQ.0.0) THEN
       PRINT*, 'NO UNIQUE SOLUTION EXISTS'
```

```
      ELSE
       C1 = DET(E,B,C,D)/DENOM
       C2 = DET(A,E,C,D)/DENOM
       C3 = DET(A,B,E,D)/DENOM
       C4 = DET(A,B,C,E)/DENOM

      ENDIF
*
      FREQN=FUNC(BBAR)
*     write(*,*)BBAR,freqn
      IF(FREQN.LT.0)NFLG1=1
      IF(FREQN.GT.0)NFLG2=1
      IF(BBAR.GT.0.5)GOTO 100
      IF(NFLG1.EQ.NFLG2)GOTO 22
      GOTO 2
   22 BBAR1=BBAR-DBBAR
      BBAR2=BBAR
      FREQL=FUNC(BBAR1)
 11   BBAR=(BBAR1+BBAR2)/2.0
      EPS1=DABS((BBAR-BBAR3)/BBAR)
      IF(EPS1.LT.1.E-8)GOTO 33
      FREQM=FUNC(BBAR)
```

```
      FEPS=FREQM*FREQN
      IF(FEPS.GT.0)BBAR2=BBAR
      IF(FEPS.LT.0)BBAR1=BBAR
      IF(FEPS.GT.0)FREQN=FREQM
      IF(FEPS.LT.0)FREQL=FREQM
      BBAR3=BBAR
      GOTO 11
33    BBAR=BBAR1
      BBAR1=BBAR2
      TEMP=FREQL
3     DFREQ=(FREQN-TEMP)/(BBAR-BBAR1)
      IF(DFREQ.EQ.0)GOTO 90
      BBAR1=BBAR
      BBAR=BBAR-FREQN/DFREQ
      EPS=DABS((BBAR-BBAR1)/BBAR)
      IF(EPS.LE.1.E-15)GOTO 90
      TEMP=FREQN
      FREQN=FUNC(BBAR)
      GOTO 3
90    ROOT=BBAR
      GOTO 1
100   WRITE(6,130)PBAR,ROOT,DLBAR
```

```
130    FORMAT (1X,3E16.8)
       IF(ROOT.EQ.0)GOTO 1011
       B(3) = DLOG(ROOT)
       B(4) = 1.0D0/ROOT
       C(3) = ROOT*ROOT
       C(4) = 2.0D0 * ROOT
       D(3) = ROOT*ROOT*DLOG(ROOT)
       D(4) = ROOT*2.0D0*DLOG(ROOT)+ROOT
       E(3) = DLBAR-(ROOT**4)*PBAR/(64.0D0)
       E(4) = -(ROOT**3)*PBAR/16.0D0
       I = I+1
       DENOM = DET(A,B,C,D)
       AC1(I) = DET(E,B,C,D)/DENOM
       AC2(I) = DET(A,E,C,D)/DENOM
       AC3(I) = DET(A,B,E,D)/DENOM
       AC4(I) = DET(A,B,C,E)/DENOM
       CALL SHAPE(ROOT,PBAR,I)
1011     PBAR=PBAR+0.1
       GOTO 1010
1100     STOP
       END
*--------------------------------------------------------------
```

```
------------------*

      FUNCTION FUNC(BBAR)

      IMPLICIT DOUBLE PRECISION (A-H,O-Z)

*--------------------------------------------------------

-----------------

      COMMON/CONS/C1,C2,C3,C4

      XNU=0.3D0

      FUNC= C2*(XNU-1.0D0)/(BBAR*BBAR)+ C3*2.0D0*(XNU+1.0D0) +

      +

C4*(3.0D0+2.0D0*DLOG(BBAR)+2.0D0*XNU*DLOG(BBAR)+XNU)+

      +        PBAR*(BBAR**2)/16.0D0*(3.0D0+XNU)

      RETURN

      END

*--------------------------------------------------------

----------------*

      FUNCTION DET(P,Q,R,S)

*

      IMPLICIT DOUBLE PRECISION (A-H, O-Z)

      DIMENSION P(4),Q(4),R(4),S(4)

*

      DET

=P(1)*Q(2)*R(3)*S(4)-P(1)*Q(2)*R(4)*S(3)-P(1)*R(2)*Q(3)*S(4)
```

```
     +
+P(1)*R(2)*Q(4)*S(3)+P(1)*S(2)*Q(3)*R(4)-P(1)*S(2)*Q(4)*R(3)
     +
-Q(1)*P(2)*R(3)*S(4)+Q(1)*P(2)*R(4)*S(3)+Q(1)*R(2)*P(3)*S(4)
     +
-Q(1)*S(2)*P(3)*R(4)+Q(1)*S(2)*P(4)*R(3)-Q(1)*R(2)*P(4)*S(3)
     +
+R(1)*P(2)*Q(3)*S(4)-R(1)*P(2)*Q(4)*S(3)-R(1)*Q(2)*P(3)*S(4)
     +
+R(1)*Q(2)*P(4)*S(3)+R(1)*S(2)*P(3)*Q(4)-R(1)*S(2)*P(4)*Q(3)
     +
-S(1)*P(2)*Q(3)*R(4)+S(1)*P(2)*Q(4)*R(3)+S(1)*Q(2)*P(3)*R(4)
     +
-S(1)*Q(2)*P(4)*R(3)-S(1)*R(2)*P(3)*Q(4)+S(1)*R(2)*P(4)*Q(3)
      RETURN
      END
*------------------------------------------------------------
----------------------

      FUNCTION DELBAR(ETUNG,H,XNU,DFR,DELTA,ARE,PNOT)
      IMPLICIT DOUBLE PRECISION (A-H,O-Z)
      ETUNG=1.9E11
```

```
H=65.0E-06
XNU=0.3
DFR=(ETUNG*(H**3))/(12.0D0*(1.0D0-XNU**2))
DELTA=30.00E-06
ARE=3500.0E-06
PNOT=1.01325E05
DELBAR=(DFR*DELTA)/(PNOT*(ARE**4))
RETURN
END

*--------------------------------------------------------
-------------------*
SUBROUTINE SHAPE(ROOT,PBAR,K)
IMPLICIT DOUBLE PRECISION (A-H, O-Z)
COMMON/CONS/C1,C2,C3,C4, AC1(100), AC[illegible](100),
+ AC3(100), AC4(100)
XNU=0.3 D0
H = 65.0E-06
PNOT=1.01325E05
ARE=3500.0E-06
DELTA=30.0E-06
DR=(ETUNG*(H**3))/(12.0D0*(1.0D0-XNU**2))
```

```
      DLBAR=DELBAR(ETUNG,H,XNU,DFR,DELTA,ARE,PNOT)
      RBAR=ROOT
      R=RBAR*ARE
      WBAR=DLBAR

W=WBAR*12.0D0*PNOT*(ARE**4)*(1.0D0-(XNU**2))/(ETUNG*(H**3))
      DWBAR=0.0D0
      DWDBAR=0.0D0
      SIGR=0.0D0
      SIGT=0.0D0
      WRITE(6,110)R,W,DWBAR,DWDBAR,SIGR,SIGT
 110 FORMAT(1X,(1X,6E16.8))
 10    RBAR=RBAR+0.01
      WBAR=
AC1(K)+AC2(K)*DLOG(RBAR)+AC3(K)*RBAR*RBAR+AC4(K)*RBAR*RBAR
      +    *DLOG(RBAR)+(RBAR**4)*PBAR/6 . D0

W=WBAR*12.0D0*PNOT*(ARE**4)*(1.0D0-(XNU**2))/(ETUNG*(H**3))
      R=RBAR*ARE
C    PR=PNOT*PBAR

DWBAR=AC2(K)/RBAR+2.0D0*AC3(K)*RBAR+2.0D0*AC4(K)*RBAR*DLOG(R
```

```
BAR)
     +  +AC4(K)*RBAR+PBAR*(RBAR**3)/16.0D0

DWDBAR=-AC2(K)/(RBAR**2)+2.0D0*AC3(K)+2.0D0*AC4(K)*DLOG(RBAR)+
     +  3.0D0*AC4(K)+3.0D0*PBAR*(RBAR**2)/16.0D0
      SIGRBAR=-(DWDBAR+XNU*DWBAR/RBAR)
      SIGTBAR=-((DWBAR/RBAR)+XNU*DWDBAR)
      SIGR=SIGRBAR*6.0D0*PNOT*(ARE**2)/(H**2)
      SIGT=SIGTBAR*6.0D0*PNOT*(ARE**2)/(H**2)
      WRITE(6,120)R,W,DWBAR,DWDBAR,SIGR,SIGT
  120 FORMAT(1X,(1X,6E16.8))
      IF(RBAR.LE.1.0D0) THEN

      GOTO 10
      ELSE
      GOTO 15
 15   CONTINUE
      ENDIF
      RETURN
      END
```